

**NUMERICAL INVESTIGATION OF SPRAY DEHUMIDIFICATION
PROCESS OF MOIST AIR**

ALI FARNOUD

**A THESIS SUBMITTED IN PARTIAL FULFILLMENT OF THE
REQUIREMENTS FOR THE DEGREE OF**

MASTER OF SCIENCE

THE DEPARTMENT OF MECHANICAL ENGINEERING

TOBB UNIVERSITY OF ECONOMICS AND TECHNOLOGY

THE GRADUATE SCHOOL OF NATURAL AND APPLIED SCIENCES

DECEMBER 2014

ANKARA

Approval of the Graduate School of Natural and Applied Sciences.

Prof. Dr. Osman EROĞUL
Director

I certify that this thesis satisfies all the requirements as a thesis for the degree of Master of Science.

Assoc. Dr. Murat Kadri AKTAŞ
Head of Department

This is to certify that we have read this thesis and that in our opinion it is fully adequate, in scope and quality, as a thesis for the degree of Master of Science.

Assoc. Dr. Murat Kadri AKTAŞ
Supervisor

Examining Committee Members

Chair : Prof. Dr. Haşmet TÜRKOĞLU

Member : Assoc. Dr. Murat Kadri AKTAŞ

Member : Asst. Dr. Özgür BAYER

TEZ BİLDİRİMİ

Tez içindeki bütün bilgilerin etik davranış ve akademik kurallar çerçevesinde elde edilerek sunulduğunu, ayrıca tez yazım kurallarına uygun olarak hazırlanan bu çalışmada orijinal olmayan her türlü kaynağa eksiksiz atıf yapıldığını bildiririm.

I hereby declare that all the information provided in this thesis was obtained with rules of ethical and academic conduct. I also declare that I have cited all sources used in this document, which is written according to the thesis format of the Institute.

Ali FARNOUD

University : TOBB University of Economics and Technology
Institute : Graduate School of Natural and Applied Sciences
Science Programme : Mechanical Engineering
Supervisor : Associate Professor Murat Kadri AKTAŞ
Degree Awarded and Date : M.Sc. – December 2014

ALI FARNOUD

**NUMERICAL INVESTIGATION OF SPRAY DEHUMIDIFICATION PROCESS
OF MOIST AIR**

ABSTRACT

This investigation focuses on the heat and mass transfer in dehumidification process of the moist air. The interaction of water droplets with the hot, moist air which is flowing in contrary to the water spray is studied in a chamber. Two dimensional and three dimensional simulations are performed in order to study the effect of various parameters on heat and mass transfer. The parameters such as droplet diameter, spray mass flow rate, droplet temperature, number of injections, spray cone angle, and spray location are considered. The results show that smaller droplets lead to higher humidity reduction at the outlet. However droplet size effect on temperature and relative humidity depends on the optimum radius. If droplets are smaller than optimum radius, increasing their size results in enhancement of heat transfer. On the other hand, if droplets are larger than the optimum radius, by increasing the droplet diameter heat transfer decreases. It is found that heat and mass transfer are proportional to mass flow rate of the spray. Furthermore results indicate that decreasing the coolant temperature causes humidity and temperature reduction at the outlet. In addition, spray cone angle effect is found to be negligible. Results demonstrate that using more sprays in the chamber helps to diffuse the droplets to regions close to the wall. It is concluded that location of the spray does not have significant effect on bulk temperature at the outlet.

Key words: droplet, spray dehumidification, direct contact condensation, multiphase flow.

Üniversitesi : TOBB Ekonomi ve Teknoloji Üniversitesi
Enstitüsü : Fen Bilimleri
Anabilim Dalı : Makine Mühendisliği
Tez Danışmanı : Doç. Dr. Murat Kadri AKTAŞ
Tez Türü ve Tarihi : Yüksek Lisans – Aralık 2014

ALİ FARNOUD

SPREYLE NEM ALMA İŞLEMİNİN SAYISAL ANALİZİ

ÖZET

Bu çalışmada nemli havanın neminin alınması işlemindeki ısı ve kütle transferi araştırılmıştır. Yapılan çalışmada su spreyinin tersi yönünde akan sıcak nemli hava ile su damlacıklarının etkileşimi bir kanal içerisinde incelenmiştir. Çeşitli parametrelerin ısı ve kütle transferine etkisini incelemek için iki boyutlu ve üç boyutlu simülasyonlar geliştirilmiştir. Bir parametrenin etkisinin incelenmesi üzerine çalışılırken, diğer tüm parametreler sabit tutulmuştur. Damlacık çapı, sprey kütle akış hızı, damlacık sıcaklığı, enjeksiyon sayısı ve sprey açısı gibi parametreler çalışmada analiz edilmiştir. Ancak, damlacık boyutunun sıcaklık ve bağıl nem üzerine etkisi optimum yarıçapa bağlıdır. Eğer damlacıkların boyutu optimum yarı çaptan küçük olursa, damlacık boyutlarındaki büyüme ısı transferini iyileştirmeye yönelik etki gösterir. Öte yandan, damlacıkların boyutu optimum yarı çaptan büyük olursa, damlacık boyutları büyüdükçe ısı transferi azalır. Isı ve kütle transferi miktarının, spreyin kütleli debisi ile orantılı olduğu görülmüştür. Ayrıca elde edilen sonuçlar soğutucu sıcaklığındaki azalmanın, çıkışta nem ve sıcaklık değerlerinin azalmasına sebep olduğunu göstermektedir. Ek olarak, sprey açısı etkisinin ihmal edilebilir olduğu görülmüştür. Elde edilen sonuçlar doğrultusunda, kanalda fazla sayıda sprey kullanımının nem alma etkisini duvara yakın bölgelere yaydığı gözlemlenmiştir. Ayrıca spreyin konumunun çıkıştaki yağın sıcaklığına önemli bir etkisi olmadığı belirlenmiştir.

Anahtar Kelimeler: damlacık, sprey nem alma, doğrudan temas yoğuşması, iki fazlı akış

ACKNOWLEDGEMENT

Many people have made significant contributions to this work. I am using this opportunity to express my gratitude to everyone who supported me throughout my studies.

Firstly I would like to thank my lovely parents who always supported me and taught me the ethics of life. I am sincerely grateful to them for sharing their truthful and illuminating views on a number of issues related to humanity and philosophy of life.

I would like to express my sincere gratitude to my research advisor, Associate Professor Murat Kadri AKTAŞ for his support, guidance and encouragement throughout this work.

I would like to thank the Turkish Ministry of Science, Industry and Technology and ARÇELİK Company for their support of research funding. This work was supported under grant number of 1488.STZ.2012-2.

I would like to thank all members of the Heat Transfer Laboratory that always helped me when I had any problem or difficulty in Turkey.

CONTENT

TEZ BİLDİRİMİ.....	ii
ABSTRACT.....	iii
ÖZET.....	iv
ACKNOWLEDGEMENT	v
CONTENT	vi
LIST OF TABLES	x
LIST OF FIGURES	xi
ABBREVIATIONS	xvi
LIST OF SYMBOLS	xvii
1. INTRODUCTION AND MOTIVATION	1
2. LITERATURE REVIEW.....	4
2.1. Experimental Investigations.....	4
2.2. Analytical Investigations.....	9
2.3. Numerical Investigations	10
3. PROBLEM DESCRIPTION.....	15
3.1. Mathematical Model	15
3.1.1. Mass Conservation Equation.....	16
3.1.2. Momentum Transfer Equation	16
3.1.3. Energy Equation.....	16
3.1.4. Turbulence Model	17

3.1.5. Equation of Motion for Droplets.....	17
3.1.6. Species Transport Equations	18
3.1.7. Heat and Mass Transfer Mechanism.....	18
3.1.7.1. Evaporation Model.....	20
3.1.7.2. Condensation Model	20
3.1.8. Integration of Particle Motion Equation	22
3.1.9. Turbulent Dispersion of Particles	22
3.2. Boundary Conditions	23
3.2.1. Continuous Phase Boundary Conditions.....	23
3.2.2. Spray Initial Conditions	23
3.2.3. Wall Boundary Conditions.....	24
3.2.4. Outlet Boundary Conditions	24
3.3. Numerical Model	24
3.3.1. Air-Vapor Mixture Model.....	24
3.3.2. Solution Method.....	25
3.4. Material Properties	25
3.5. Grid Independency Analysis	26
4. TWO DIMENSIONAL ANALYSIS	27
4.1. A Base Case Study	27
4.1.1. Evaporation and Condensation Mechanism.....	34
4.2. Parametric Study	36

4.2.1. Effect of Droplet Diameter.....	36
4.2.1.1. Effect of Droplet Size on Penetration	40
4.2.1.2. Effect of the droplet diameter on flow pattern on the horizontal centerline	41
4.2.1.3. Effect of droplet diameter on flow pattern at the outlet cross section	44
4.2.1.4. Effect of droplet diameter on mass-weighted average values of the parameters	47
4.2.2. Effect of Spray Mass Flow Rate	49
4.2.2.1. Effect of mass flow rate on flow pattern on the horizontal centerline	51
4.2.2.2. Effect of mass flow rate on flow pattern at the outlet cross section .	53
4.2.2.3. Effect of mass flow rate on mass-weighted average values of the parameters	56
4.2.3. Effect of Water Droplet Temperature	58
4.2.3.1. Effect of water droplet temperature on flow pattern on the horizontal centerline	59
4.2.3.2. Effect of water droplet temperature on flow pattern at the outlet cross section	61
4.2.3.3. Effect of water droplet temperature on mass-weighted average values of the parameters	64
4.2.4. Effect of Spray Cone Angle	66
4.2.5. Effect of Number of the Sprays	68
4.2.5.1. Effect of number of injections on flow pattern on the horizontal centerline	71
4.2.5.2. Effect of number of injections on flow pattern at the outlet cross section	73
4.2.5.3. Effect of number of injections on mass-weighted average values of the parameters	76
4.2.6. Effect of the Location of the Spray	79

4.2.6.1. Effect of the location of the spray on flow pattern on the centerline	81
4.2.6.2. Effect of the location of the spray on flow pattern at the outlet cross section	83
4.2.6.3. Effect of the location of the spray on mass-weighted average values of the parameters	85
5. THREE DIMENSIONAL SIMULATIONS	88
6. CONCLUSIONS	97
REFERENCES.....	99
RESUME	106

LIST OF TABLES

Table 3-1. Inlet boundary conditions of the continuous phase.	23
Table 3-2. Thermo-physical properties of the water (dispersed phase).	25
Table 3-3. Thermo-physical properties of air.	25
Table 4-1. Spray initial conditions.	28
Table 4-2. Initial conditions of the injection.	36
Table 4-3. Effect of heating the air-vapor mixture on RH.	47
Table 4-4. Effect of heating the air-vapor mixture on RH.	55
Table 4-5. Effect of heating the air-vapor mixture on RH.	64
Table 4-6. Initial conditions of each spray.	68
Table 4-7. Effect of heating the air-vapor mixture on RH.	75

LIST OF FIGURES

Figure 1-1. Schematic for the drying cycle.....	2
Figure 2-2. Droplet distributions in the cross-sections for different injection angles with $Re = 25700$. Zhang et al. [25].	9
Figure 2-3. Comparisons between experimental and calculated results for differential liquid film temperature in injection regions [32].	11
Figure 2-4. Distribution of drop bulk temperature with time [33].	12
Figure 2-5. The drop growth rate [33].	12
Figure 3-1. Schematic for the spray dryer.....	15
Figure 3-2. "Reflect" Boundary Condition for the Discrete Phase.	24
Figure 3-3. Grid on the channel.	26
Figure 3-4. Grid independence test.	26
Figure 3-5. Location of the mesh study cases.	26
Figure 4-1. Non-dimensional droplet temperature vs time.	27
Figure 4-2. Droplet non-dimensional temperature [10].	28
Figure 4-3. Droplet non-dimensional temperature [7].	29
Figure 4-4. Velocity magnitude distribution at different horizontal distances from nozzle.	30
Figure 4-5. Pressure distribution on the horizontal centerline.	31
Figure 4-6. Effect of gravity on droplet velocity distribution.....	32
Figure 4-7. Humidity distribution at different horizontal distances from the nozzle.	32
Figure 4-8. Temperature distribution at different horizontal distances from the nozzle.	33
Figure 4-9. Relative humidity distribution at different distances from the nozzle. ...	34
Figure 4-10. Dehumidification and cooling process.	35
Figure 4-11. Effect of droplet diameter on gas-phase bulk temperature at the outlet.	37
Figure 4-12. Nu variation with droplet radius [58].	38
Figure 4-13. Temperature contours for different droplet diameters, (a) $d_p = 10 \mu\text{m}$, (b) $d_p = 15 \mu\text{m}$, (c) $d_p = 30 \mu\text{m}$, (d) $d_p = 40 \mu\text{m}$, (e) $d_p = 60 \mu\text{m}$, (f) $d_p = 80 \mu\text{m}$	38

Figure 4-14. Humidity contours for different droplet diameters, (a) $d_p = 10 \mu\text{m}$, (b) $d_p = 15 \mu\text{m}$, (c) $d_p = 30 \mu\text{m}$, (d) $d_p = 40 \mu\text{m}$, (e) $d_p = 60 \mu\text{m}$, (f) $d_p = 80 \mu\text{m}$	39
Figure 4-15. Particle trajectories for $d_p = 10 \mu\text{m}$ and mass flow rate = 3 gr/s.	40
Figure 4-16. Particle trajectories for $d_p = 40 \mu\text{m}$ and mass flow rate = 3 gr/s.	41
Figure 4-17. Particle trajectories for $d_p = 80 \mu\text{m}$ and mass flow rate = 3 gr/s.	41
Figure 4-18. Effect of droplet diameter on relative humidity distribution on the horizontal centerline.....	42
Figure 4-19. Effect of droplet diameter on temperature distribution on the horizontal centerline.....	42
Figure 4-20. Effect of droplet diameter on humidity distribution on the horizontal centerline.....	43
Figure 4-21. Effect of droplet diameter on relative humidity at the outlet.	44
Figure 4-22. Effect of droplet diameter on temperature at the outlet.....	45
Figure 4-23. Effect of droplet diameter on humidity at the outlet.	45
Figure 4-24. Effect of droplet diameter on mass-weighted average relative humidity.	47
Figure 4-25. Effect of droplet diameter on mass-weighted average humidity.....	48
Figure 4-26. Effect of droplet diameter on mass-weighted average humidity.....	48
Figure 4-27. Temperature contours for different mass flow rates , (a) Mass flow rate = 3 gr/s, (b) Mass flow rate = 4gr/s, (c) Mass flow rate = 6 gr/s.	49
Figure 4-28. Humidity contours for different mass flow rates, (a) Mass flow rate = 3 gr/s, (b) Mass flow rate = 4 gr/s, (c) Mass flow rate = 6 gr/s.....	50
Figure 4-29. Effect of spray mass flow rate on relative humidity distribution on the horizontal centerline.....	51
Figure 4-30. Effect of spray mass flow rate on temperature distribution on the horizontal centerline.....	52
Figure 4-31. Effect of spray mass flow rate on humidity distribution on the horizontal centerline.....	52
Figure 4-32. Effect of mass flow rate on relative humidity at the outlet.	53
Figure 4-33. Effect of mass flow rate on temperature distribution at the outlet.	54
Figure 4-34. Effect of mass flow rate on humidity distribution at the outlet.....	54
Figure 4-35.Effect of mass flow rate on mass-weighted average relative humidity..	56
Figure 4-36. Effect of mass flow rate on mass-weighted average temperature	57

Figure 4-37. Effect of mass flow rate on mass-weighted average humidity.....	57
Figure 4-38. Temperature contours for different water droplet temperature,	58
Figure 4-39. Humidity contours for different water droplet temperature, (a) $T_w = 288$ K, (b) $T_w = 313$ K, (c) $T_w = 323$ K, (d) $T_w = 330$ K.....	59
Figure 4-40. Effect of droplet temperature on relative humidity distribution on the horizontal centerline.....	60
Figure 4-41. Effect of droplet temperature on temperature distribution on the horizontal centerline.....	60
Figure 4-42. Effect of droplet temperature on humidity distribution on the horizontal centerline.	61
Figure 4-43. Effect of water temperature on relative humidity distribution at the outlet.....	61
Figure 4-44. Effect of water temperature on temperature distribution at the outlet. .	62
Figure 4-45. Effect of water temperature on humidity distribution at the outlet.	63
Figure 4-46. Effect of water droplet temperature on mass-weighted average relative humidity.	64
Figure 4-47. Effect of water droplet temperature on mass-weighted average temperature.....	65
Figure 4-48. Effect of water droplet temperature on mass-weighted average humidity.	65
Figure 4-49. Effect of spray cone angle on relative humidity distribution on the centerline after the nozzle.	67
Figure 4-50. Effect of spray cone angle on temperature distribution on the centerline after the nozzle.	67
Figure 4-51. Effect of spray cone angle on humidity distribution on the centerline after the nozzle.	68
Figure 4-52. Temperature contours, (a) one injection, (b) two injections, (c) three injections, (d) four injections.	69
Figure 4-53. Humidity contours, (a) one injection, (b) two injections, (c) three injections, (d) four injections.	70
Figure 4-54. Effect of number of injections on relative humidity distribution on the horizontal centerline.....	71
Figure 4-55. Effect of number of injections on temperature distribution on the horizontal centerline.....	72

Figure 4-56. Effect of number of injections on humidity distribution on the horizontal centerline.	72
Figure 4-57. Effect of number of injections on relative humidity distribution at the outlet cross section.	73
Figure 4-58. Effect of number of injections on temperature distribution at the outlet cross section.	74
Figure 4-59. Effect number of injections on humidity distribution at the outlet cross section.	74
Figure 4-60. Effect of number of injections on mass-weighted average relative humidity.	76
Figure 4-61. Effect of number of injections on mass-weighted average temperature.	76
Figure 4-62. Effect of number of injections on mass-weighted average humidity....	77
Figure 4-63. Particle trajectories colored by humidity.....	78
Figure 4-64. Particle trajectories colored by temperature.....	78
Figure 4-65. Temperature contours for sprays at different locations, (a) $x = 44.5$ cm, (b) $x = 80$ cm, (c) $x = 120$ cm.	79
Figure 4-66. Humidity contours for sprays at different locations, (a) $x = 44.5$ cm, (b) $x = 80$ cm, (c) $x = 120$ cm.	80
Figure 4-67. Effect of the spray location on relative humidity distribution on the horizontal centerline.....	81
Figure 4-68. Effect of the spray location on temperature distribution on the horizontal centerline.	81
Figure 4-69. Effect of the spray location on humidity distribution on the horizontal centerline.	82
Figure 4-70. Effect of spray location on the relative humidity at the outlet.	83
Figure 4-71. Effect of spray location on the temperature at the outlet.	83
Figure 4-72. Effect of spray location on the humidity at the outlet.	84
Figure 4-73. Effect of the spray location on mass-weighted average relative humidity.	85
Figure 4-74. Effect of the spray location on bulk temperature.	86
Figure 4-75. Effect of the spray location on mass-weighted average humidity.....	86
Figure 5-1. Three dimensional geometry of the pipe.	88

Figure 5-2. Particle trajectories for $d_p = 80 \mu\text{m}$	88
Figure 5-3. Particle trajectories for $d_p = 40 \mu\text{m}$	89
Figure 5-4. Particle trajectories for $d_p = 10 \mu\text{m}$	89
Figure 5-5. Particle traces colored by gas-phase temperature ($d_p = 80 \mu\text{m}$).	89
Figure 5-6. Particle traces colored by humidity ($d_p = 80 \mu\text{m}$).	90
Figure 5-7. Particle traces colored by gas-phase temperature ($d_p = 40 \mu\text{m}$).	90
Figure 5-8. Particle traces colored by humidity ($d_p = 40 \mu\text{m}$).	91
Figure 5-9. Particle traces colored by gas-phase temperature ($d_p = 10 \mu\text{m}$).	91
Figure 5-10. Particle traces colored by humidity ($d_p = 10 \mu\text{m}$).	92
Figure 5-11. Particle traces colored by temperature ($T_w = 288 \text{ K}$).	92
Figure 5-12. Particle traces colored by humidity ($T_w = 288 \text{ K}$).	93
Figure 5-13. Particle traces colored by temperature ($T_w = 323 \text{ K}$).	93
Figure 5-14. Particle traces colored by humidity ($T_w = 323 \text{ K}$).	94
Figure 5-15. Particle traces colored by temperature (mass flow rate = 3 gr/s).	94
Figure 5-16. Particle traces colored by humidity (mass flow rate = 3 gr/s).	95
Figure 5-17. Particle traces colored by temperature (mass flow rate = 6 gr/s).	95
Figure 5-18. Particle traces colored by humidity (mass flow rate = 6 gr/s).	96

ABBREVIATIONS

Abbreviations	Description
CFD	Computational Fluid Dynamics
DCC	Direct Contact Condensation
DPM	Discrete Phase Model
RH	Relative Humidity
RNG	Renormalization Group

LIST OF SYMBOLS

Symbol	Description
A	surface area
Bi	Biot number
B_m	Spalding mass number
C_D	Drag coefficient
C_e	Atomization rate constant
C_p	Heat capacity of the droplet
d_p	Diameter of particle
$D_{i,m}$	Diffusion coefficient for species i in the mixture
$D_{T,i}$	Thermal diffusion coefficient
E	Energy
e_n	Restitution coefficient
F	Force
h	Convective heat transfer coefficient
h_{fg}	Latent heat of droplet
J_i	Diffusion flux of species i
k	Thermal conductivity
k_c	Mass transfer coefficient
m_p	droplet mass
Nu	Nusselt number

P	Pressure
Pr	Prandtl number
R_i	Net rate of production of species i
Re	Reynolds number
S_i	Source term for component i
Sc_t	Turbulent Schmidt number
t	Time
T	Temperature
T_{w0}	Droplet initial temperature
u	Velocity x-component
v	Velocity y-component
x	Cartesian horizontal axis direction
y	Cartesian vertical axis direction
Y_i	Mass fraction of the species i
$Y_{i,s}$	Vapor mass fraction at the surface
ρ	Density
μ	Dynamic viscosity
μ_t	Turbulent viscosity
τ	Stress tensor
σ	Stefan-Boltzmann constant
ε	Emissivity

θ_R Radiation temperature

Subscripts

d Droplet

i Species

p Particle

s Saturated steam

x Cartesian horizontal axis direction

y Cartesian vertical axis direction

∞ Continuous phase

max Maximum

1. INTRODUCTION AND MOTIVATION

Air conditioning is the process in which the properties of the air are changed to desirable conditions [1]. One of these processes is the dehumidification process of the humid air. During dehumidification, humidity of the air is reduced due to reasons such as health, comfort and industrial need [2]. Dehumidification can be achieved by means of sub-cooled water sprays as long as the temperature of the spray is lower than the dew point of the humid air passing through the unit. This process is known as “spray dehumidification”.

The main physical phenomenon in this process is direct contact condensation (DCC) of steam on water surface. Direct contact heat transfer occurs whenever two substances touch each other physically at different temperatures. Direct and indirect contact processes differ in many perspectives. In indirect transfer, the process is limited by the surface area and the possible heat transfer rate through this surface. In direct contact transfer, the process is controlled by the interplay between the latent heat of condensation and the amount of sensible heat the liquid can absorb [3]. In this process sensible heat and latent heat transfer play a crucial role. Since the air is in contact with water, the sensible heat will be absorbed by droplet. However latent heat of condensation will be removed from the steam to the surrounding.

Nowadays DCC has a great role in many industrial projects like air conditioning, nuclear reactor cooling system, mixing-type heat exchangers, steam jet spray and desalination. For this reason many researchers have investigated the physics of the phenomenon. However due to complexity of the heat and mass transfer process and limitations in numerical methods and measurement devices, number of the available publications are not adequate in order to fully understand physics of the problem.

Recently air or water cooled condensers are used to dehumidify the drum air in washing-drying machines. The most common disadvantages in these machines are the long drying time, high energy and water consumption. Within this project, a dehumidification system is developed for hybrid washer / dryer machines. The following figure describes the drying cycle. The data from experiments show that hot and moist air

with relative humidity of 90 % and temperature of 348 K exits from the drum. The drum air enters the channel with the velocity of 10 m/s. It is observed that by using a spray after the drum, the humid drum air is dehumidified. Accordingly, the humidity and the temperature decrease. It should be mentioned that by using spray in the system drying time decreases.

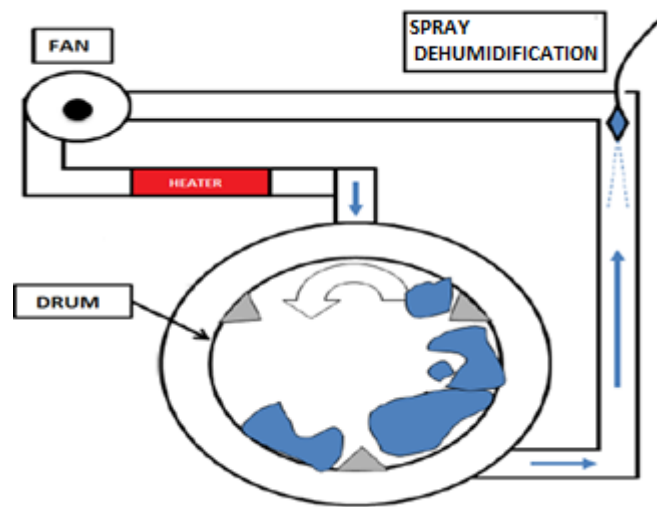


Figure 1-1. Schematic for the drying cycle.

The objective of this thesis study is to study the effect of various parameters on direct contact condensation of steam on the surface of sprayed chilled water droplets in a horizontal channel. The thesis is organized as follows:

Chapter two presents a critical review of analytical, experimental, and numerical investigations in the field of direct contact condensation of steam on liquid droplets.

Chapter three describes the details of the problem and equations which are governing the problem. Furthermore this chapter discusses the computational methods and boundary conditions which are utilized to simulate the problem. All the simulations are performed by utilizing ANSYS Fluent 14.5.

Chapter four explains the results of the numerical simulations. This chapter completely describes the effects of various parameters on pattern of the flow field. Various parameters such as spray mass flow rate, droplet diameter, droplet

temperature and cone angle of the spray are altered in order to investigate their effect on flow pattern. Finally, Chapter five presents the conclusions.

The major aim of this thesis is to develop a model and investigate the effect of various parameters on dehumidification process.

2. LITERATURE REVIEW

Sprays have many applications such as spray drying, turbine combustor cooling, air conditioning, nuclear reactor cooling and mixing-type heat exchangers. Depending on the droplet characteristics such as size, temperature, cone angle, spray mass flow rate, and velocity of sprays have different utilizations. In the field of air conditioning, sprays are used in cooling towers and evaporative coolers and air washers. Direct contact condensation plays a crucial role in the study of the humidification and dehumidification of the moist air in contact with the sub-cooled water spray. There has been great number of publications in the literature concerning film condensation and also drop-wise condensation; however the investigations on direct contact condensation are limited. Investigations on direct contact condensation are reviewed at three major branches of experimental, numerical, and analytical studies.

2.1. Experimental Investigations

Hasson et al. experimentally studied the heat transfer in steam condensation on laminar water sheets generated by the fan spray nozzle. They showed that heat transfer coefficient could be reduced by as much as 50 % for a concentration of one percent air in steam [4].

Ford et al. experimentally studied the droplet size increase in direct contact condensation of steam on liquid droplets. They estimated a correlation for this phenomenon. They utilized a high-speed photography to calculate the particle size enhancement through the condensation process [5].

Simpson et al. experimentally studied the condensation process and hydrodynamic pressure oscillations when steam was discharged into a sub-cooled water pool. They explained that behavior of the subsonic jet is different from sonic jet. They noticed that pool sub-cooling had the largest influence on dynamic behavior [6].

Jeje et al. investigated the growth of vapor-liquid interfaces which are influenced by inertial and thermal effects. In their experiments high speed photography and frequency measurements systems were used. Convective heat transfer coefficients at vapor-liquid interfaces depended on bubbling regime and the stage of interface growth and its value increased up to $2.4 \text{ MWm}^{-2}\text{K}^{-1}$ [7].

Garimella et al. measured the effect of non-condensable gas mass fraction on heat transfer coefficient in small enclosures. They found that when the initial non-condensable gas amount is small the heat transfer coefficient depends on it. But when the non-condensable gas amount is great, the heat transfer coefficient is independent of it [8].

Celata et al. investigated the effect of droplet velocity on the heat transfer rate of saturated steam condensation on chilled water sprays. Furthermore they performed the average droplet temperature on the centerline of the spray injection [9].

Aya et al. experimentally studied the heat transfer coefficient evaluated assuming simple interface shapes for complicated surfaces. They predicted the heat transfer coefficient at chugging, condensation oscillation, jet region, and surface of satisfied flow [10].

Liang through experiments studied the regimes associated with the condensation of steam on water. He developed a transient conduction-diffusion model to analyze the effect of non-condensable gas on chugging transition steam condensation. Furthermore he found that the chugging boundary was not affected by water velocity. For this reason chugging process is controlled by localized eddies around the interface [11].

Mayinger et al. experimentally measured the growth of liquid droplet diameter due to condensation of saturated vapor on sub-cooled liquid. In order to measure the drop diameter they used pulsed laser holography. They found out that the geometry of the spray and the vapor pressure has a specific relation. For this reason, designers of nozzles which work at high vapor pressure conditions have to consider the relation of

the high pressure and the condensation and how it can have influence on the flow [12].

Akira et al. studied the direct contact condensation of the steam on sub-cooled water in a horizontal channel. In order to model the lowest limit of the heat transfer, the heat conduction model was used. They found that modified k- ϵ model shows more improved prediction compared with the wall k- ϵ model and agrees better with experimental results with smooth interfaces [13].

Lock has categorized all the different modes of condensation and evaporation which can happen in direct contact heat transfer. One of these approaches is the evaporation and condensation interactions with droplets and jets in the presence of a non-condensable gas. When an amount of non-condensable gas is present with the vapor the condensation rate decreases [14].

Kuhn et al. did many experiments in a vertical tube to figure out the effect of non-condensable gas. Pure steam, air-steam, and air-steam and Helium mixtures investigated. The results depicted that presence of non-condensable gases reduce the heat transfer performance [15].

Karl et al. utilized the linear Raman spectroscopy method to get temperature distribution in the water phase or the concentration pattern in the vapor phase to the heat transfer coefficient in condensation process of mixtures with and without condensable gas [16].

Anderson et al. investigated the steam condensation on the surface of AP600 containment. Heat transfer reduction due to presence of non-condensable gas has been investigated for different mixtures of air and helium. Effect of various parameters such as bulk temperature, cold surface temperature, non-condensable mass fraction on condensation heat transfer has been analyzed. For lowest mass fraction of the non-condensable and the highest surface temperature highest heat transfer coefficient was found [17].

Ju et al. measured the heat transfer coefficients around steam bubbles using the holographic interferometer and high speed camera. They investigated the condensation regime map associated with the downward injection of steam into water. They showed that the boundary of chugging and subsonic jetting with the larger diameter pipe is shifted to the larger steam mass flux [18].

Lee et al. experimentally investigated the effect of non-condensable gas on direct contact condensation of moist air. They led to the conclusion that higher mass fractions of non-condensable gas have inverse relation with the average heat transfer coefficient. Increasing the mass fraction of the non-condensable gas, results in reduction of average heat transfer coefficient. In addition, they noted the abatement of the average heat transfer coefficient by increasing the Jacob number [19].

Kim et al. performed experiments on direct contact condensation of steam discharging into cold water tank. They used five nozzles with different sizes and investigated various steam mass flux and pool temperature conditions. They noticed that the average heat transfer coefficient is in the range of 1.24-2.05 MWm⁻² °C⁻¹ and increases as the temperature of the pool decreases. The heat transfer coefficient is reduced as the nozzle size reduces [20].

Pikkula et al. analyzed the effect of droplet diameter on heat transfer in spray cooling by measuring the maximum heat removal for different average droplet diameters. They noticed that by increasing the particle diameter heat transfer increases, but after optimum radius, increasing the diameter reduces heat transfer [21].

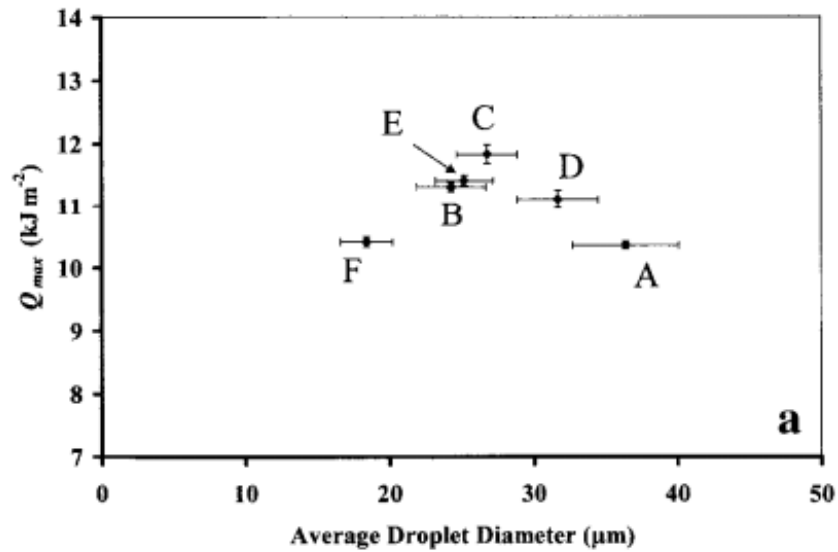


Figure 2-1. Maximal heat removal (Q_{max}) achieved at spraying distance DQ_{max} immediately upon termination of a 200-ms spurt as a function of average diameter [21].

Cheng et al. studied the effect of spray mass flow rate on heat transfer. They noticed that by increasing the spray mass flow rate heat transfer enhances [22].

Chen et al. experimentally studied the effect of droplet mean diameter on heat transfer coefficient. They altered particle mean diameter from 62.2 to 191.4 μm while other parameters were fixed in a constant value. They did not find a clear heat transfer pattern for different droplet diameters. This can be due to the range of droplet diameters in their research. The droplets that they studied were not small enough to find a pattern for heat transfer by changing droplet diameters [23].

Martinez-Galvan et al. analyzed the effect of spray cone angle on heat transfer by doing experiments with different nozzles. By using a methodology based on utilization of high speed camera, it is found that the thermal performance decreases as spray cone angle decreases [24].

Zhang et al. by using the PIV visualization system studied the spray in cross flow. They divided the flow field into three main parts of upper counter-rotating vortex pair zone, mainstream zone, and bottom counter-rotating vortex pair zone. Figure 2-2 illustrates droplet pattern and distribution at different cross sections. Due to coherent

structure at $\alpha = 60^\circ$, the upper counter-rotating vortex pair is prevented strongly. In addition in this case mixing rate is higher and it is obvious in the results from experiments [25].

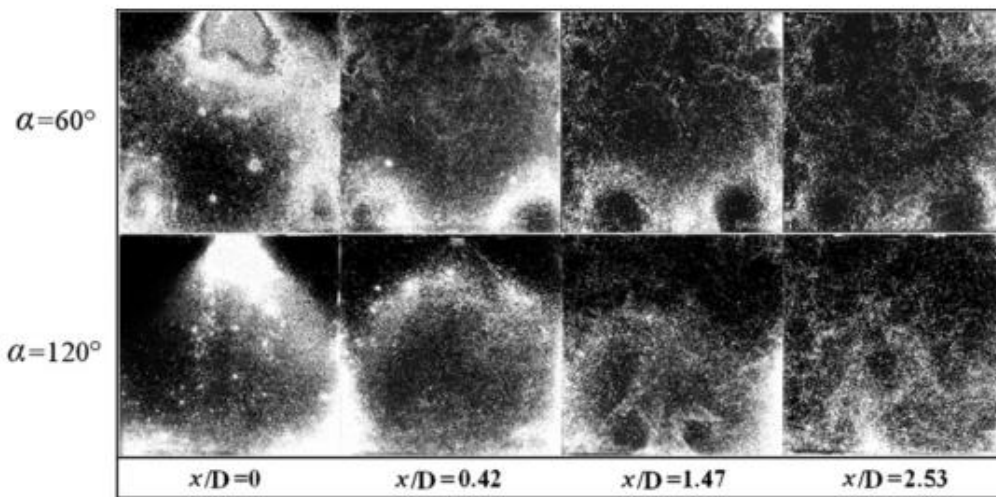


Figure 2-1. Droplet distributions in the cross-sections for different injection angles with $Re = 25700$. Zhang et al. [25].

2.2. Analytical Investigations

Minkowycz et al. studied the forced convection condensation of binary mixture of gases. In order to solve the coupled equations for gas phase and continuous phase similarity method is used. They noticed that the presence of non-condensable gas reduced the heat transfer [26].

Sparrow et al. analyzed the forced convection condensation on a horizontal surface of a binary mixture and non-condensable gas. Equations are solved using similarity method. They found that condensation reduction due to the presence of the non-condensable gas is lower when forced convection is the case. For free convection case presence of non-condensable gas plays a crucial role and decreases the heat transfer rate [27].

Taitel et al. investigated the DCC (direct contact condensation) on the falling liquid water. Based on integral solutions of the boundary layer equations and similarity

method condensation of vapor and air is studied. They explained that by increasing the mass fraction of the non-condensable gas the water interface temperature reduces [28].

Sage et al. solved the condensation problem of multicomponent mixture of alcohol vapors by using similarity solution. Their solution did not consider the presence of the non-condensable gas and the diffusivity coefficients were taken as constant values [29].

Frediani et al. mathematically modelled a large scale spray cooling system. For a single spray energy and continuity equations are solved. The equations are solved using a finite-difference solution along a drop trajectory for both water and air parameters. The model is applied towards solution of large systems involving multiple passes of sprays operating in conjunction with power stations. They found that there is agreement between data and the predictions of wind velocity and air-water temperatures [30].

Ghosh et al. mathematically studied the motion of the droplet in a droplet driven vertical jet. They simulated one and two-dimensional models to find the average air velocity in the spray. In order to validate the theoretical result they did some experiments which also gave a good perspective to some important mechanisms in the problem. They found that normal turbulent jets are characterized by large turbulent structures; on the other hand, droplet-driven jets are having small scales of turbulence [31].

2.3. Numerical Investigations

Akimoto et al. studied the direct contact condensation of steam on water droplets during a loss-of-coolant accident. They found that the droplet diameter strongly effect the condensation rate. Moreover they noticed that finer droplets lead to higher condensation rate. Figure 2-3 explains the liquid film temperature distribution with respect to C_e (atomization rate constant). Liquid film temperature increases with atomization rate and it remains below the saturation temperature [32].

Figure 2-3 depicts the liquid film temperature for different distances from the nozzle. As the liquid gets far from the nozzle its temperature increases and its value approximately enhances to saturation temperature. It should be emphasized that the liquid temperature is not able reach the saturation temperature.

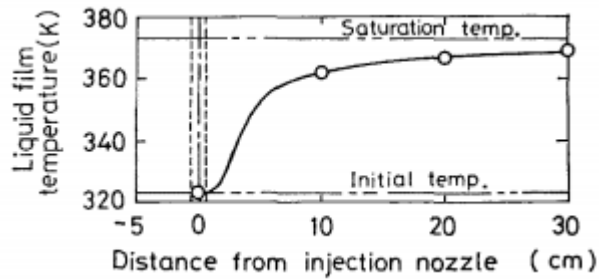


Figure 2-2. Comparisons between experimental and calculated results for differential liquid film temperature in injection regions [32].

Huang et al. numerically studied the heat and mass transfer on droplet in direct contact with the environment. The environment consists of saturated vapor and non-condensable gas. They provided new correlations for averaged condensation rate and heat flux associated with condensation on a moving droplet. The correlations are extracted from transient numerical calculations. Figure 2-4 illustrates the time variation of the dimensionless bulk temperature. The droplet bulk temperature increases with time [33].

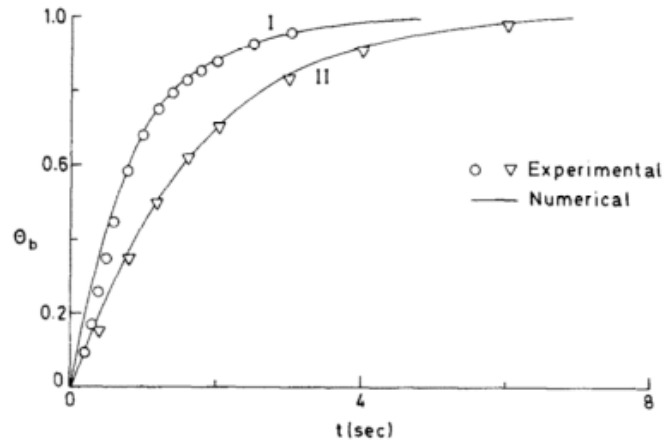


Figure 2-3. Distribution of drop bulk temperature with time [33].

In addition, they found that for a given droplet size, change in cone angle of the spray does not have any significant effect on the enhancement of the dimensionless bulk temperature.

Droplet non-dimensional radius is also predicted and plotted (Figure 2-5). Due to condensation of vapor on the surface of the droplet, droplet grows. This increase in size is found to be linear with temperature difference.

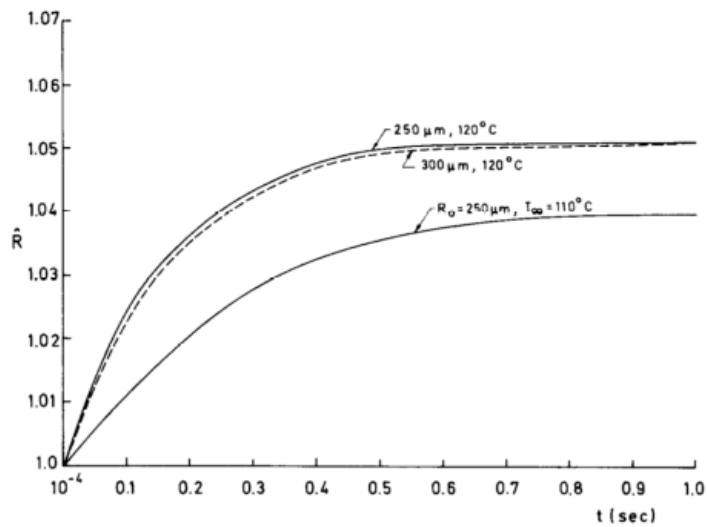


Figure 2-4. The drop growth rate [33].

Turkoglu et al. developed a three dimensional model to study the effect of droplet diameter and mass flow rate on the efficiency of the direct contact metal recovery condenser. They found that condensation rate enhances by increasing the liquid mass flow rate. They noticed that increasing the droplet diameter reduces the condensation efficiency. Their droplet diameters ranges are between 2 and 4 mm [34].

Lin et al. numerically studied the characteristics of spray cooling in a closed loop. A miniature nozzle array with eight nozzles is sprayed to the chamber in which nucleate boiling heat transfer, convection heat transfer, and evaporation phenomenon was observed. At heat fluxes lower than the critical heat flux presence of the non-condensable gas has reverse effect on heat transfer performance [35].

Shah et al. modelled the direct contact condensation of supersonic steam jet in water pool. They simulated the two phase flow problem by using Euler-Euler model in FLUENT 6.3 software. They found that increasing the water temperature leads to reduction of condensation rate. As the temperature difference of the water and the steam increases, the condensation rate enhances. In addition they concluded that the condensation heat transfer coefficients is in the range of 0.75- 0.917 MW.(m²K)-1 for water temperatures in the interval of 293 K and 343 K [36].

Shaver et al. computationally studied the fundamental physical phenomena governing steam-jet/water interaction. They studied two different models for investigating fluid flow and heat transfer in a high speed steam jet. One is a simplified theoretical model in two dimensions which is modeled in Lagrangian and Eulerian approach. The other one is a multidimensional computational multiphase fluid dynamics (CMFD) model. Their two dimensional model is able to explain the hydrodynamic behavior of the droplets where the condensation is neglected. Their model is able to predict the droplet trajectories and the condensation rate [37].

Alnaimat et al. developed a transient one dimensional model to analyze the heat and mass transfer through direct contact condensers and evaporators. In the heat and mass transfer model the inlet air, water temperature and humidity ratio calculated by variation of time. Experiments were conducted and used to validate the models [38].

Cui et al. numerically developed a method for heat and mass transfer incorporated with the volume of fluid surface tracking method in a two dimensional channel, including DCC and a distillation effect. They investigated the interfacial temperature and composition. While changing different parameters of boundary conditions interfacial latent heat and mass transfer are studied [39].

Lan et al. developed a mathematical model of droplet to investigate the vapor molecules condensing on the chilled surface in presence of non-condensable gas. By using homogeneous nucleation model their model was able to describe the effect of non-condensable gas presence and also the size of the clusters. They concluded that a small amount of non-condensable gas reduces the heat transfer rate [40].

3. PROBLEM DESCRIPTION

A two dimensional channel in which water is injected in a counter flow direction into air-water vapor mixture via a cone spray nozzle with a degree of 60 is considered. The height and the length of the channel are 6.5 cm and 128 cm, respectively. The height corresponds to the dimension of a washing-drying machine in Arçelik's product range. The hot and moist air is entering from the right side and the sub-cooled water is sprayed into the humid air through a nozzle located at (44.5 cm, 0 cm). The channel and water-spray nozzle configuration used in this study is shown in Figure 3-1. This geometry has been adopted for all simulations.

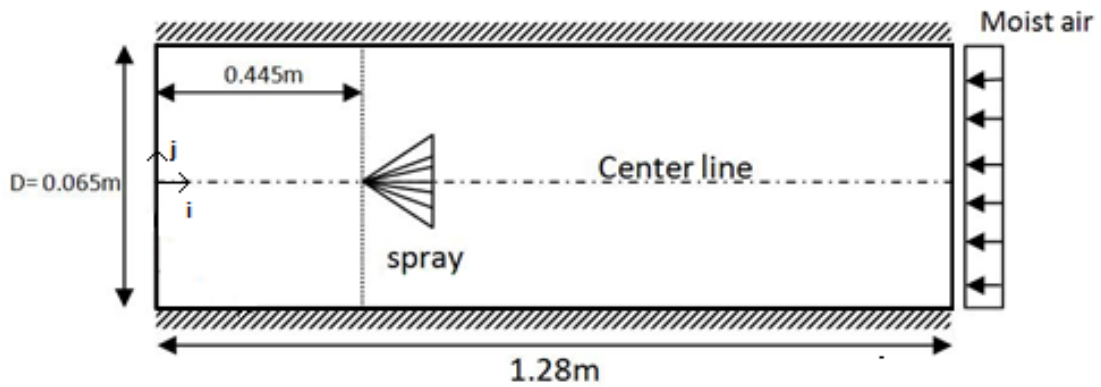


Figure 3-1. Schematic for the spray dryer.

3.1. Mathematical Model

This chapter discusses the equations which govern the heat and mass transfer between droplets and the air-vapor mixture. In the Lagrangian-Eulerian method the continuous phase (air-vapor mixture) is modelled using mass, momentum, energy, and species transport equations. The secondary phase (droplets) is solved by tracking a large number of particles into the solved continuous phase. These particles will have mass, momentum and energy exchange with the flow field. This method is available when the dispersed phase volume fraction is less than 10% [41]. In this case we can neglect the particle-particle interaction of droplets. During the flow field calculations at specific intervals, the particle trajectories of droplets are calculated.

In order to simulate the present study the following assumptions are accepted:

- ✓ Mixture (air and vapor) is considered as incompressible fluid.
- ✓ The gravitational force is neglected.
- ✓ Radiation heat transfer is neglected.
- ✓ Droplet rotation is neglected.
- ✓ Temperature inside the water droplet is considered as uniform. This assumption is accepted just for $Bi < 0.1$ [46].
- ✓ Pressure gradient and virtual mass forces are neglected.
- ✓ Droplet-Droplet interaction is neglected.

The governing equations for the continuous are as following:

3.1.1. Mass Conservation Equation

$$\frac{\partial u}{\partial x} + \frac{\partial v}{\partial y} = S_m \quad (3.1)$$

S_m is the mass source added to the continuous phase due to mass transfer between dispersed phase and gas-phase.

3.1.2. Momentum Transfer Equation

$$\rho \frac{\partial(uu)}{\partial x} + \rho \frac{\partial(uv)}{\partial y} = -\frac{\partial P}{\partial x} + \frac{\partial \tau_{xx}}{\partial x} + \frac{\partial \tau_{xy}}{\partial y} + F_x \quad (3.2)$$

$$\rho \frac{\partial(uv)}{\partial x} + \rho \frac{\partial(vv)}{\partial y} = -\frac{\partial P}{\partial y} + \frac{\partial \tau_{yx}}{\partial x} + \frac{\partial \tau_{yy}}{\partial y} + F_y \quad (3.3)$$

Here F represents the momentum source due to the interaction between the dispersed phase and the continuous phase.

3.1.3. Energy Equation

$$\rho \frac{\partial}{\partial x}(uE) + \rho \frac{\partial}{\partial y}(vE) = k \frac{\partial}{\partial x} \left(\frac{\partial T}{\partial x} \right) + k \frac{\partial}{\partial y} \left(\frac{\partial T}{\partial y} \right) + S_h \quad (3.4)$$

S_h is the energy source term due to droplets in the continuous phase.

3.1.4. Turbulence Model

Since the Reynolds number is 68200, the flow in the channel is turbulent. For this reason k - ε turbulence model is used to simulate the turbulence. However it should be mentioned that the renormalization group (RNG) method of the k - ε model has been randomly consulted for different cases and results were in good agreement with this model.

3.1.5. Equation of Motion for Droplets

The trajectories are solved by integrating the equation of the motion of the droplets.

$$\frac{d\vec{u}_p}{dt} = F_D(\vec{u} - \vec{u}_p) + \vec{F} \quad (3.5)$$

The first term in right hand side of the equation (3.5) represents the drag force per unit droplet mass. The second term is the additional force term which is neglected in this investigation. The pressure force, unsteady forces, virtual mass and Basset terms are in the order of the air/droplet density which is approximately 10^{-3} . For this reason they could be neglected [56].

$$F_D = \frac{18\mu C_D \text{Re}}{24\rho_p d_p^2} \quad (3.6)$$

Where,

\vec{u} = continuous phase velocity

\vec{u}_p = particle velocity

μ = molecular viscosity of the continuous phase fluid

ρ = density of the continuous phase fluid

ρ_p = density of the particle

d_p = diameter of the particle

Reynolds number is defined as

$$\text{Re} = \rho_{\infty} |u_{\infty} - V| d / \mu_{\infty} \quad (3.7)$$

In order to compute the drag coefficient the following equation is used:

$$C_D = a_1 + \frac{a_2}{\text{Re}} + \frac{a_3}{\text{Re}^2} \quad (3.8)$$

Here, a_1 , a_2 , a_3 are constants given by Morsi and Alexander [42].

3.1.6. Species Transport Equations

$$\frac{\partial}{\partial t} (\rho Y_i) + \nabla \cdot (\rho \vec{v} Y_i) = -\nabla \cdot \vec{J}_i + R_i + S_i \quad (3.9)$$

$$\vec{J}_i = -(\rho D_{i,m} + \frac{\mu_t}{Sc_t}) \nabla Y_i - D_{T,i} \frac{\nabla T}{T} \quad (3.10)$$

Where,

$D_{i,m}$ = Diffusion coefficient for species i in the mixture

$D_{T,i}$ = Thermal diffusion coefficient

Sc_t = Turbulent Schmidt number

J_i = Diffusion flux of species i

R_i = Net rate of production of species i

S_i = Source term for component i

Y_i = Mass fraction of the species i

The continuous phase mixture consists of air and vapor.

3.1.7. Heat and Mass Transfer Mechanism

DPM (Discrete Phase Model) approach of ANSYS Fluent 14.5 can model the particle motion and its heat and mass transfer effect on the mixture. In order to formulate the heat transfer mechanism, the heat balance equation of a droplet is considered.

$$m_p c_p \frac{dT_p}{dt} = hA_p (T_\infty - T_p) + \varepsilon_p A_p \sigma (\theta_R^4 - T_p^4) + \frac{dm_p}{dt} h_{fg} \quad (3.11)$$

Where,

m_p = mass of the droplet (kg)

c_p = heat capacity of the droplet (J/kg-K)

A_p = surface area of the droplet (m²)

T_∞ = local temperature of the continuous phase (K)

h = convective heat transfer coefficient (W/m²-K)

θ_R = radiation temperature, $(\frac{G}{4\sigma})^{1/4}$

h_{fg} = Latent heat of water

Second term in the right hand side represents the radiation heat transfer which is neglected in this calculation.

By using Ranz and Marshall [43] correlation for heat transfer coefficient, Nusselt Number is expressed as following:

$$Nu = \frac{hd_p}{k_\infty} = 2.0 + 0.6 Re_d^{1/2} Pr^{1/3} \quad (3.12)$$

Where

d_p = particle diameter (m)

k_∞ = thermal conductivity of the mixture (W/m-K)

Re_d = Reynolds number of the droplet

Pr = Prandtl number of the mixture

3.1.7.1. Evaporation Model

In order to simulate evaporation, convection-diffusion model is utilized. When the effect of the evaporating water droplet on the gas phase becomes stronger convection term should be considered.

ANSYS Fluent uses the following equations to calculate the mass transfer which are adopted from Miller [44] and Sazhin [45]:

$$\frac{dm_p}{dt} = k_c A_p \rho_\infty \ln(1 + B_m) \quad (3.13)$$

Where,

m_p = droplet mass (kg)

k_c = mass transfer coefficient (m/s)

A_p = droplet surface area (m²)

ρ_∞ = density of the continuous phase (kg/m³)

B_m in equation 3.13 is Spalding mass number.

$$B_m = \frac{Y_{i,s} - Y_{i,\infty}}{1 - Y_{i,s}} \quad (3.14)$$

In this equation $Y_{i,s}$ is the vapor mass fraction at the surface and $Y_{i,\infty}$ is the vapor mass fraction in the air-vapor mixture.

3.1.7.2. Condensation Model

In order to simulate the steam condensation on water droplets a user-defined function is implemented to ANSYS Fluent 14.5 software [64]. When the relative humidity of the mixture exceeds 100 %, steam starts to condense on water surface. For this reason, mass and diameter of the droplets increase. By using this code a mass source is added to the droplet due to condensation of vapor on it. In addition an energy source is adjusted depending on the latent heat of condensation and the amount of

mass source. The following equations (3.15 and 3.17) depict the mass and energy sources which are added to the continuity and energy equations. It should be mentioned that the momentum source is added to the continuous phase by Discrete Phase Model itself.

$$\dot{m}_p = (\text{condensation factor})\sqrt{A}\left(\frac{RH}{100} - 1\right) \quad (3.15)$$

$$m_p = m_{p0} + \dot{m}_p \quad (3.16)$$

$$S_h = \dot{m}_p h_{fg} \quad (3.17)$$

Equation 3.15 calculates the mass source to the continuous phase which is recommended by ANSYS Fluent UDF Manual [64]. Here, A is the droplet area and RH is the relative humidity of the air-vapor mixture. It is obvious that for the case in which condensation occurs the mass source will be positive. This means that steam condensation on water surface increases mass of the water droplet. The condensation factor in equation 3.15 is recommended to be 1e-4 [64]. Droplet mass is calculated by equation 3.16. In this equation, m_{p0} is the initial droplet mass and \dot{m}_p is the rate of condensation. It should be mentioned that latent heat is calculated depending on the temperature.

When condensation of the steam on water droplet takes place, the droplet diameter is calculated by using the following equation:

$$d_p = \left(\frac{6m_p}{\rho_p \pi}\right)^{1/3} \quad (3.18)$$

During condensation the droplet mass increases, accordingly the droplet diameter enhance.

3.1.8. Integration of Particle Motion Equation

By using stepwise integration over discrete time steps, particle trajectories and heat and mass transfer to/from droplet is solved. Integrating the equation 3.5 yields to find the particle velocity along each point in the trajectory [41]. In addition, the trajectories can be predicted by equation 3.19. Equation 3.5 could be written as equation 3.20, and discretizing it in trapezoidal method yields to equation 3.21.

$$u_p = \frac{dx}{dt} \quad (3.19)$$

$$\frac{du_p}{dt} = \frac{1}{\tau_p}(u - u_p) \quad (3.20)$$

$$u_p^{n+1} = \frac{u_p^n (1 - \frac{1}{2} \frac{\Delta t}{\tau_p}) + \frac{\Delta t}{\tau_p} (u^n + \frac{1}{2} \Delta t u_p^n \cdot \nabla u^n)}{1 + \frac{1}{2} \frac{\Delta t}{\tau_p}} \quad (3.21)$$

It should be mentioned that equation 3.19 and 3.5 are coupled ordinary differential equations. Locations of the droplets are predicted by discretizing equation 3.19 in implicit and the trapezoidal scheme.

$$x_p^{n+1} = x_p^n + \frac{1}{2} \Delta t (u_p^n + u_p^{n+1}) \quad (3.22)$$

3.1.9. Turbulent Dispersion of Particles

In order to implement the effect of the turbulence of the mainstream flow, instantaneous fluid velocity is utilized in trajectory equation. Instantaneous value of the fluid velocity is:

$$u = \bar{u} + u' \quad (3.23)$$

The Discrete Random Walk model is used to model the instantaneous gas velocity. In this model fluctuating part of the velocity is assumed to be constant linear function

of time. This model which is also famous as Eddy-Lifetime model simulates the interaction of continuous phase turbulent eddies with particles [41].

3.2. Boundary Conditions

In this section of the thesis boundary conditions are discussed. Boundary conditions are generally divided into continuous phase and dispersed phase conditions.

3.2.1. Continuous Phase Boundary Conditions

The continuous phase consists of air-vapor mixture which enters from the right end and it interacts with the injected water droplets. Boundary conditions of the mainstream flow are strongly affecting the calculations. These conditions include the mixture temperature, relative humidity, and velocity. The mixture temperature, velocity and relative humidity are presented in Table 3-1. These values correspond to a Reynolds number of 68200.

Table 3-1. Inlet boundary conditions of the continuous phase.

RH(%)	Temperature (K)	Velocity (m/s)	Mass Flow Rate (kg/s)
90	348	10	0.57

3.2.2. Spray Initial Conditions

Spray initial conditions such as location of the spray, droplet diameter, droplet temperature, mass flow rate of the spray, and velocity of the injected droplets are significantly affecting the heat and mass transfer between two phases. In order to study the effect of these parameters on the dehumidification process, each time all parameters are kept constant and just one parameter is varied to check its effect on temperature, humidity, and relative humidity pattern of the mainstream flow.

3.2.3. Wall Boundary Conditions

No-slip boundary condition is considered for the wall. The “reflect” boundary condition is used for the discrete phase model. e_n is the restitution coefficient. In this study the restitution coefficient is taken as default which is the constant value of 1 for normal and tangent reflection factors [41]. This means all the normal and tangential momentum retains when the droplet hits the wall. Here 1 represents the condition before the collision of the droplet to the wall and 2 represents the condition after the collision of the droplet to the wall.

$$e_n = \frac{v_{2,n}}{v_{1,n}} \quad (3.24)$$

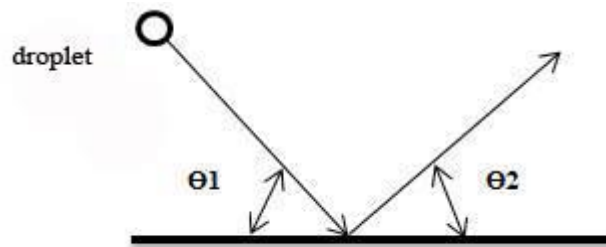


Figure 3-2. "Reflect" Boundary Condition for the Discrete Phase.

3.2.4. Outlet Boundary Conditions

Pressure-Outlet boundary condition is implemented for the channel outlet.

3.3. Numerical Model

This chapter discusses the numerical model which is used for this simulation.

3.3.1. Air-Vapor Mixture Model

In order to model the air-vapor mixture Species Transport model is used. ANSYS FLUENT 14.5 provides the species transport model which simulates the transport of the species by solving the diffusion and convection equations. By solving

convection-diffusion equations for each species FLUENT predicts the mass fraction of the species.

3.3.2. Solution Method

The pressure-velocity coupling is solved by using coupled scheme. In addition Pseudo transient method is utilized.

Momentum, Energy and species transport equations are discretized by using second order upwind approach to get more accurate results.

In order to be able to converge the problem, Discrete Phase Sources relaxation factors should be decreased to values like 0.1.

3.4. Material Properties

This section presents the properties of the continuous and dispersed phase. The properties of the water are listed in Table 3-2.

Table 3-2. Thermo-physical properties of the water (dispersed phase).

Property	Value	Unit
Density	998.2	Kg/m ³
Specific Heat	4182	J/Kg-K

Table 3-3. Thermo-physical properties of air.

Property	Value	Unit
Density	1.22	Kg/m ³
Specific Heat	1006.4	J/Kg-K
Thermal Conductivity	0.026	W/m-K

Table 3-3 describes the thermo-physical properties of the air. Water vapor pressure strongly depends on the temperature, for this reason, a piecewise linear function is used to predict it.

3.5. Grid Independency Analysis

In this investigation a computational mesh independency study has been carried out with square grids of 20 mm, 10 mm, 8 mm, and 7 mm. The grid evaluation aims to make sure that the physical result from numerical simulation is independent of the number of grid cells. It is seen that the results from the three sets of grids with sizes of 10 mm, 8mm, and 7mm coincide. Accordingly the structural grid size of 7 mm is chosen for the simulations. The grid used for this study is shown in figure 3-3. Figure 3-4 depicts the independency of the solution from the domain mesh. Velocity magnitudes at different locations of the centerline are checked and analyzed. Figure 3-5 illustrates the locations of the points in the chamber. Point number 1 represents the location of the $x = 44$ cm and $y = 0$ cm. Point number 2 demonstrates the location of $x = 0$ and $y = 0$ cm.

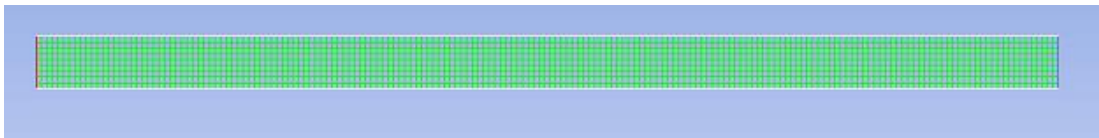


Figure 3-3. Grid in the channel.

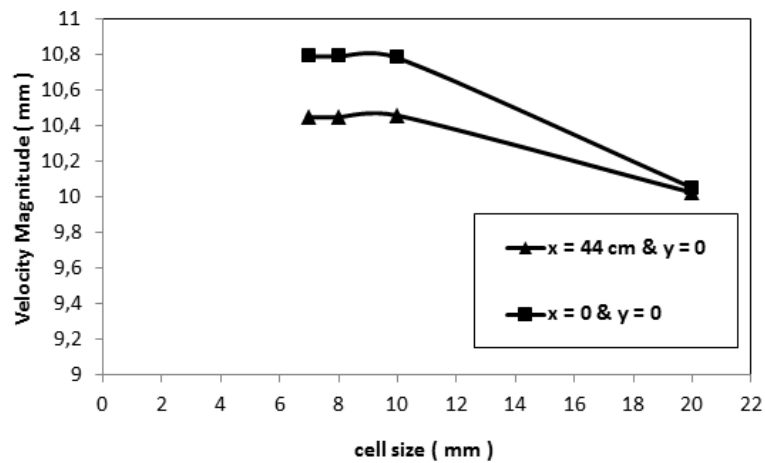


Figure 3-4. Grid independence test.

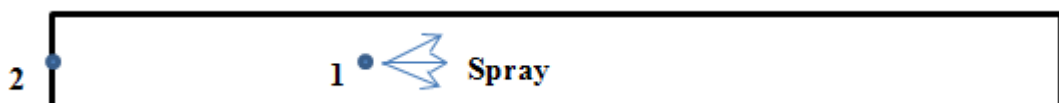


Figure 3-5. Location of the mesh study cases.

4. TWO DIMENSIONAL ANALYSIS

This section presents the predictions of the present numerical investigations. First a validation study is performed. A parametric study on the effect of different parameters on pattern of humidity, relative humidity, temperature distribution and other flow variables is studied, next.

4.1. A Base Case Study

Validation of the results with available experimental or analytical data is necessary to ensure that results are reliable to optimize the effect of different parameters on spray dehumidification process.

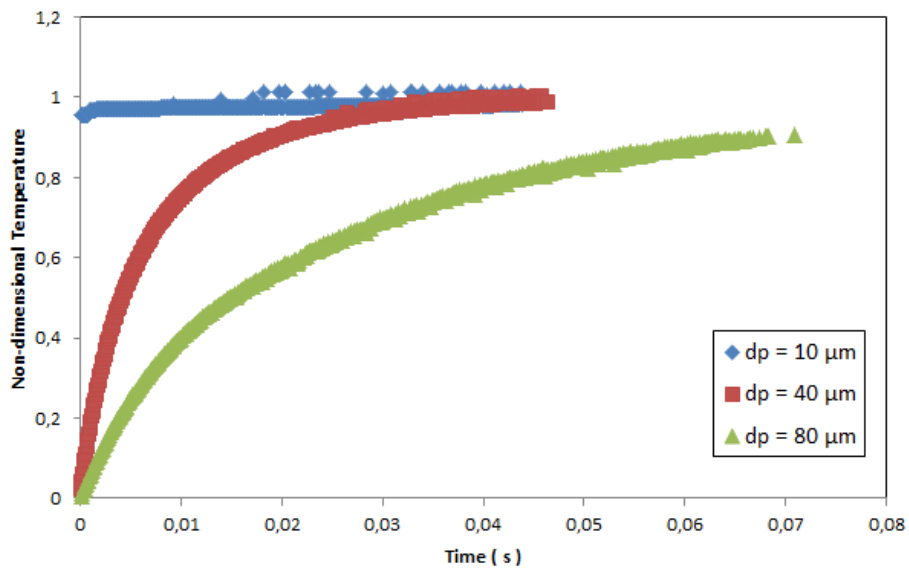


Figure 4-1. Non-dimensional droplet temperature vs time.

Figure 4-1 illustrates the variation of non-dimensional droplet temperature with time. Various droplet diameters are compared in figure 4-1. In each case spray initial conditions are kept fixed and they are summarized in table 4-1.

Table 4-1. Spray initial conditions.

Spray Temperature (K)	Spray Cone Angle	Spray Mass Flow Rate (gr/s)
288	60	3

The droplet temperature is increasing with time. It is found that by reducing the droplet diameter, droplet temperature quickly enhances to values close to the saturation temperature. The temperature of the larger droplets grows slower since they are bigger. In addition, when the droplet diameter is larger, its residence time larger.

These results qualitatively compare well with the results of Celata et al.[10], Mayinger et al.[7], and Takahashi et al.[47] obtained for similar direct contact condensation problem. Figure 4-2 and 4-3 illustrate the non-dimensional droplet temperature found by Celata and Myinger, respectively.

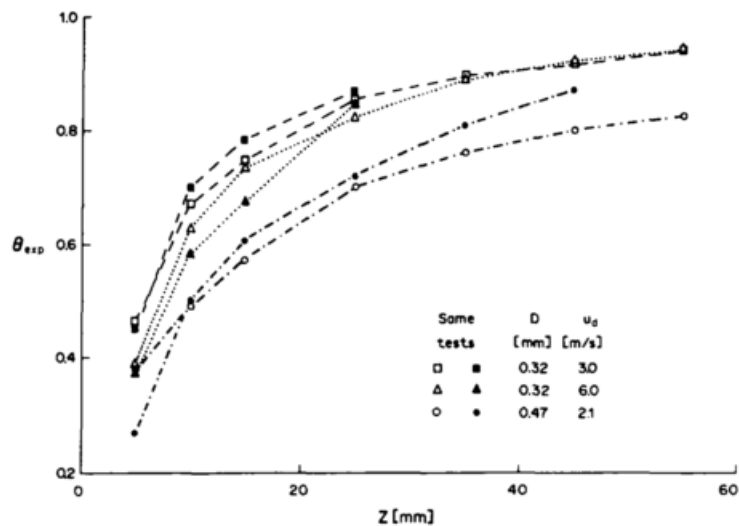


Figure 4-2. Droplet non-dimensional temperature [10].

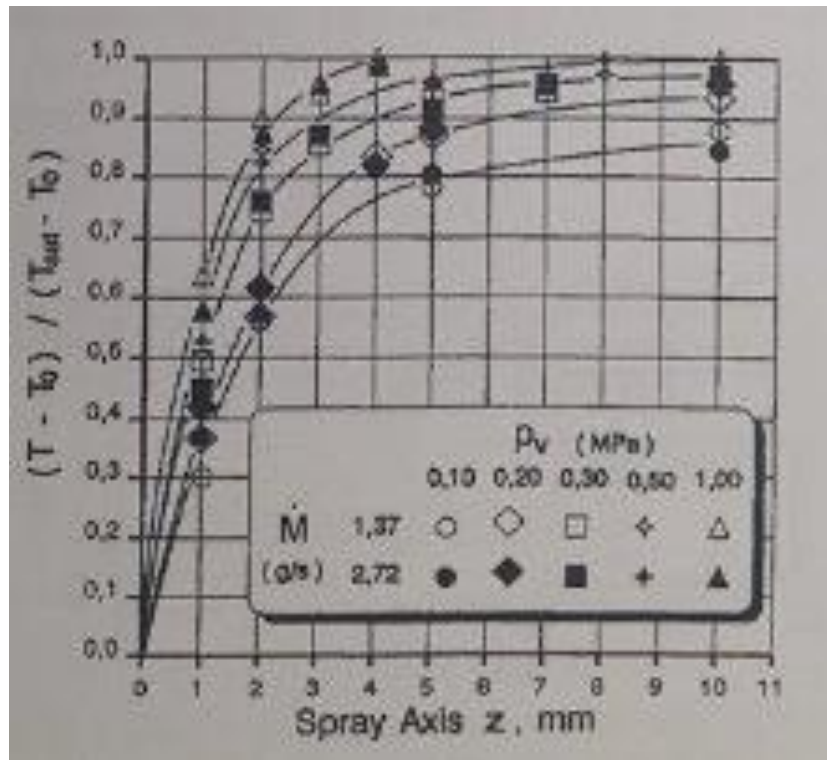


Figure 4-3. Droplet non-dimensional temperature [7].

Due to high turbulence and interaction between continuous phase and the dispersed phase violent condensation occurs and the droplet temperature approaches to saturation temperature of the steam. The droplet non-dimensional temperature which is also called as condensation efficiency is defined as following:

$$\theta = \frac{T_d - T_{w0}}{T_s - T_{w0}} \quad (4.1)$$

In this equation T_d is the droplet temperature at time t and T_s is the saturated steam temperature; T_{w0} is the droplet initial temperature [10].

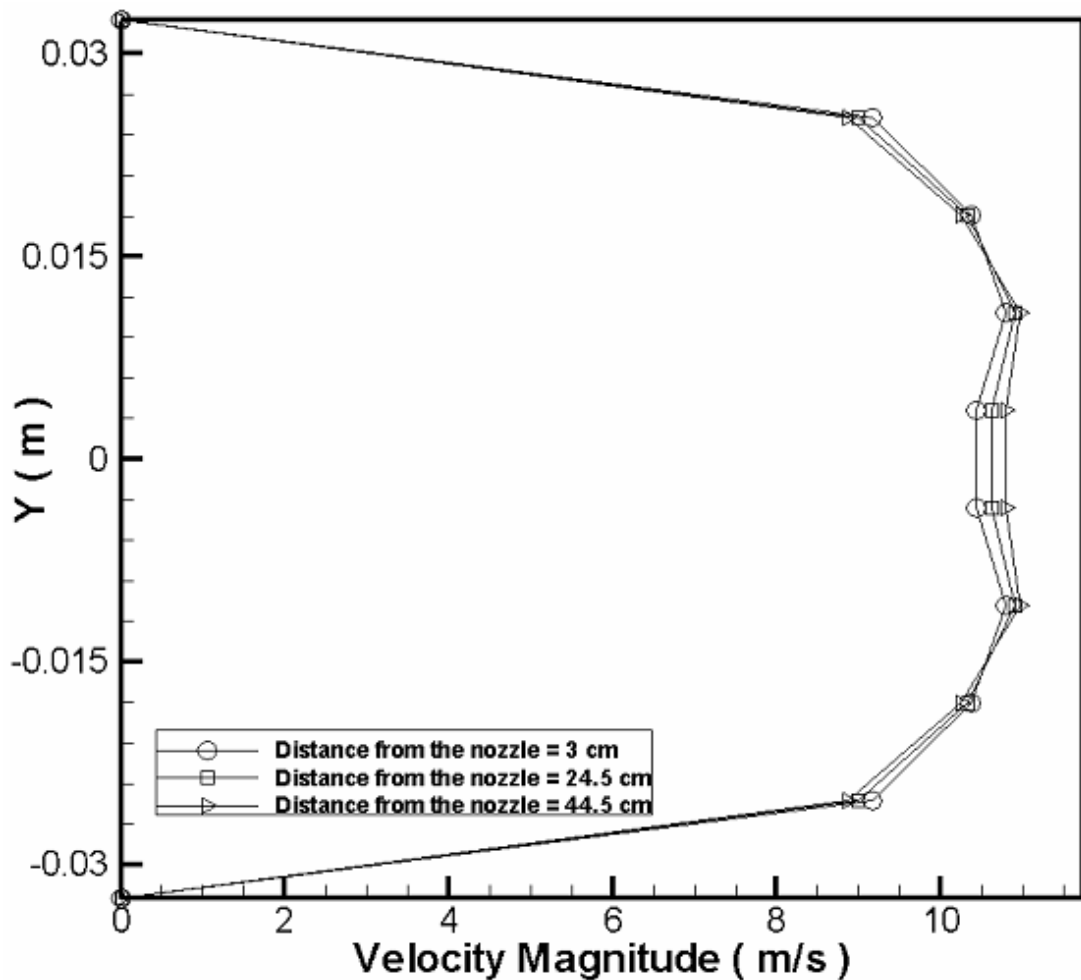


Figure 4-4. Velocity magnitude distribution at different horizontal distances from nozzle.

Figure 4-4 depicts the distribution of the velocity magnitude at different horizontal distances from the nozzle in the downstream direction. Since the spray and air-vapor mixture are in contrary direction to each other, at regions close to the spray velocity of the mixture is slightly less compared to regions far from the nozzle in the downstream direction. The momentum of the air-vapor mixture is very large, for this reason spray droplets could not change the mainstream velocity profile noticeably. There is a slight velocity reduction at the central core of the chamber due to presence of the spray.

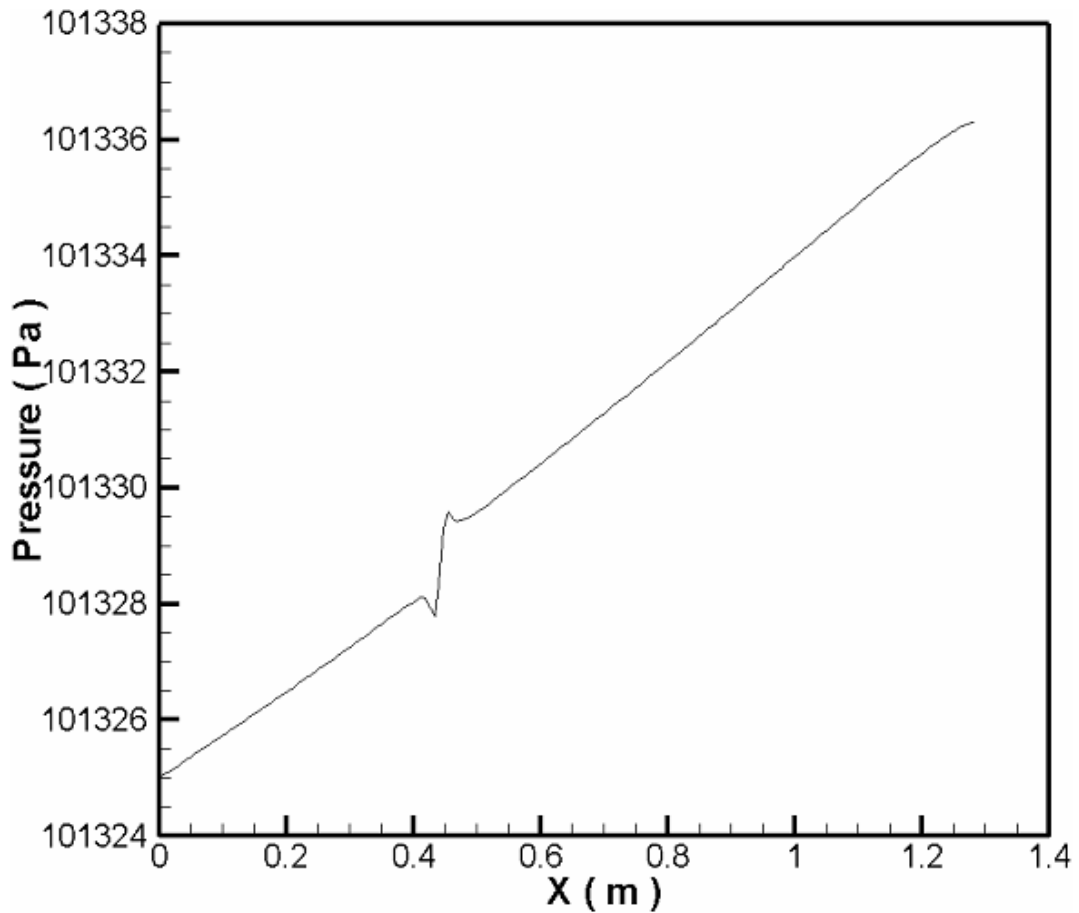


Figure 4-5. Pressure distribution along the horizontal centerline.

Figure 4-5 depicts the pressure distribution on the horizontal centerline of the channel. Figure 4-6 illustrates the effect of gravity on the droplet velocity. The effect of gravity should be included in the right hand side of the equation (3.5). However Figure 4-6 indicates that gravity does not affect the droplet velocity. Because of the large momentum of the air-vapor mixture, gravity does not affect the trajectories of the droplets. In addition, droplets immediately change their direction and flow to the same direction with the air-vapor mixture. Consequently effect of gravity on the simulations could be neglected.

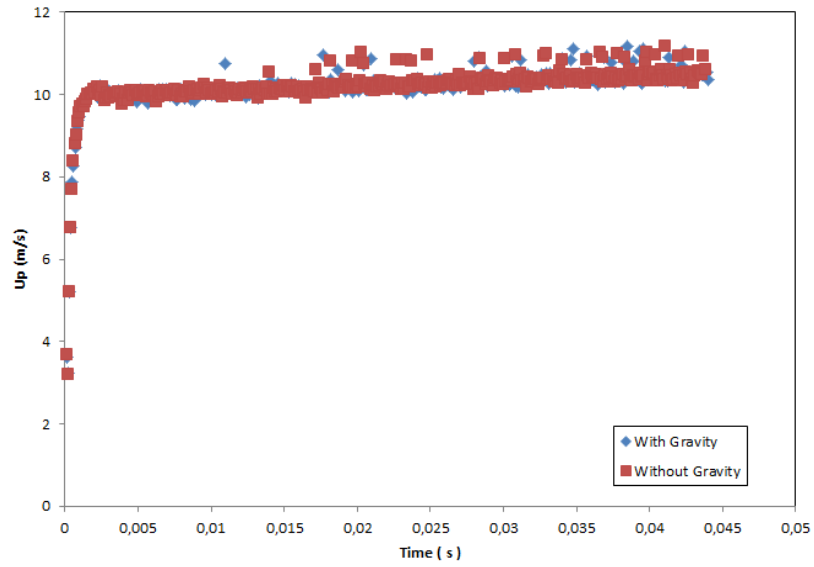


Figure 4-6. Effect of gravity on droplet velocity distribution.

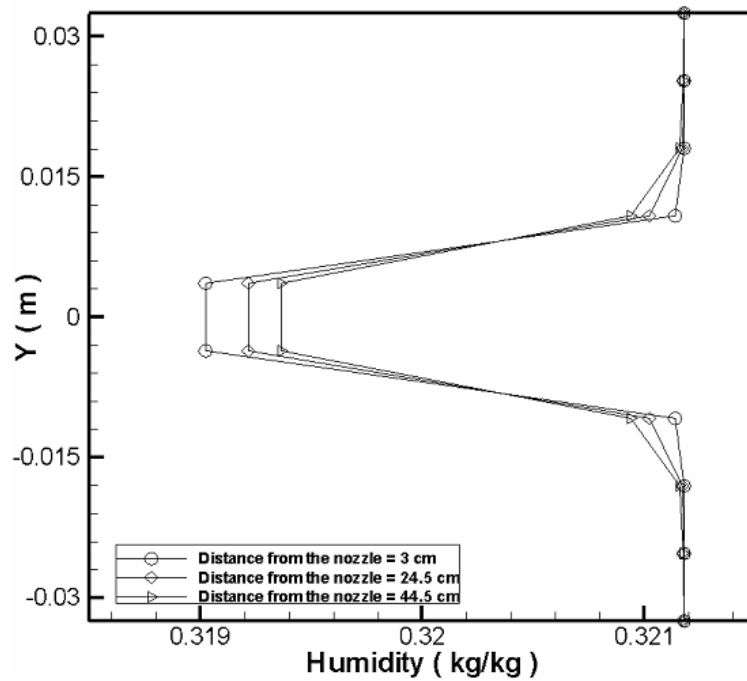


Figure 4-7. Humidity distribution at different horizontal distances from the nozzle.

This section shortly discusses the effect of chilled-water spray on relative humidity, temperature, and humidity distribution of the continuous phase. In this part the distributions of various parameters are illustrated for the case with the mass flow rate of 3gr/s, water temperature of 288 K, spray cone angle of 60° and droplet diameter of

10 μm . Figure 4-7 depicts the humidity pattern at different distances from the nozzle. It is illustrated that there is a remarkable humidity reduction close to the nozzle. For the locations far from the nozzle humidity reduction is less noticeable. The results show that at distances close to the nozzle, condensation rate is higher than distances far from the nozzle. At 3cm from the nozzle drastic reduction of humidity indicates a large amount of condensation taking place right after the nozzle.

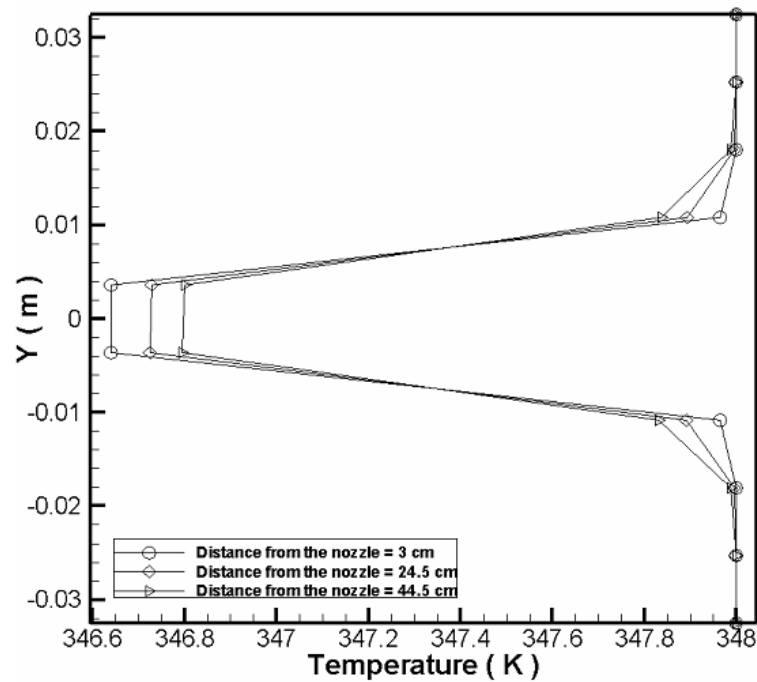


Figure 4-8. Temperature distribution at different horizontal distances from the nozzle.

Figure 4-8 illustrates the temperature distribution at different horizontal distances from the nozzle at downstream direction. Due to presence of the spray in the channel centerline, the highest temperature reduction takes place in this region. Figure 4-8 depicts that close to the nozzle temperature reduction is higher compared to regions far from the nozzle in the downstream direction.

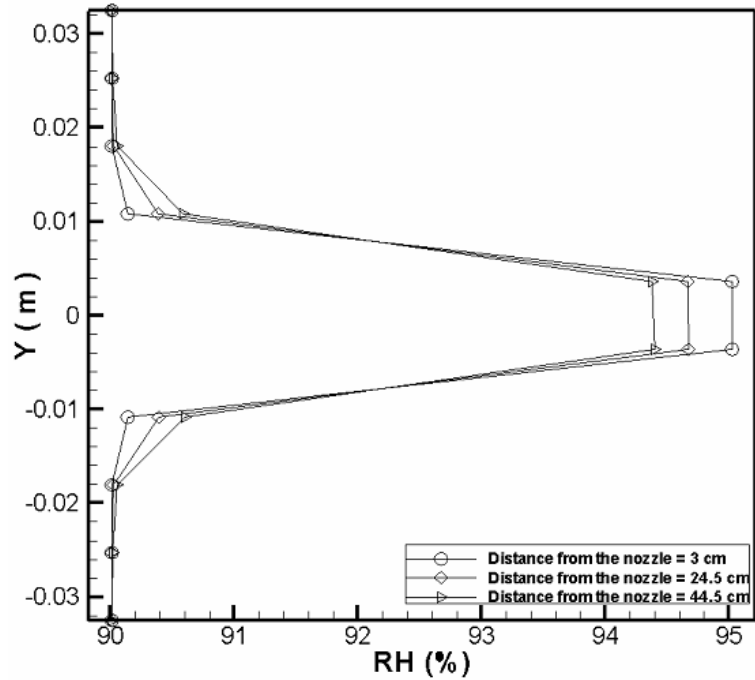


Figure 4-9. Relative humidity distribution at different distances from the nozzle.

Figure 4-9 depicts the relative humidity distribution at different distances from the nozzle. Due to sensible heat cooling relative humidity of the mixture enhances [48]. It is shown that relative humidity before the injection was 90 % and after the injection it is increased due to decrease in temperature. Decrease in temperature reduces the vapor carrying capacity of the air to contain vapor. It is observed that relative humidity enhancement rate right after the nozzle is higher than regions far from the nozzle in the downstream direction.

4.1.1. Evaporation and Condensation Mechanism

Since water droplets absorb the sensible heat of the mixture, surrounding air temperature decreases. During the sensible cooling process the moisture content is constant and dry-bulb temperature of the air is decreased. At the same time when the vapor pressure at the surface of the water is greater than that of the surrounding mixture, evaporation will take place. Latent heat of evaporation which is the energy required to change the phase of the water droplet (liquid) to water vapor (gas) will reduce the surrounding air temperature [48].

When the continuous phase temperature reaches the dew point, condensation of steam on water droplets takes place [49]. This process involves not only sensible heat cooling, but also latent heat release due to condensation [50]. When the air is cooled sufficiently that its temperature is lower than the dew point normally condensation happens. The latent heat of condensation of steam will be released to its surrounding (air and droplet) and this heat will decrease the normal reduction of the temperature due to cooling [51]. Normally when there is no condensation happening, the droplet and the mixture temperature decreases more, but due to increase in the temperature of the air and the droplet this reduction in temperature is reduced. It should be mentioned that the sensible cooling is dominant compared to latent heat warming. This means that the overall temperature of the mixture reduces. Because of the condensation of the steam on water droplets temperature and moisture content of the mixture reduces [52, 53]. After this step that the mixture temperature is reduced to lower temperatures, dehumidification is usually done at the same time as the sensible cooling process at the droplet surface [54, 55]. Figure 4-10 sketches dehumidification and cooling process in a psychrometric chart.

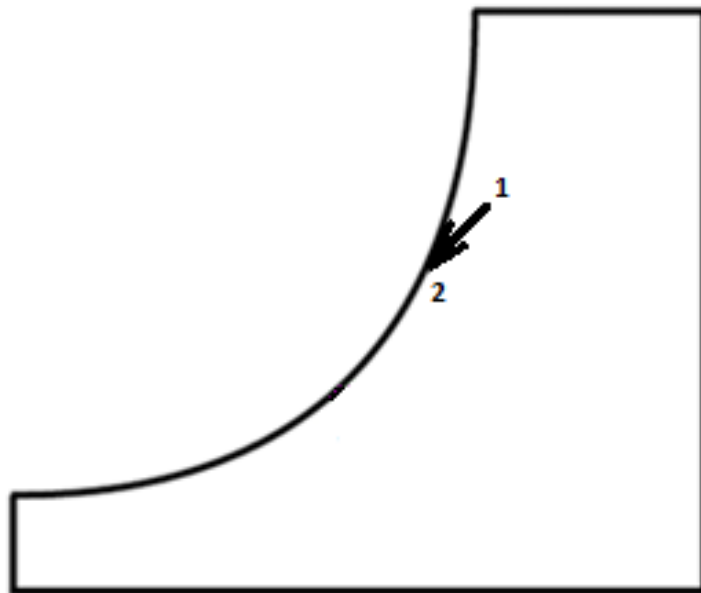


Figure 4-10. Dehumidification and cooling process.

4.2. Parametric Study

This section presents the results of the parametric study of the spray dehumidification process. This investigation studies the effect of different parameters on flow pattern after the spray. It is vital to figure out how different characteristics of spray affect the channel. In each study all parameters are kept constant and just one parameter is altered to check its effect on temperature, humidity, and relative humidity pattern of the mainstream flow. Table 4-2 summarizes various spray conditions which are studied.

Table 4-2. Initial conditions of the injection.

Droplet Diameter (μm)	10	15	30	40	80
Spray Mass Flow Rate (gr/s)	3	4	6	-	-
Droplet Temperature (K)	288	313	323	330	-
Spray Cone Angle	18	45	60	90	120
Number of Injections	1	2	3	4	-
Location of the Spray (cm)	44.5	80	120	-	-

4.2.1. Effect of Droplet Diameter

Droplet diameter is one of the most important characteristics of the spray which can directly affect the heat and mass transfer. In this section effect of droplet diameter on dehumidification process is discussed. Accordingly sprays with different droplet diameters of 10 μm , 15 μm , 30 μm , 40 μm , 60 μm , and 80 μm are considered to analyze the effect of drop diameter on temperature, humidity, and relative humidity profiles. The reason of analyzing this vast range of droplet diameter is to include large and small droplets at the same study.

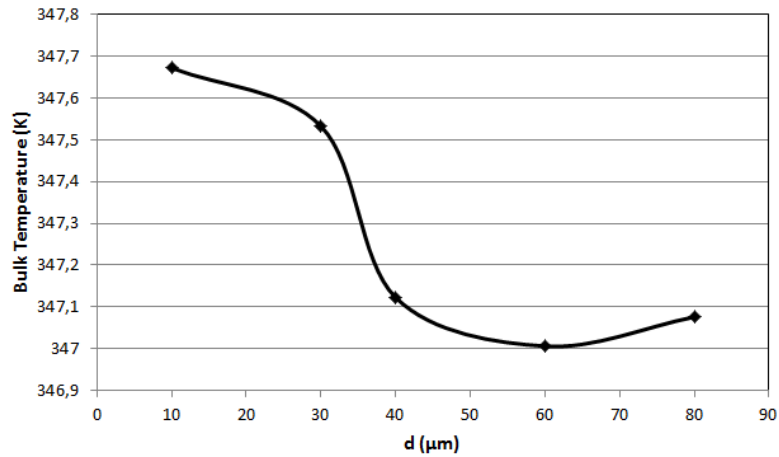


Figure 4-11. Effect of droplet diameter on gas-phase bulk temperature at the outlet.

Figure 4-11 illustrates the effect of droplet diameter on the gas-phase bulk temperature at the outlet. It is found that initially gas-phase bulk temperature decreases by increasing the droplet diameter. After reaching the droplet optimum size, temperature reduction rate decreases by increasing the droplet diameter which means heat transfer is decreased. There is an optimum droplet diameter for maximum heat transfer. As droplet size increases the heat transfer enhances. After a specific droplet size heat transfer starts to decrease by increase in droplet size [21].

Most of the studies in the literature include large droplets. Most of these investigations concluded that enhancement of droplet diameter leads to heat transfer reduction. In fact, they have studied the effect of particle size on heat transfer for droplets larger than the optimum size. In this region droplet diameter has reverse effect on heat transfer which means by enhancing the droplet diameter heat transfer decreases. In order to determine the optimum diameter, droplet diameter is varied from 10 μm to 80 μm. Chen et al. [57] studied the effect of droplet diameter on heat transfer while keeping other parameters constant. In their study droplets were varied in the range of 62 μm and 190 μm. They concluded that droplet diameter does not have any effect on the heat transfer. This could be due to the large droplets which they used in their investigations. However, Sarkar [58] studied the effect of droplet diameter on heat transfer (Figure 4-12). Droplet diameters varied in vicinity of 7 μm and 40.49 μm. It was found that heat transfer initially increased and after reaching an

optimum droplet size heat transfer started to decrease. In this study the same effect is concluded.

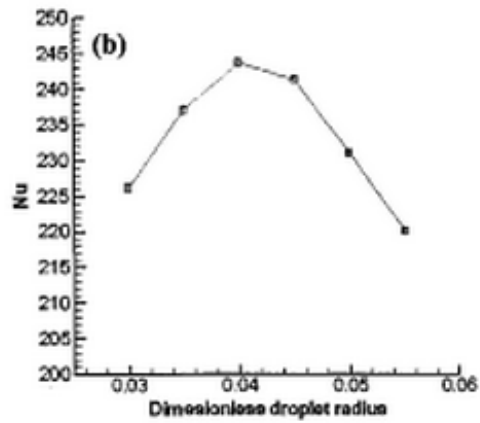


Figure 4-12. Nu variation with droplet radius [58].

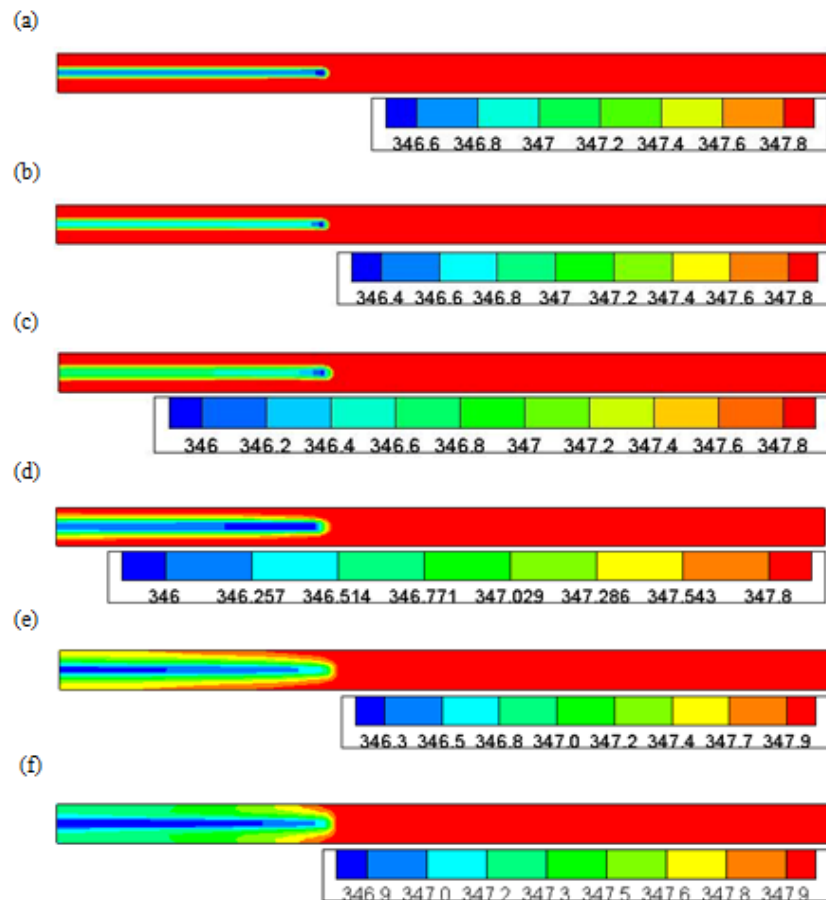


Figure 4-13. Temperature contours for different droplet diameters, (a) $d_p = 10 \mu\text{m}$, (b) $d_p = 15 \mu\text{m}$, (c) $d_p = 30 \mu\text{m}$, (d) $d_p = 40 \mu\text{m}$, (e) $d_p = 60 \mu\text{m}$, (f) $d_p = 80 \mu\text{m}$.

Figure 4-13 illustrates the effect of droplet diameter on the air-vapor mixture temperature. It is found that large momentum of the coming air-vapor mixture does not let the droplets penetrate in the flow field and droplets are forced to move back to the outlet. It is observed that temperature values in regions close to the nozzle are lower. This is directly because of presence of sub-cooled water in this region.

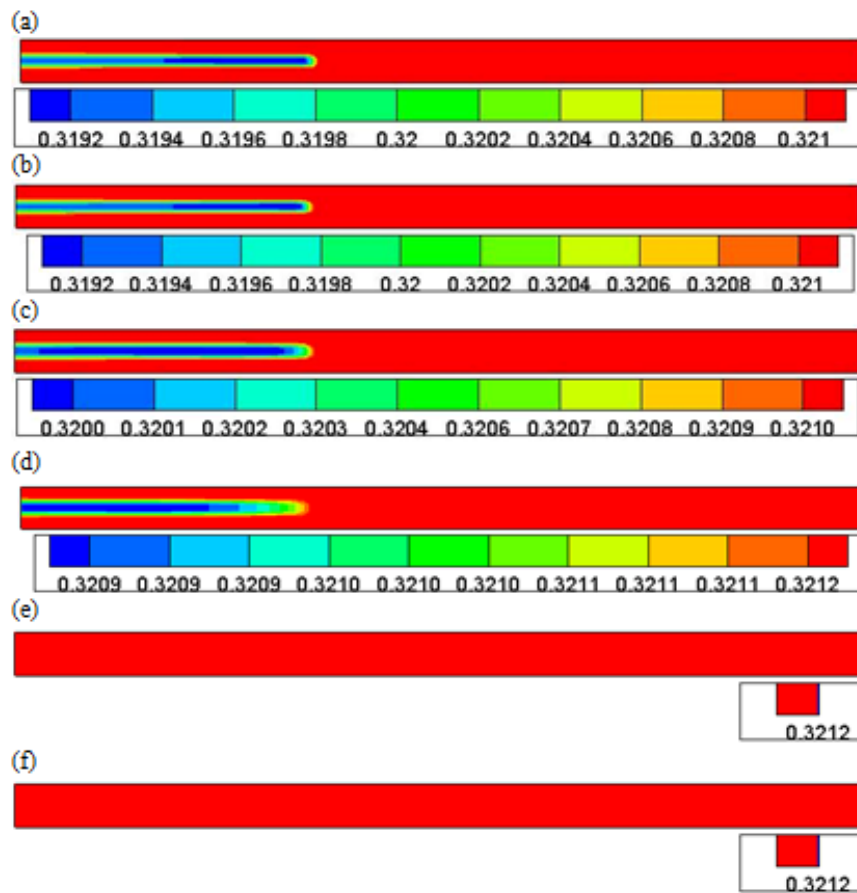


Figure 4-14. Humidity contours for different droplet diameters, (a) $d_p = 10 \mu\text{m}$, (b) $d_p = 15 \mu\text{m}$, (c) $d_p = 30 \mu\text{m}$, (d) $d_p = 40 \mu\text{m}$, (e) $d_p = 60 \mu\text{m}$, (f) $d_p = 80 \mu\text{m}$.

Figure 4-14 describes the effect of droplet diameter by showing humidity contours. Unlike the temperature, droplet diameter has different effect on humidity distribution. By reducing the droplet diameter humidity decreases more. It means that the moisture content of the mixture is reduced. Large droplets like $60 \mu\text{m}$ and $80 \mu\text{m}$ does not have humidity reduction [56]. There is no condensation happening on these larger droplets. For this reason when spray cooling without any condensation is the goal, larger droplets are better [56]. During condensation, steam releases the latent

heat of condensation to the surrounding which does not let the surrounding air to cool better.

4.2.1.1. Effect of Droplet Size on Penetration

Droplet diameter strongly affects the penetration rate of the particle in the vertical direction. One of the objectives of this study is to spread the effect of dehumidification in the y direction at the outlet. Since the vapor-air mixture has a drastic momentum, the particles are not able to penetrate in the flow direction. Larger droplets can penetrate better in the y direction due to their larger momentum which is an advantage for larger droplets (Figure 4-16, Figure 4-17). On the other hand, bigger droplets do not effectively reduce the humidity of the chamber. Since reducing the moisture content of the mixture is the main goal of this study, smaller droplets are preferred even they just dehumidify the core center of the chamber. In order to resolve this drawback using two or more nozzles is suggested which will be discussed in chapter 4.2.5. The following figures depict the particle trajectories for different droplet diameters. Firstly the whole view of the channel is shown and under it just the region after the spray is demonstrated.

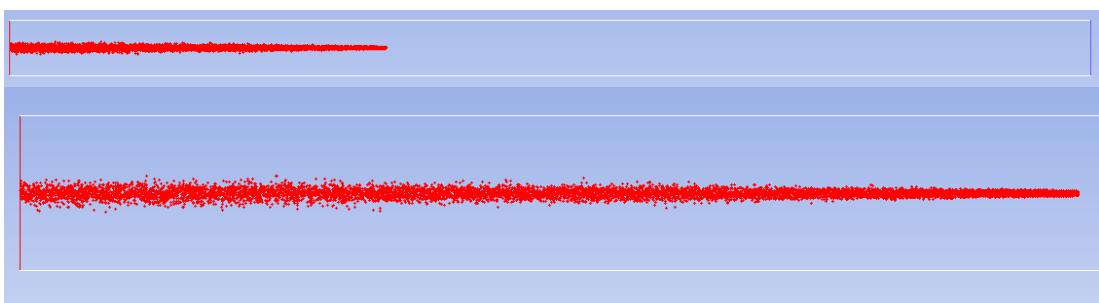


Figure 4-15. Particle trajectories for $d_p = 10 \mu\text{m}$ and mass flow rate = 3 gr/s.

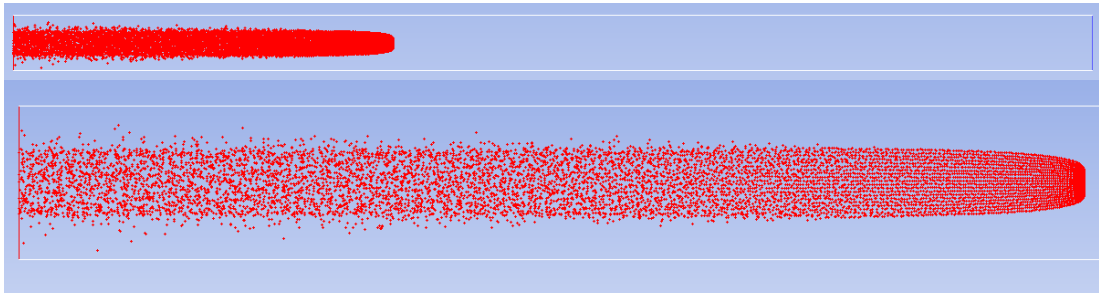


Figure 4-16. Particle trajectories for $d_p = 40 \mu\text{m}$ and mass flow rate = 3 gr/s.

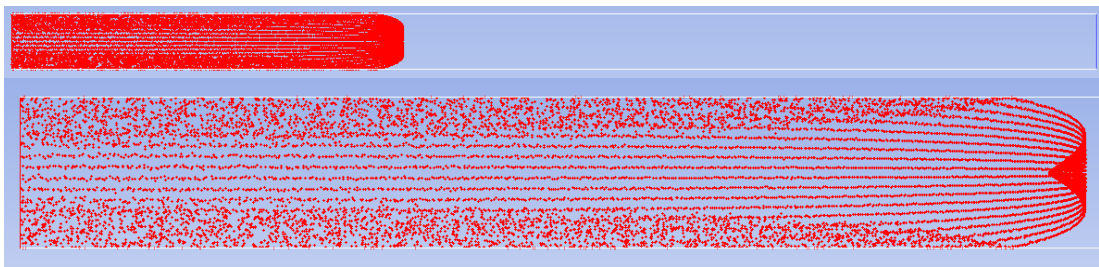


Figure 4-17. Particle trajectories for $d_p = 80 \mu\text{m}$ and mass flow rate = 3 gr/s.

4.2.1.2. Effect of the droplet diameter on flow pattern on the horizontal centerline

Effect of droplet diameter on heat transfer has always been a critical point in spray heat transfer studies. Figure 4-18 illustrates the relative humidity distribution along the centerline of the nozzle. Figure 4-18 depicts that at first relative humidity enhancement rate increases by increasing the droplet diameter. Later on by reaching to the optimum droplet diameter this procedure changes. After this step, increase in droplet diameter leads to reduction of the relative humidity enhancement.

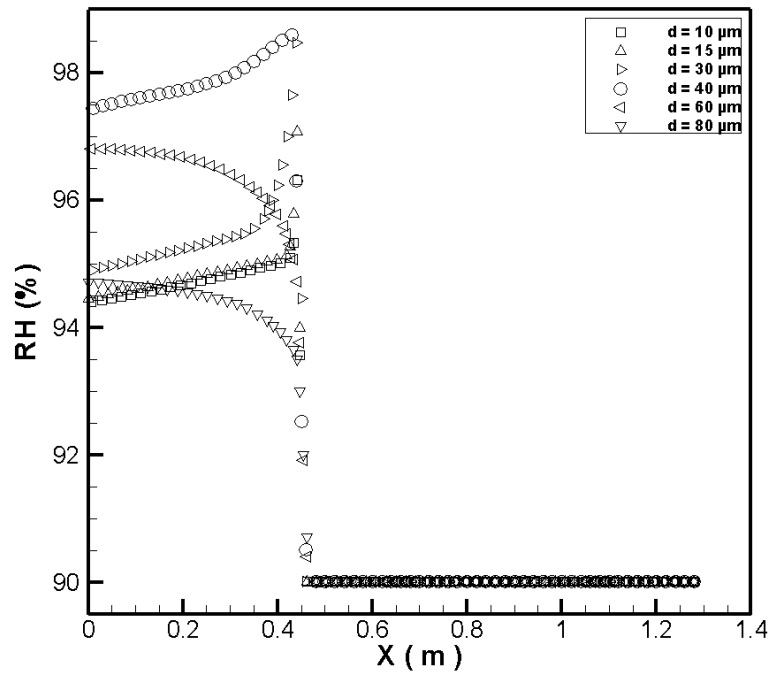


Figure 4-18. Effect of droplet diameter on relative humidity distribution on the horizontal centerline.

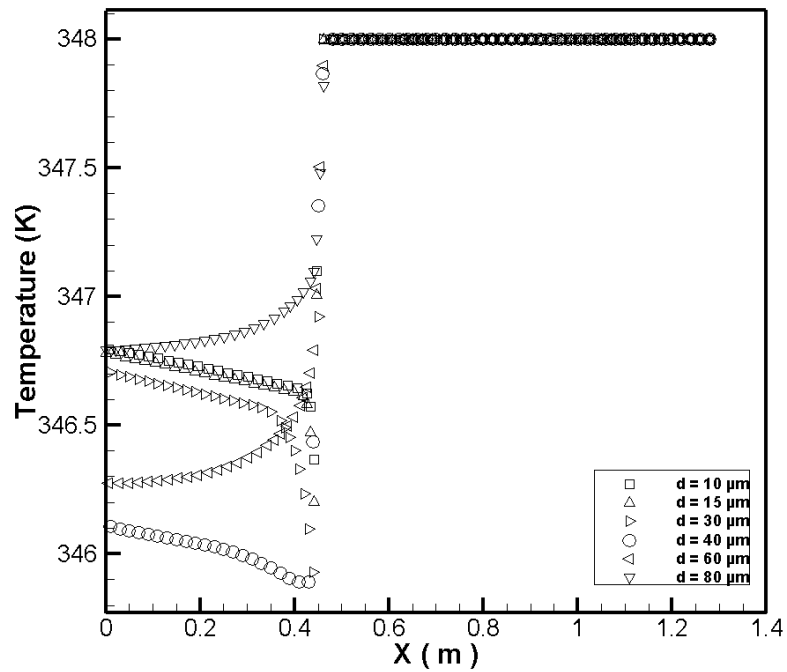


Figure 4-19. Effect of droplet diameter on temperature distribution on the horizontal centerline.

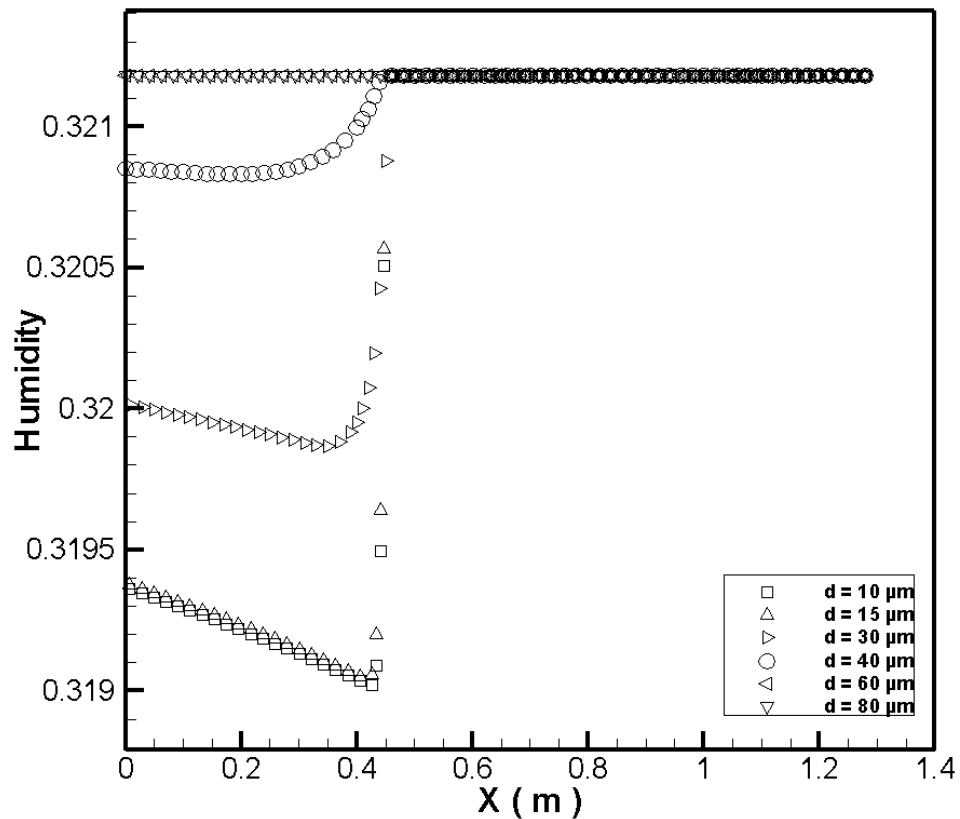


Figure 4-20. Effect of droplet diameter on humidity distribution on the horizontal centerline.

Figure 4-19 shows the effect of the droplet diameter on temperature pattern on the horizontal centerline. The temperature reduces more by increasing the droplet diameter until a specific value. If the diameter increases to values higher than the optimum diameter, temperature reduction decreases.

Figure 4-20 depicts the droplet size effect on humidity pattern in the channel. Smaller particles have higher condensation rate and as a result humidity reduces more. Spray with droplets of 10 μm causes the highest humidity abatement.

4.2.1.3. Effect of droplet diameter on flow pattern at the outlet cross section

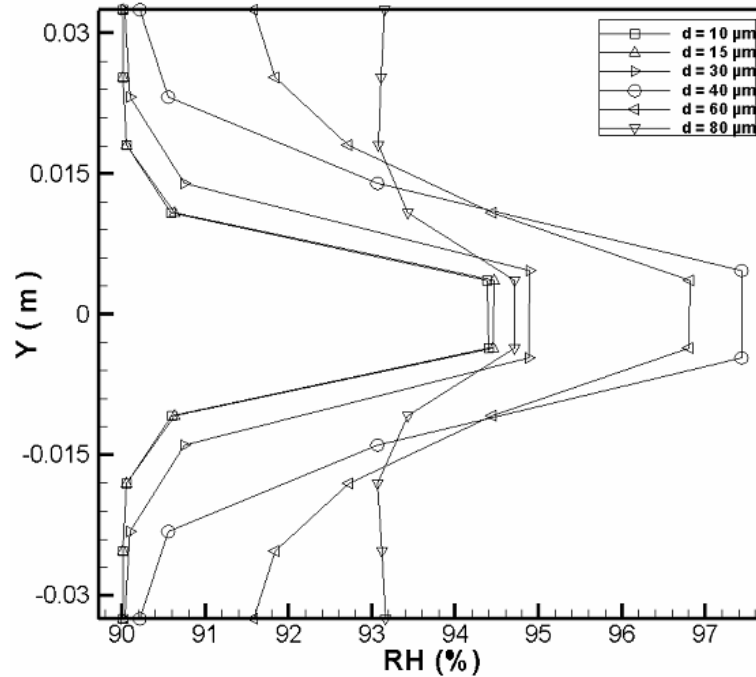


Figure 4-21. Effect of droplet diameter on relative humidity at the outlet.

Figure 4-21 describes the effect of droplet diameter on relative humidity distribution at the outlet cross section of the channel. Droplets with optimum diameter increase the relative humidity to its highest value.

Larger droplets radially penetrate in the chamber and decrease the temperature of the mixture at regions close to the wall too. Accordingly at regions close to the wall relative humidity is increased. On the other hand, smaller droplets could not penetrate to regions close to the wall to decrease the temperature. Therefore for cases with smaller droplets, relative humidity values close to the wall are approximately 90 %.

The same phenomenon is observed for gas-phase temperature distribution at the outlet which is depicted in Figure 4-22. Larger droplets reduce the temperature at parts close to the wall but temperature at the core center is not reduced noticeably. Spray with optimum droplet sizes causes the highest temperature reduction.

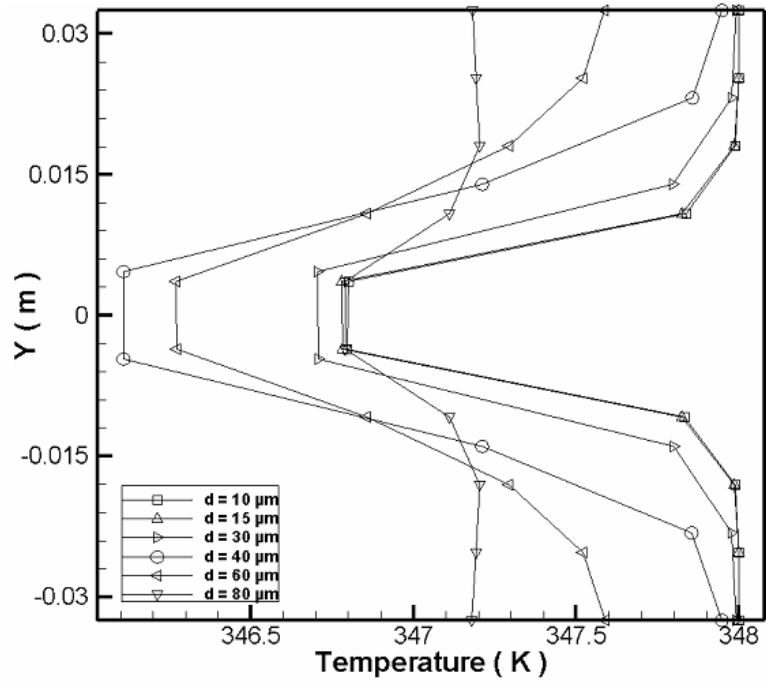


Figure 4-22. Effect of droplet diameter on temperature at the outlet.

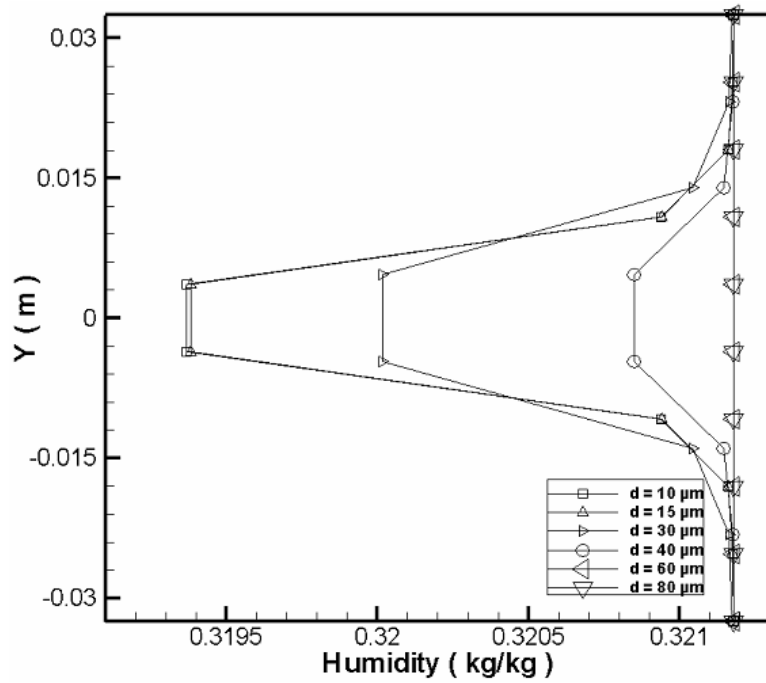


Figure 4-23. Effect of droplet diameter on humidity at the outlet.

Figure 4-23 shows the influence of particle size on humidity pattern at the outlet cross section. Spray with particle diameters of 10 μm has the highest humidity reduction. Larger particles do not penetrate in the radial direction, but there is no condensation of steam on them, therefore, there is no vapor reduction in the air. That is why they are not used in the dehumidification process.

If the mixture is heated again to increase its temperature up to 348 K for the case with droplet diameter of 10 μm , the mass weighted average relative humidity at the outlet cross section will decrease from 91.2 % to 89.39 %. If the same process is implemented for the case with droplet diameter of 60 μm , the relative humidity will decrease from 93.87 % to 89.48 %. Since the humidity of the mixture is constant in this heating process, the relative humidity values will decrease more for mixtures with lower humidity. The mixture humidity in the case with droplet diameter of 10 μm is lower than the humidity values in the case with droplet diameter of 60 μm . For this reason, by increasing the mixture temperature to 348 K, relative humidity of the case with particle diameters of 10 μm decreases to lower values compared to case with droplet diameter of 60 μm . Table 4-3 summarizes the effect of heating on relative humidity.

Spray with optimum droplets reduce the temperature of the mixture more, therefore mixture requires more heat to increase its temperature to 348 K compared to sprays with smaller droplet diameters. For the case with droplet diameters of 10 μm , 335.7 Watt energy is required to increase the mixture temperature to 348 K. Similarly for the case with droplet diameters of 60 μm , 691.2 Watt energy is needed to increase the temperature to 348 K.

Table 4-3. Effect of heating the air-vapor mixture on RH.

Case	RH (%)	RH (%) at T = 348 K
$d_p = 10 \mu\text{m}$	91.2	89.39
$d_p = 40 \mu\text{m}$	93.87	89.48

4.2.1.4. Effect of droplet diameter on mass-weighted average values of the parameters

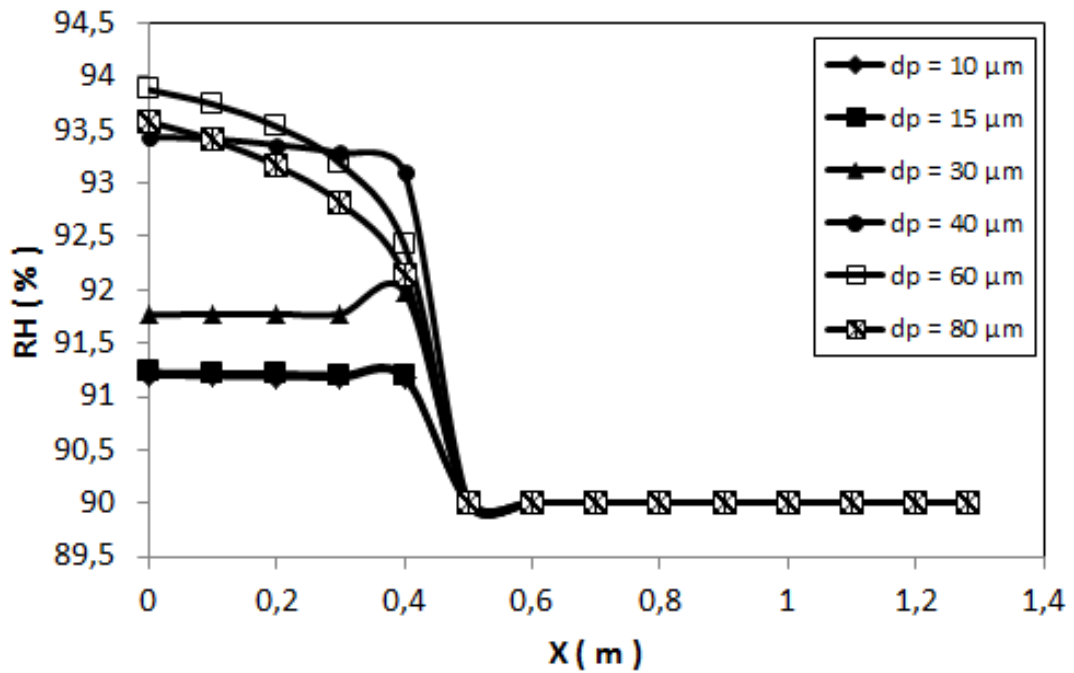


Figure 4-24. Effect of droplet diameter on mass-weighted average relative humidity.

Figure 4-24 depicts effect of the droplet diameter on the mass weighted average values of the relative humidity. Mass weighted average relative humidity for droplets with diameters of $60 \mu\text{m}$ has the highest enhancement.

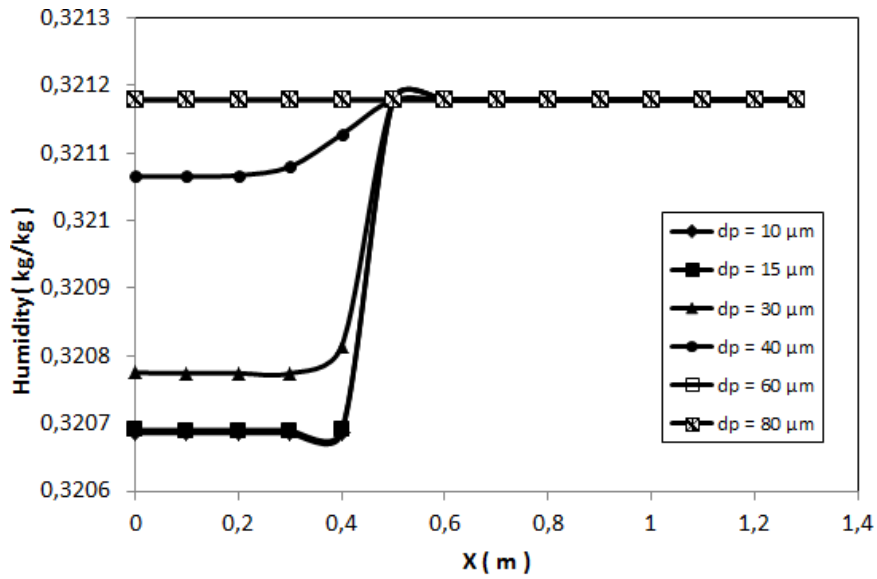


Figure 4-25. Effect of droplet diameter on mass-weighted average humidity.

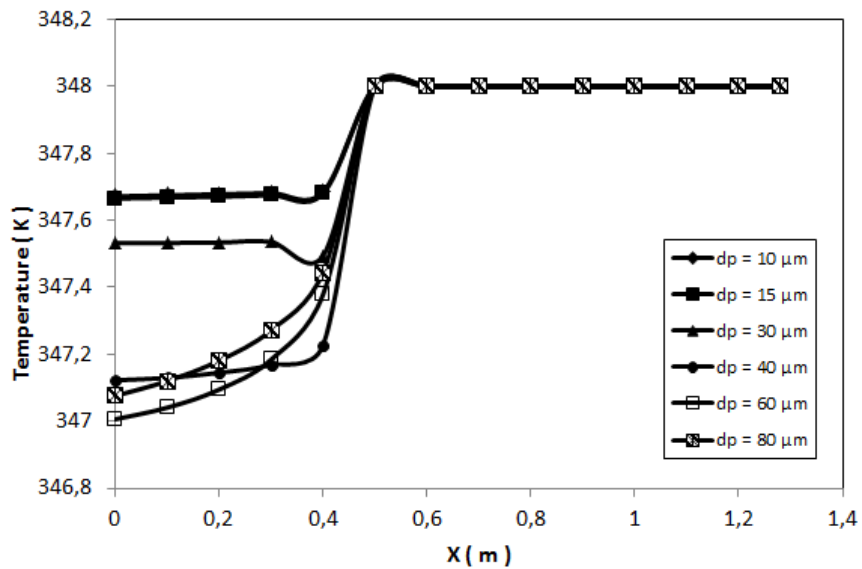


Figure 4-26. Effect of droplet diameter on mass-weighted average humidity.

Figure 4-25 shows the effect of droplet diameter on mass weighted average humidity. It is found that smaller droplets reduce the humidity more, because their contact probability with the steam is more compared to larger droplets. For this reason more steam could condense on the droplet.

Figure 4-26 illustrates the effect of droplet diameter on the bulk temperature of the mixture. As it is observed in Figure 4.26, bulk temperature reduction for the case with optimum droplet diameter has the highest amount.

4.2.2. Effect of Spray Mass Flow Rate

In this part effect of mass flow rate on flow pattern is analyzed. Spray mass flow rates of 3, 4, 6 gr/s are investigated to analyze mass flow rate effect on heat and mass transfer. Obviously increasing the mass flow rate will lead to heat transfer and mass transfer enhancement [48, 59, 60, 61, 62]. The following figure illustrates the temperature contours for different mass flow rates. The figure illustrates that mass flow rate is proportional to heat transfer. By enhancing the mass flow rate of the spray, temperature at the core center of the channel reduces more [63].

Figure 4-27 illustrates the temperature contours for various mass flow rates. It is noticed that spray with mass flow rate of 6 gr/s has the highest temperature reduction.

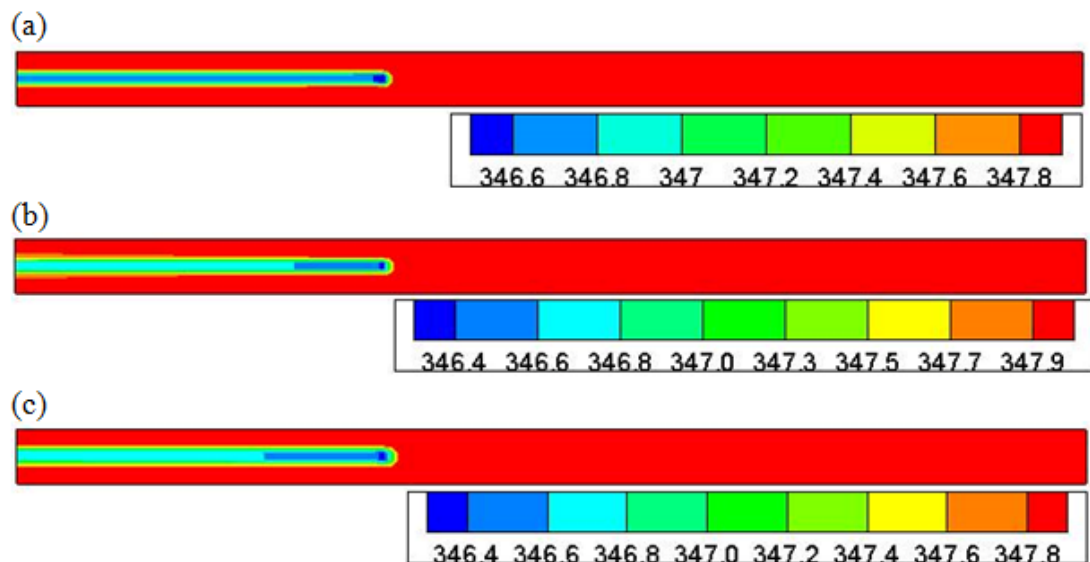


Figure 4-27. Temperature contours for different mass flow rates , (a) Mass flow rate = 3 gr/s, (b) Mass flow rate = 4gr/s, (c) Mass flow rate = 6 gr/s.

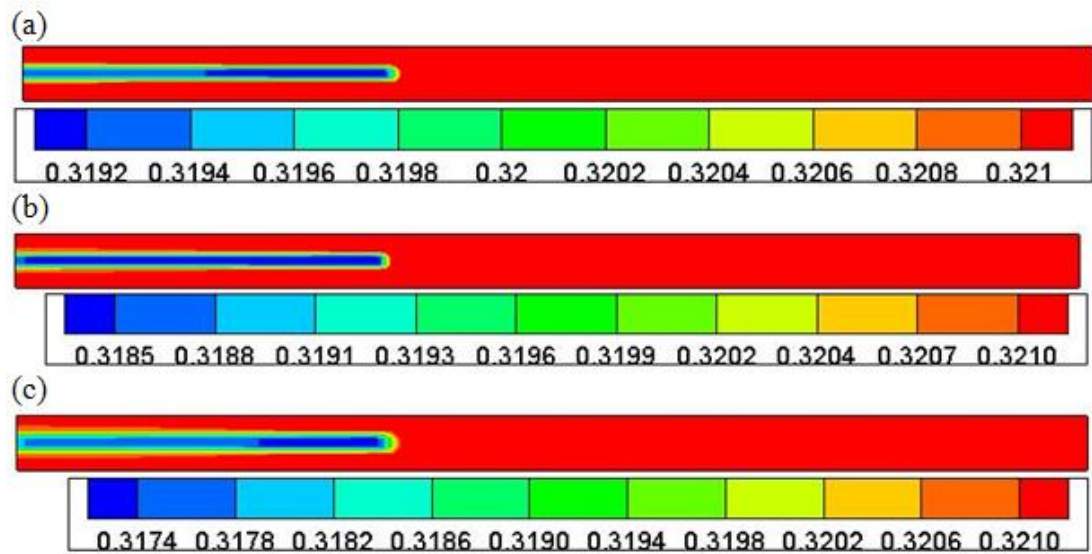


Figure 4-28. Humidity contours for different mass flow rates, (a) Mass flow rate = 3 gr/s, (b) Mass flow rate = 4 gr/s, (c) Mass flow rate = 6 gr/s.

Figure 4-28 shows the effect of mass flow rate on the humidity distribution. Spray with mass flow rate of 6 gr/s leads to the lowest humidity at the outlet. It is concluded that increasing the mass flow rate of the spray increases heat and mass transfer.

4.2.2.1. Effect of mass flow rate on flow pattern on the horizontal centerline

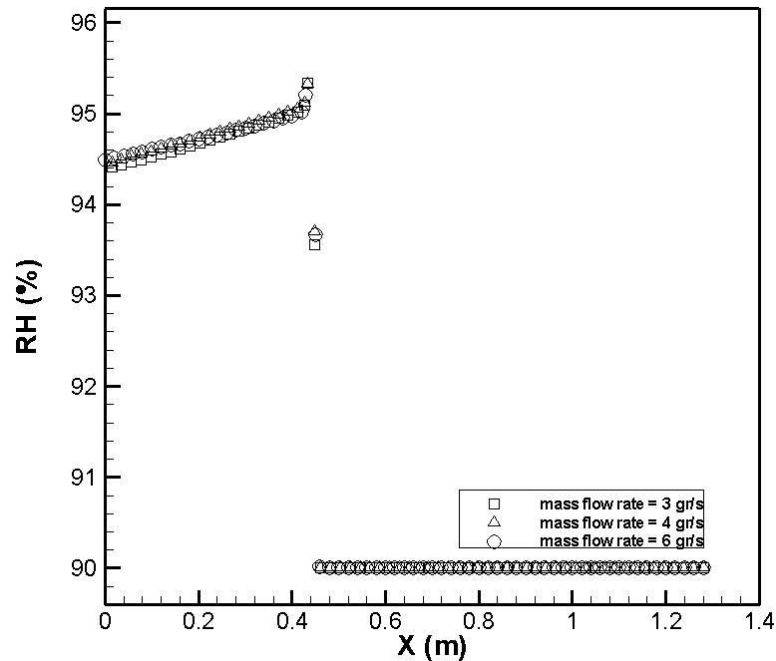


Figure 4-29. Effect of spray mass flow rate on relative humidity distribution on the horizontal centerline.

Figure 4-29 depicts the effect of mass flow rate on relative humidity on the horizontal centerline of the chamber. As the mass flow rate increases, spray cools the mixture better. Although condensation occurs and the temperature of the air and droplet increases slightly, temperature reduction due to sensible heat is more dominant. As a result sprays with higher mass flow rates decrease the mixture temperature more. More reduction in temperature leads to enhancement in relative humidity.

Figure 4-30 illustrates the effect of mass flow rate on the temperature pattern of the gas phase on the centerline of the channel. Temperature reduction rate is increased due to enhancement of the mass flow rate of the spray.

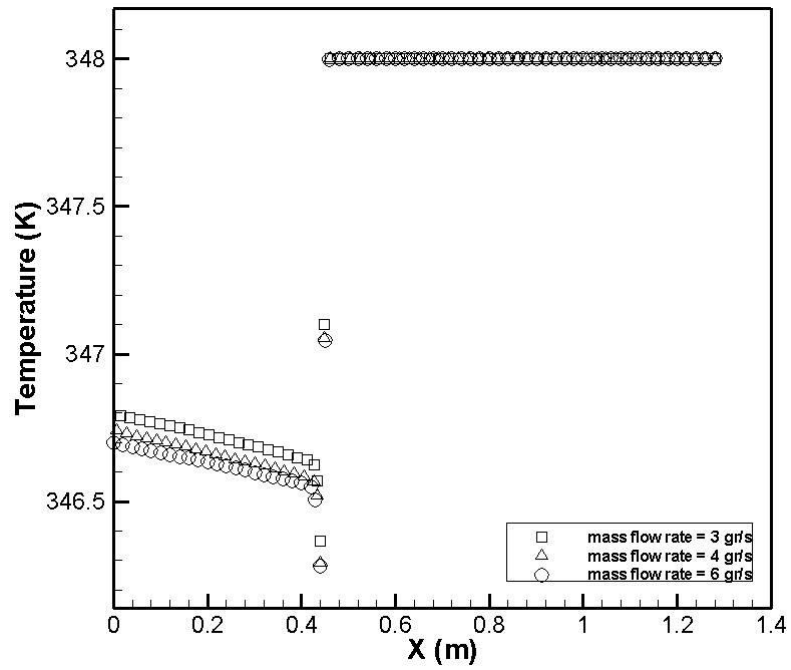


Figure 4-30. Effect of spray mass flow rate on temperature distribution on the horizontal centerline.

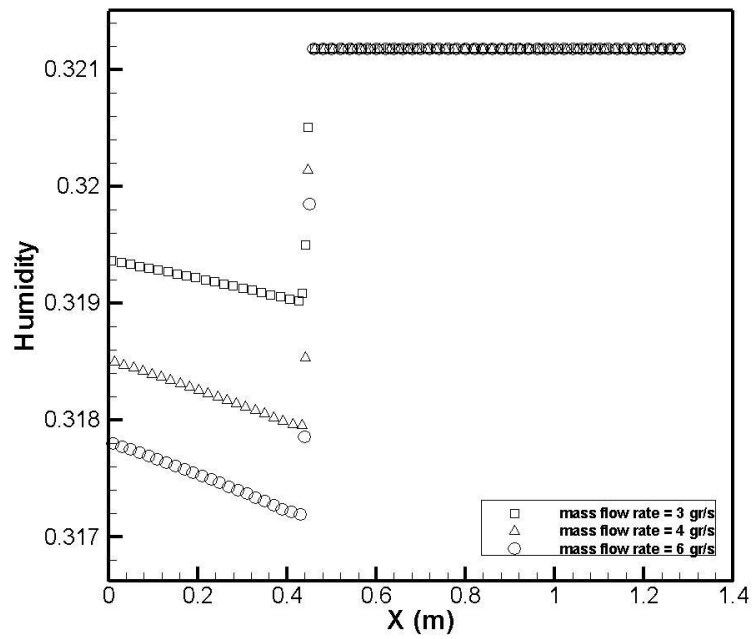


Figure 4-31. Effect of spray mass flow rate on humidity distribution on the horizontal centerline.

Figure 4-31 describes the effect of the mass flow rate of the spray on humidity. Since heat and mass transfer are proportional to mass flow rate of the spray [48], increasing the mass flow rate of the spray reduces the humidity of the mixture. It could be interpreted that increase in mass flow rate leads to higher temperature reduction due to sensible heat. Since temperature decreases below the dew point more and more, condensation rate violently increases. Accordingly, large amount of vapor is condensed on the water droplet and humidity diminishes.

4.2.2.2. Effect of mass flow rate on flow pattern at the outlet cross section

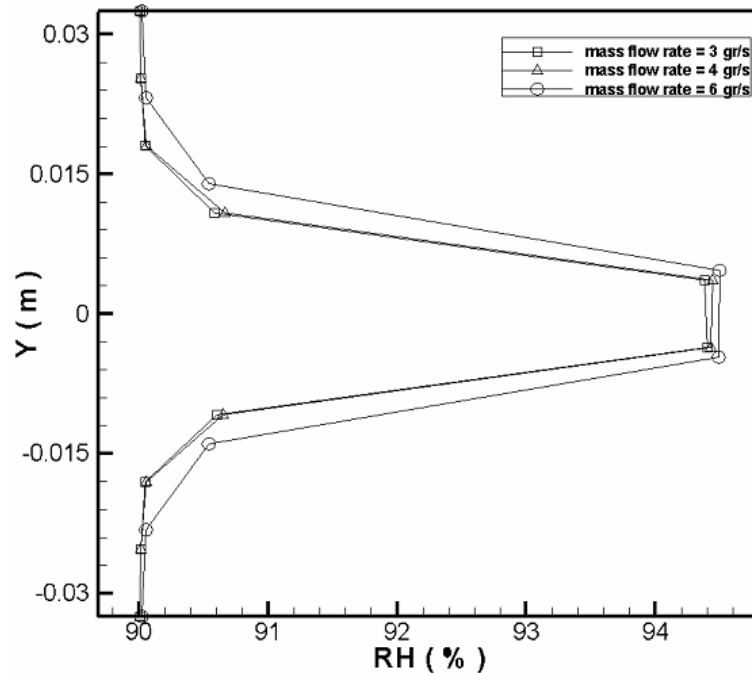


Figure 4-32. Effect of mass flow rate on relative humidity at the outlet.

Figure 4-32 shows the effect of mass flow rate on relative humidity at the outlet cross-section of the channel. It is found that the regions close to the wall are almost at the same relative humidity with the entering air-vapor mixture. On the other hand, core region has been strongly affected by condensation.

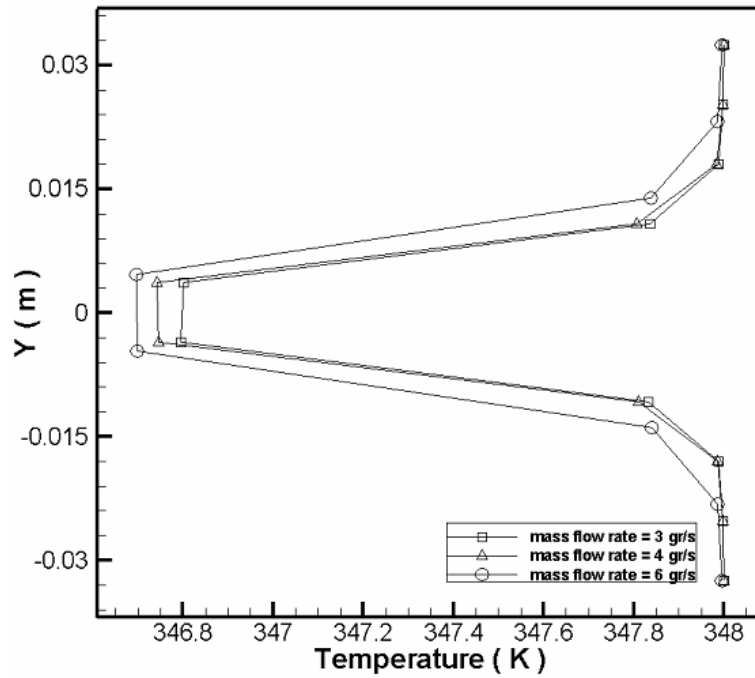


Figure 4-33. Effect of mass flow rate on temperature distribution at the outlet.

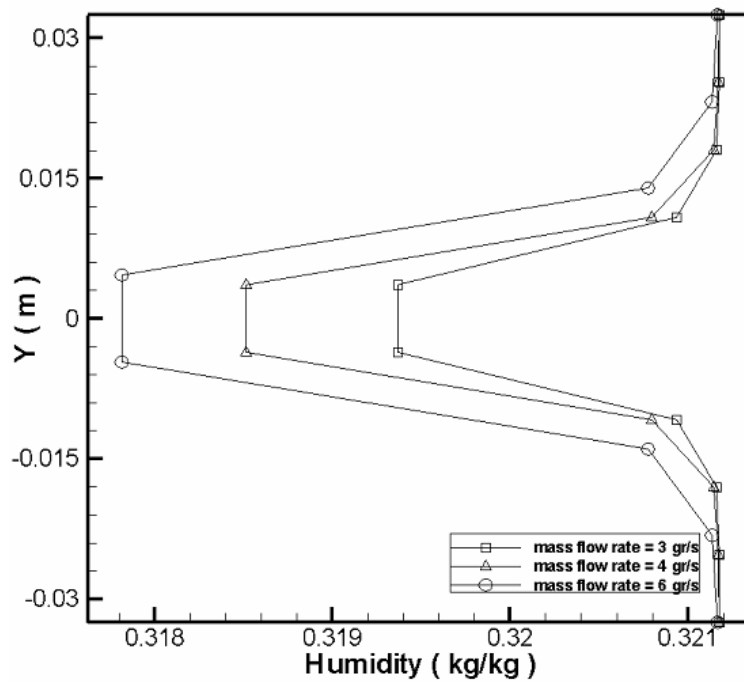


Figure 4-34. Effect of mass flow rate on humidity distribution at the outlet.

Figure 4-33 illustrates the effect of mass flow rate on gas-phase temperature at the outlet cross-section of the channel. It is observed that central core of 3 cm is cooled effectively. Figure 4-34 describes that higher mass flow rates lead to higher reduction

of the humidity in the mixture. In addition it is found that larger mass flow rates increase the effect of the spray in the channel. In other words, higher spray mass flow rates can spread dehumidification effect to regions close to the wall too. This radial diffusion of dehumidification effect helps to decrease the humidity in every part of the chamber which is so vital in many industrial processes.

If the liquid water in the discharging mixture is taken out and the air-vapor mixture is heated to increase its temperature to 348 K, the relative humidity of the mixture will decrease. If the mixture is heated again to 348 K for the case with the spray mass flow rate of 6gr/s, the mass weighted average relative humidity at the outlet will decrease from 91.51 % to 89.28 %. If the same process is done to the case with the spray mass flow rate of 3gr/s, the relative humidity will decrease from 91.2 % to 89.39 %. Since the humidity of the mixture is constant in this heating process, the relative humidity values will decrease more for mixtures with lower humidity. In other words, if the mixture has less humidity the relative humidity value will decrease more by heating the mixture up to 348 K. Table 4-4 summarizes the effect of heating on relative humidity.

Table 4-4. Effect of heating the air-vapor mixture on RH.

Case	RH (%)	RH (%) at T = 348 K
Mass flow rate = 3gr/s	91.2	89.39
Mass flow rate = 6gr/s	91.51	89.28

Obviously, the heat transfer rate of the heating process for the case with higher spray mass flow rate will be higher. Sprays with higher mass flow rates reduce the temperature of the mixture more, therefore the mixture requires more heat to increase its temperature to 348 K compared to sprays with lower mass flow rates. For example in the case of sprays with mass flow rate of 3gr/s, 335.7 Watt energy is required to increase the mixture temperature to 348 K. Similarly for the case with mass flow rate of 6 gr/s, 413 Watt energy is needed to increase the temperature to 348 K.

4.2.2.3. Effect of mass flow rate on mass-weighted average values of the parameters

The effect of spray mass flow rate on mass weighted average relative humidity is explained in figure 4-35. Spray with mass flow rate of 6 gr/s leads to higher mass weighted value of relative humidity at the outlet. Figure 4-36 illustrates that higher spray mass flow rate reduces the temperature more. Sprays with the mass flow rate of 6 gr/s decrease the mixture temperature more. Humidity reduction is proportional to mass flow rate of the water spray. In other words sprays with higher mass flow rates reduce the humidity of the mixture more (Figure 4-37.).

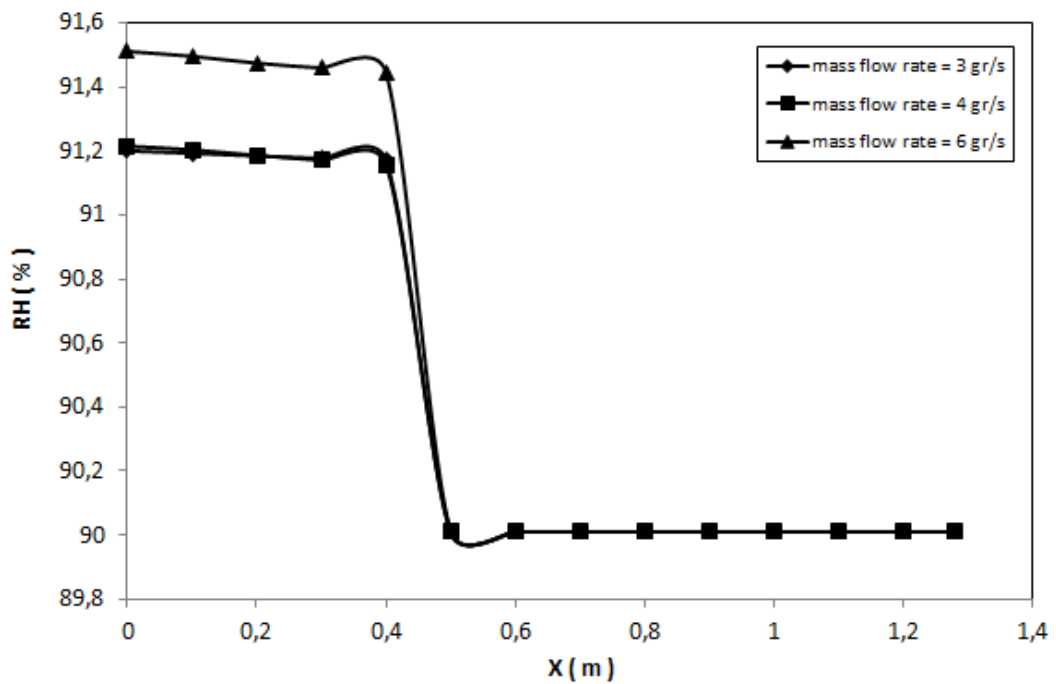


Figure 4-35. Effect of mass flow rate on mass-weighted average relative humidity.

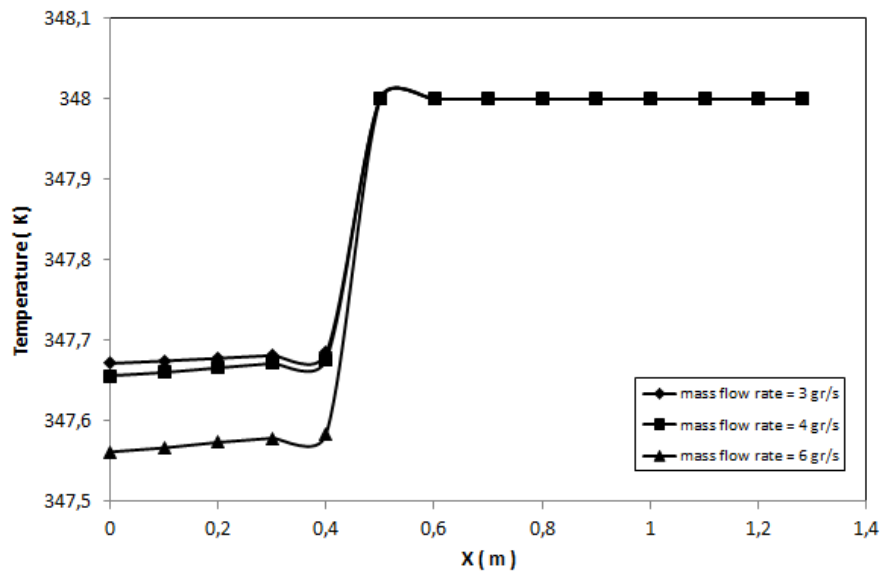


Figure 4-36. Effect of mass flow rate on mass-weighted average temperature

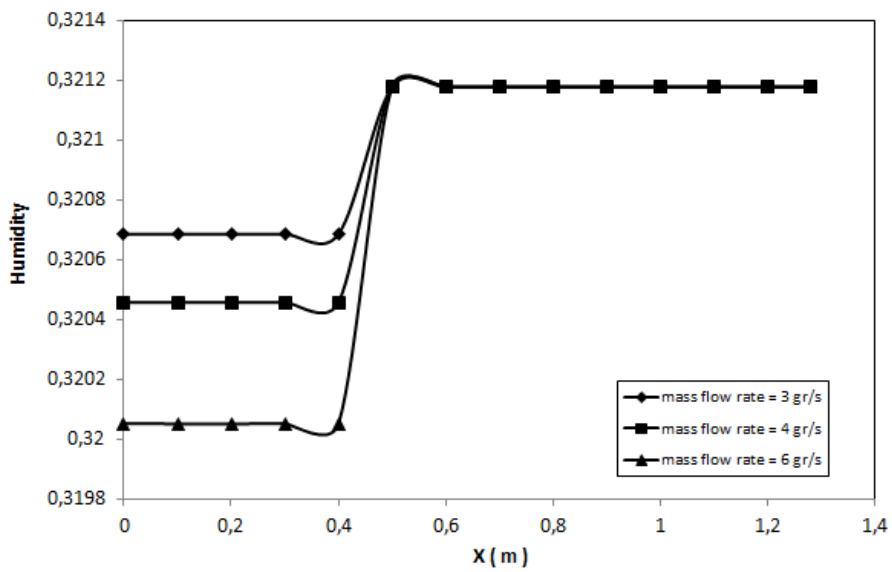


Figure 4-37. Effect of mass flow rate on mass-weighted average humidity.

4.2.3. Effect of Water Droplet Temperature

This section studies the effect of water droplet temperature on heat and mass transfer rate. In order to analyze the effect of coolant temperature, water droplet temperature is varied while keeping other parameters constant. Water droplet with temperature of 288 K, 313 K, 323 K, and 330 K has been studied. For all the cases mass flow rate of the spray and droplet diameter are kept fixed at the values of 3 gr/s and 10 μm , respectively. Temperature contours of the continuous phase for different water droplet temperatures are shown in Figure 4-38. It is noticed that decrease in water droplet temperature enhances the temperature difference between two phases which leads to enhancement of heat and mass transfer.

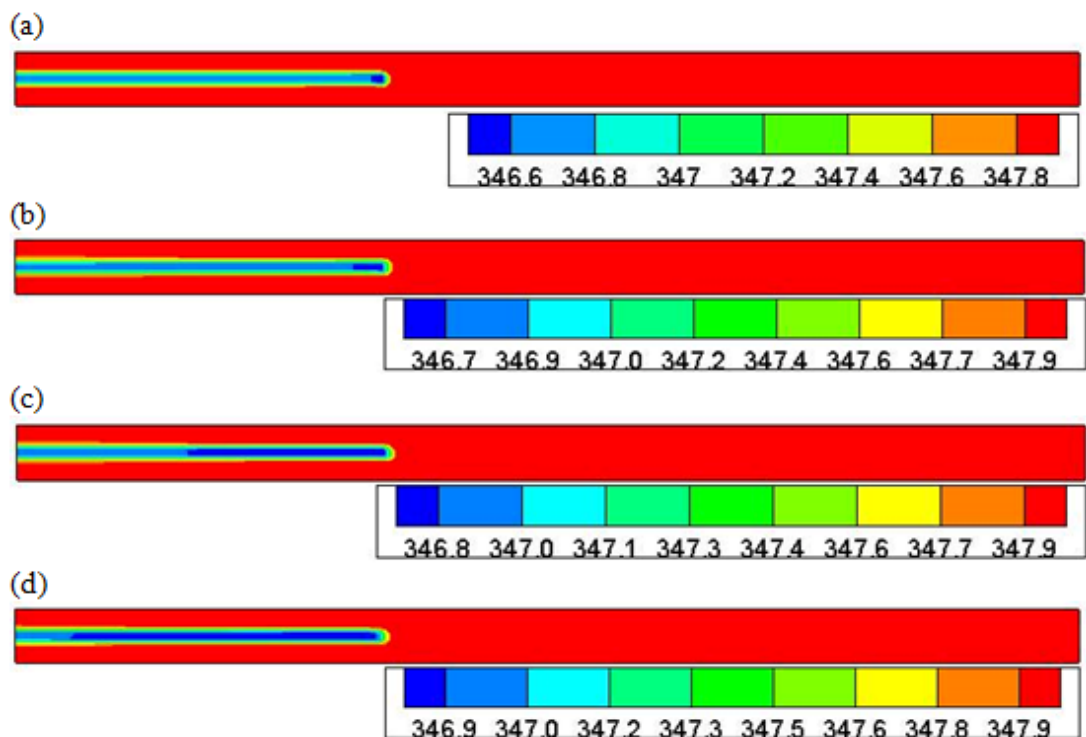


Figure 4-38. Temperature contours for different water droplet temperature, (a) $T_w = 288$ K, (b) $T_w = 313$ K, (c) $T_w = 323$ K, (d) $T_w = 330$ K.

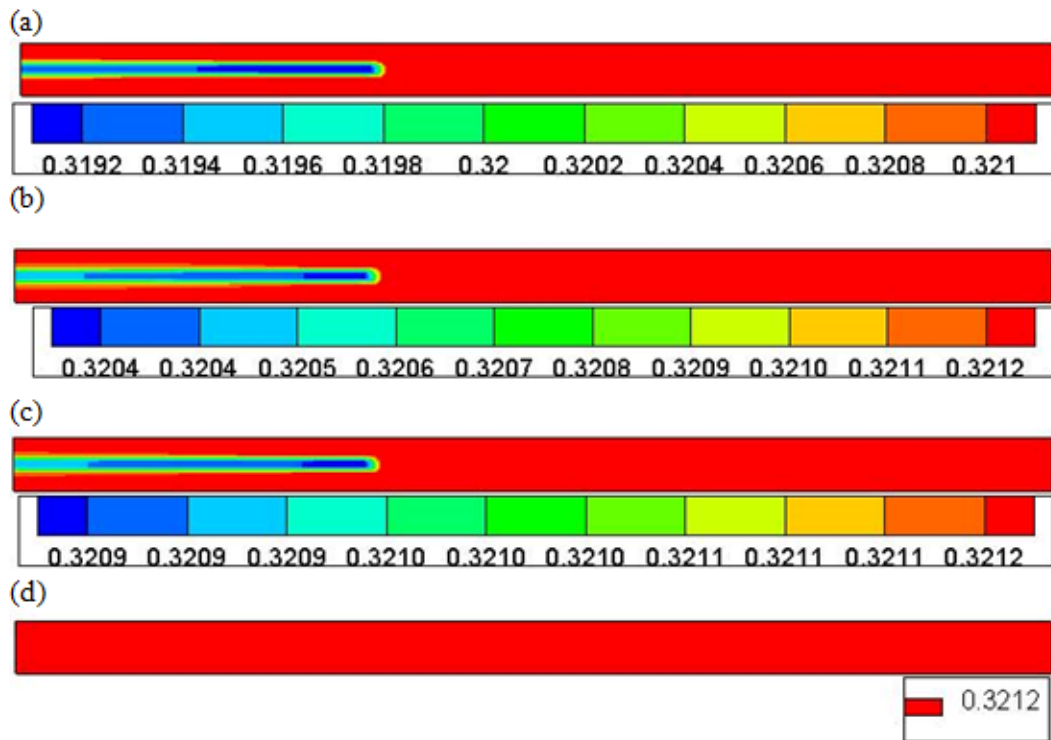


Figure 4-39. Humidity contours for different water droplet temperature, (a) $T_w = 288$ K, (b) $T_w = 313$ K, (c) $T_w = 323$ K, (d) $T_w = 330$ K.

Figure 4-39 shows the humidity contours for variety of water droplet temperatures where effect of the coolant temperature is obvious. When the water droplet is colder, sensible heat is higher. This means mixture temperature will be reduced more and as a result more steam will be condensed on the surface of the liquid water.

4.2.3.1. Effect of water droplet temperature on flow pattern on the horizontal centerline

Temperature difference plays a crucial role in heat and mass transfer between two phases. Temperature difference is proportional to heat and mass transfer [14]. When the droplet temperature is higher, due to less temperature difference with mixture, less heat transfer will happen. Therefore cooling process of the mixture will not be effective. For this reason relative humidity of the mixture will increase less compared to cases with colder coolants. In cases with colder coolants, temperature reduction will be more. Accordingly, more condensation of vapor on water droplet surface is

expected and humidity will diminish more. Figure 4-40, 4-41, and 4-42 illustrate this scenario for relative humidity, temperature, and humidity respectively.

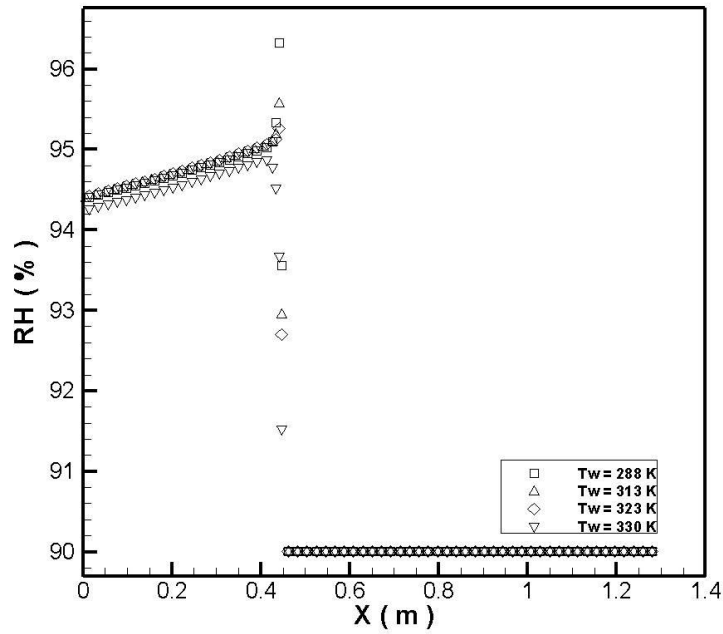


Figure 4-40. Effect of droplet temperature on relative humidity distribution on the horizontal centerline.

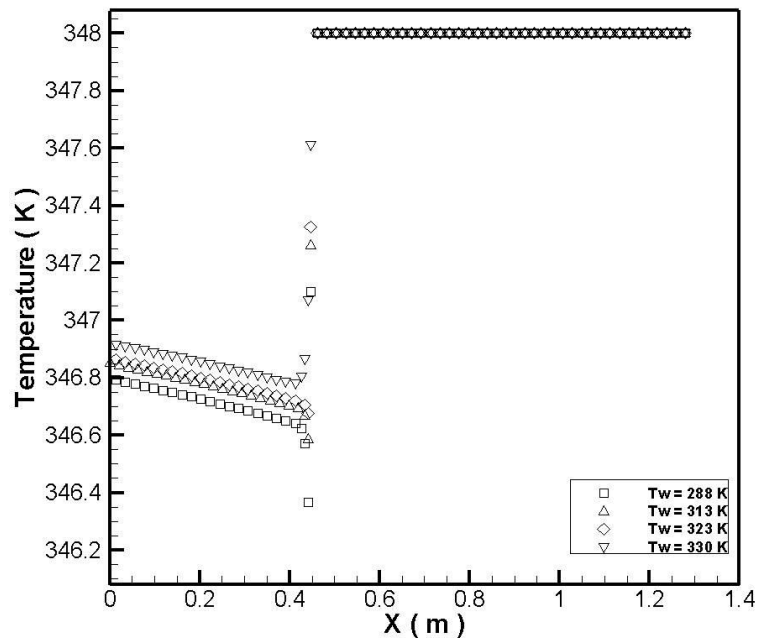


Figure 4-41. Effect of droplet temperature on temperature distribution on the horizontal centerline.

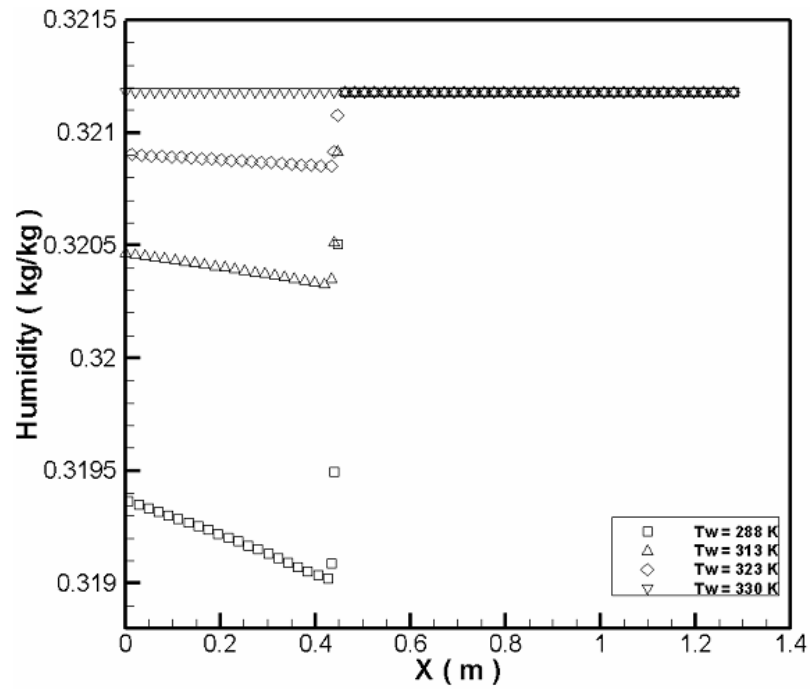


Figure 4-42. Effect of droplet temperature on humidity distribution on the horizontal centerline.

4.2.3.2. Effect of water droplet temperature on flow pattern at the outlet cross section

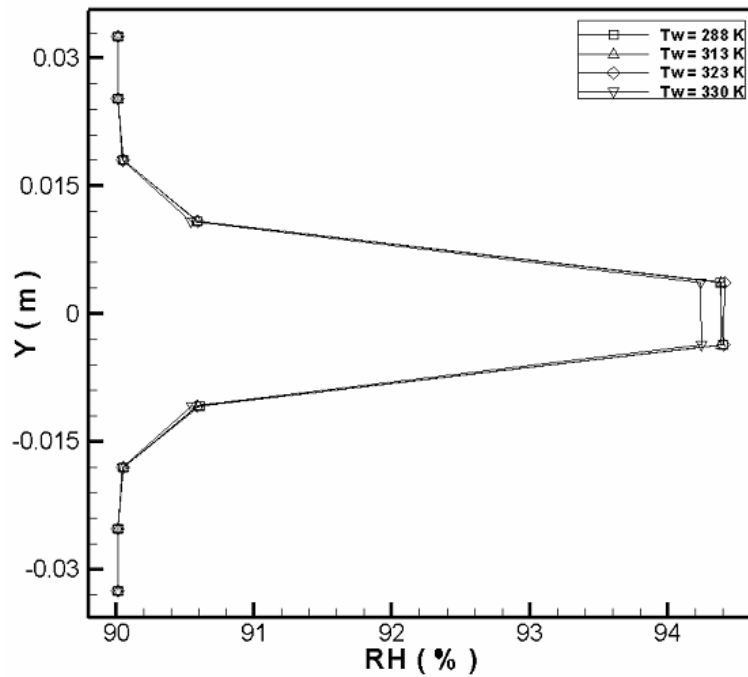


Figure 4-43. Effect of water temperature on relative humidity distribution at the outlet.

Figure 4-43 illustrates the effect of droplet temperature on relative humidity pattern at the outlet cross section. It is found that reduction of the coolant temperature causes enhancement in relative humidity. This enhancement is found to be slight due to balance between latent heat and sensible heat transfer.

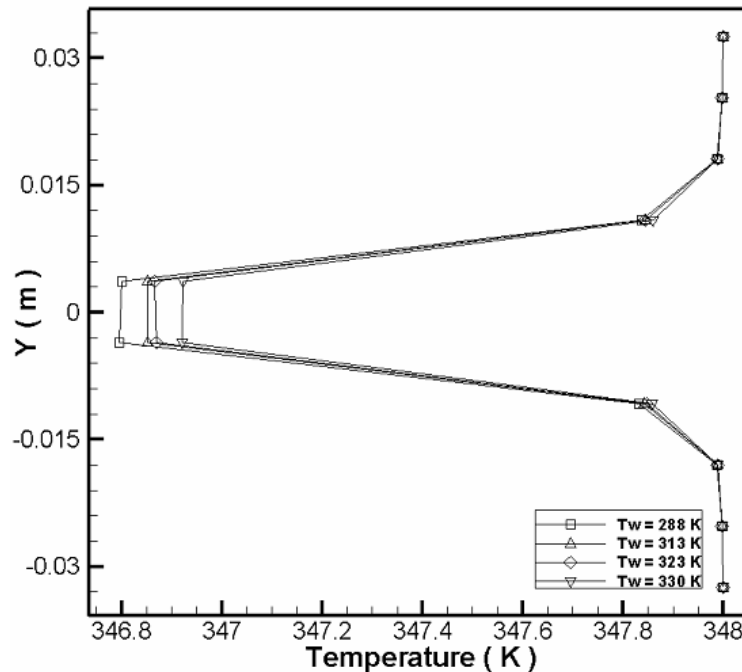


Figure 4-44. Effect of water temperature on temperature distribution at the outlet.

Figure 4-44 represents the effect of spray temperature on gas-phase temperature distribution at the outlet. It is observed that by reducing the spray temperature continuous phase temperature decreases more. As mentioned before temperature gradient enhancement causes higher heat transfer. Thus sensible heat transfer will decrease the mixture temperature more. In this case mixture temperature drops more below its dew point and more condensation occurs. Because of high condensation rate condensing vapor releases its latent heat to the droplets and surrounding air. This balance between latent heat and sensible heat does not let the colder sprays to reduce the mixture temperature remarkably [52, 55].

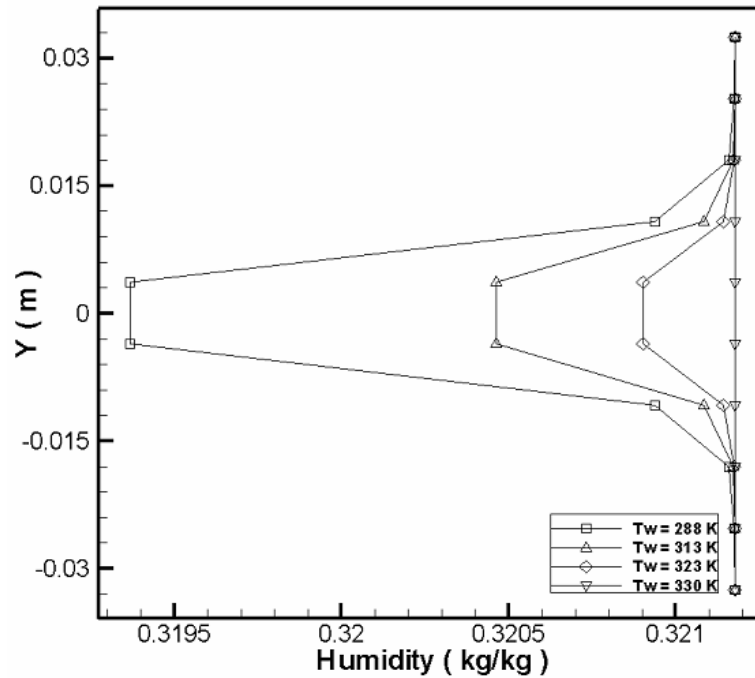


Figure 4-45. Effect of water temperature on humidity distribution at the outlet.

Figure 4-45 clarifies the influence of spray temperature on the humidity dispersion at the outlet. Spray temperature reduction causes remarkable abatement in mixture humidity.

If the outlet mixture is heated again to increase its temperature to 348 K, for the case with droplet temperature of 288 K, the mass weighted average relative humidity will decrease from 91.2 % to 89.39 %. If the same process is implemented for the case with droplet temperature of 330 K, the relative humidity will decrease from 91.15 % to 89.48 %. Since during the heating process humidity is kept constant, mixtures with lower humidity will lead to lower relative humidity. Accordingly, by increasing the mixture temperature to 348 K, the relative humidity of the case with particle temperature of 288 K decreases to lower values compared to case with droplet temperature of 330 K. Table 4-5 summarizes the effect of heating on relative humidity.

Table 4-5. Effect of heating the air-vapor mixture on RH.

Case	RH (%)	RH (%) at T = 348 K
$T_w = 288$ K	91.2	89.39
$T_w = 330$ K	91.15	89.48

Sprays with lower droplet temperature reduce the temperature of the mixture more, therefore mixture requires more heat to increase its temperature to 348 K compared to sprays with higher droplet temperatures. For example in the case of sprays with droplet temperature of 288 K, 335.7 Watt energy is required to increase the mixture temperature to 348 K. Similarly for the case with droplet temperature of 330 K, 309 Watt energy is needed to increase the temperature to 348 K.

4.2.3.3. Effect of water droplet temperature on mass-weighted average values of the parameters

In this section effect of droplet temperature on mass weighted average values of different parameters is studied.

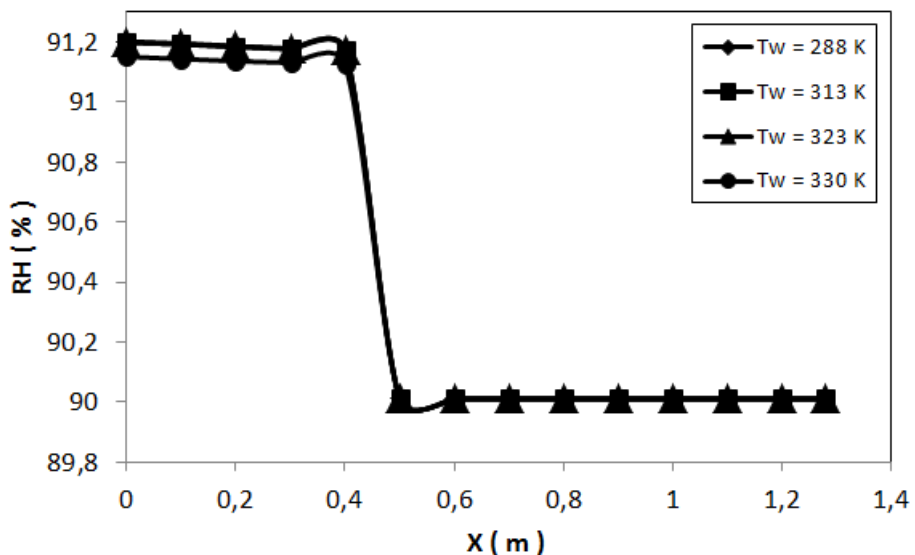


Figure 4-46. Effect of water droplet temperature on mass-weighted average relative humidity.

Figure 4-46 shows that relative humidity values are close to each other; however droplet temperatures of 288 K cause more increase in relative humidity.

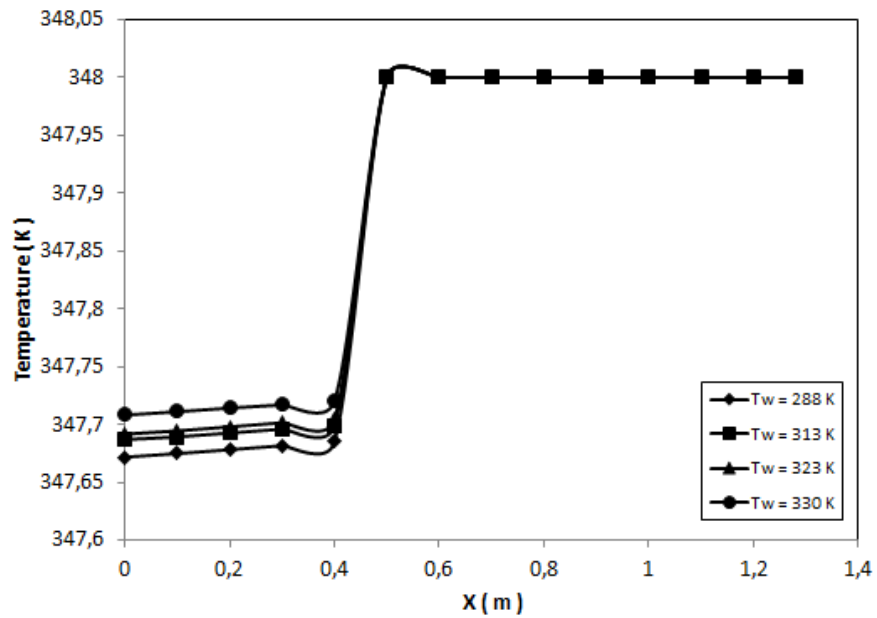


Figure 4-47. Effect of water droplet temperature on mass-weighted average temperature.

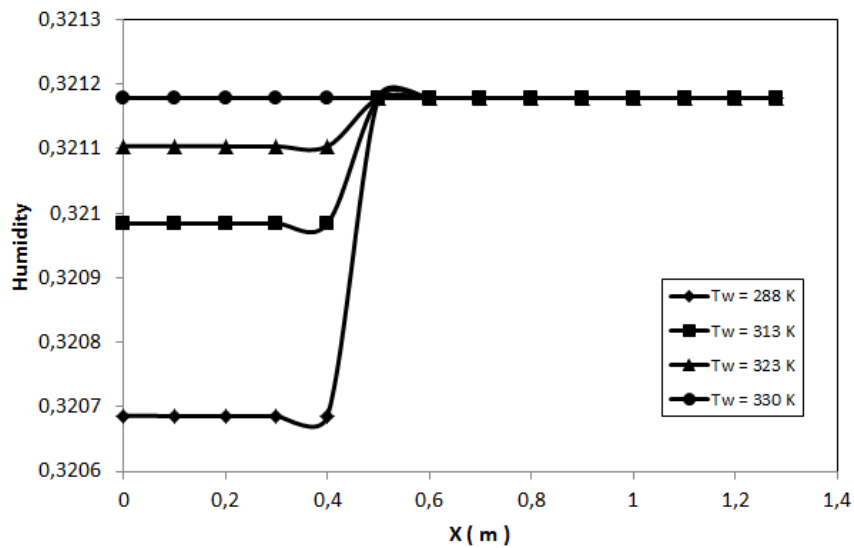


Figure 4-48. Effect of water droplet temperature on mass-weighted average humidity.

Figure 4-47 and figure 4-48 illustrate the effect of droplet temperature on mass weighted average temperature and humidity, respectively. Colder sprays cause more reduction in bulk temperature. Effect of spray temperature is remarkable on humidity pattern.

4.2.4. Effect of Spray Cone Angle

Huang et al. [34] studied the effect of change in cone angle of the water spray in direct contact with surrounding steam. They found that change in cone angle of the spray does not have significant effect on the heat transfer enhancement. In this section of the research this fact is studied. Accordingly the cone angle of the spray is changed while keeping other parameters constant. Great variety of the cone angles are investigated to figure out this fact. Since the continuous phase momentum is large compared to spray momentum, spray cone angle gradient could not depict any effect on the flow pattern. For this reason, there is not a remarkable heat and mass transfer due to change in cone angle of the spray. However by focusing on the zone after the spray it is possible to recognize the slight effect of cone angle effect. Nevertheless it is mentioned by Huang et al. [34] and Martinez-Galvan et al. [18] that the effect of cone angle on heat and mass transfer is negligible, it is found that increasing the cone angle slightly increases heat transfer [18]. The following figures depict this fact. In this investigation it is noticed that effect of cone angle on heat transfer is very slight. The following figures (figure 4-49, figure 4-50, and figure 4-51) depict that cone angle gradient does not affect the humidity pattern.

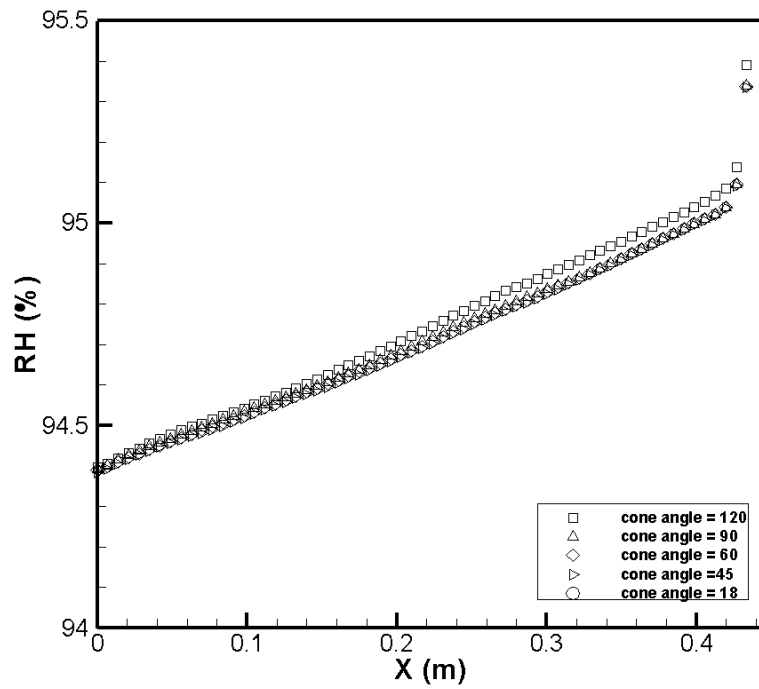


Figure 4-49. Effect of spray cone angle on relative humidity distribution on the centerline after the nozzle.

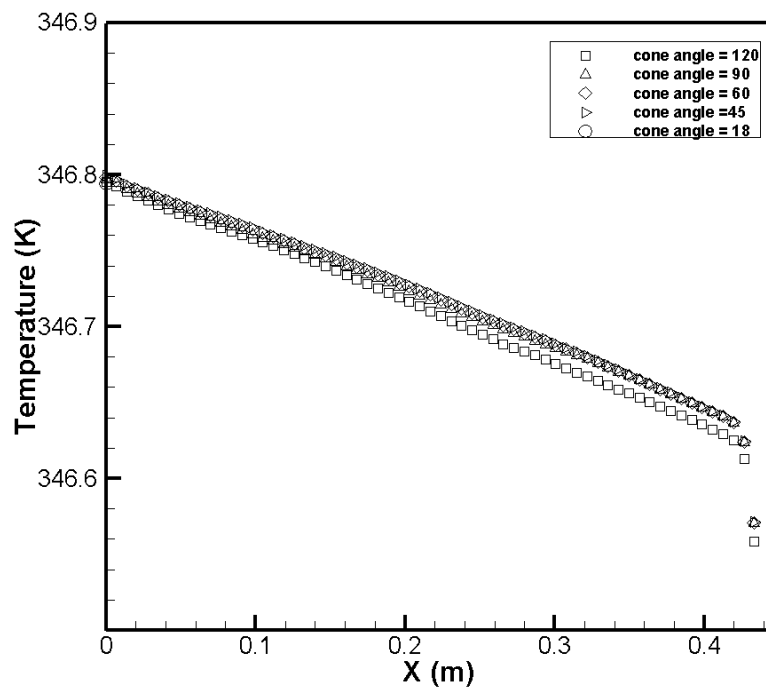


Figure 4-50. Effect of spray cone angle on temperature distribution on the centerline after the nozzle.

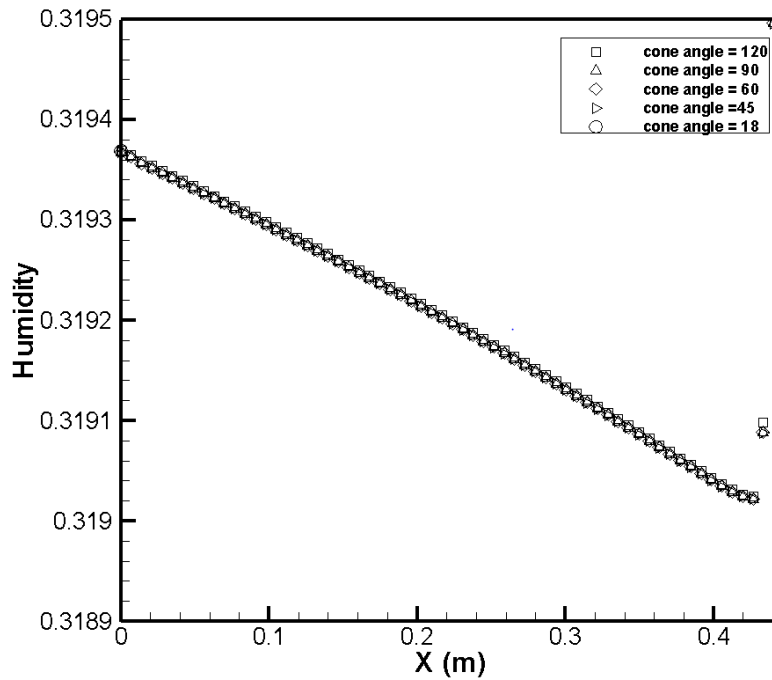


Figure 4-51. Effect of spray cone angle on humidity distribution on the centerline after the nozzle.

4.2.5. Effect of Number of the Sprays

In previous chapters effects of different parameters on a spray are analyzed. As mentioned before, due to large momentum of the air-vapor mixture, particles could not penetrate in the radial direction effectively. Therefore the spray just effects on the core center of the chamber. In order to spread the spray in vertical direction, more injections are implemented in the chamber. Accordingly effects of two, three, and four injections on the flow field are analyzed. Table 4-6 summarizes the initial conditions of each spray.

Table 4-6. Initial conditions of each spray.

Spray Temperature (K)	Spray Cone Angle	Droplet Diameter (μm)	Spray Mass Flow Rate (gr/s)
288	60	10	3

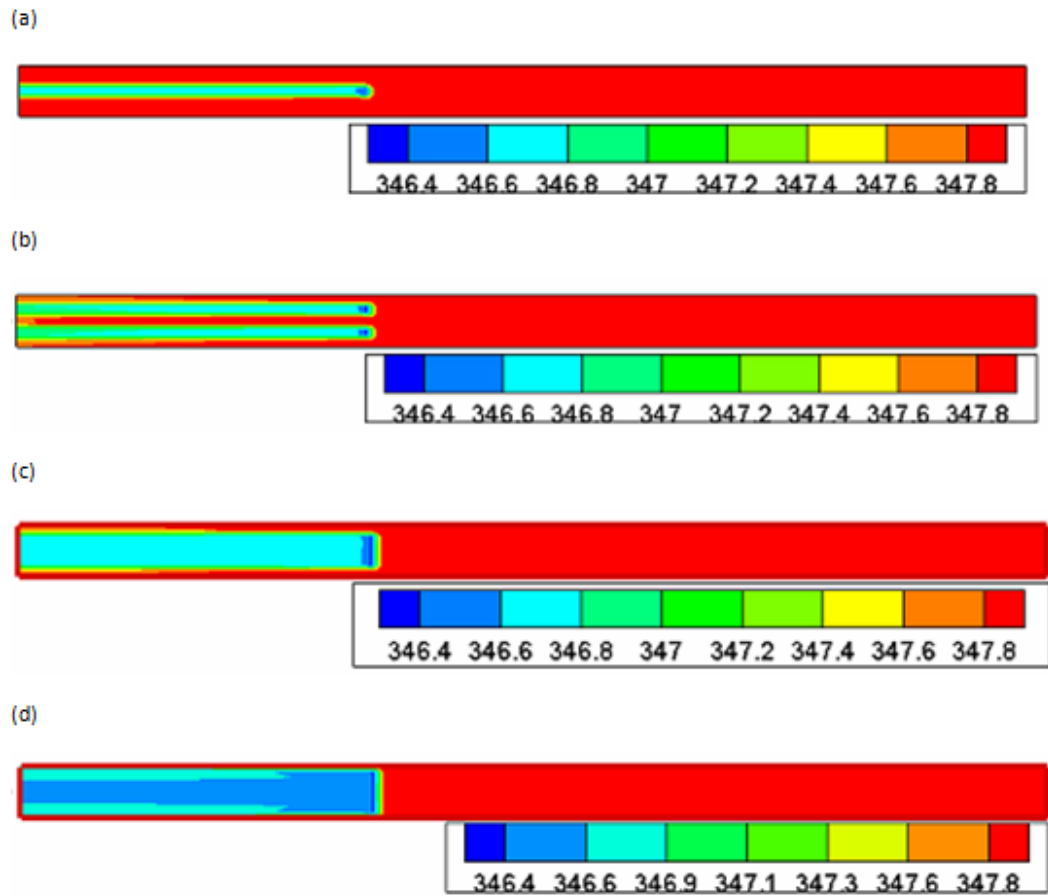


Figure 4-52. Temperature contours, (a) one injection, (b) two injections, (c) three injections, (d) four injections.

Figure 4-52 depicts the temperature contours for various numbers of injections. When one spray is utilized, just the central core of the channel is cooled. It is observed that by increasing the number of injections, effect of the spray is diffused in y-direction at the outlet cross-section. For this reason at the outlet, regions close to the wall are also cooled efficiently.

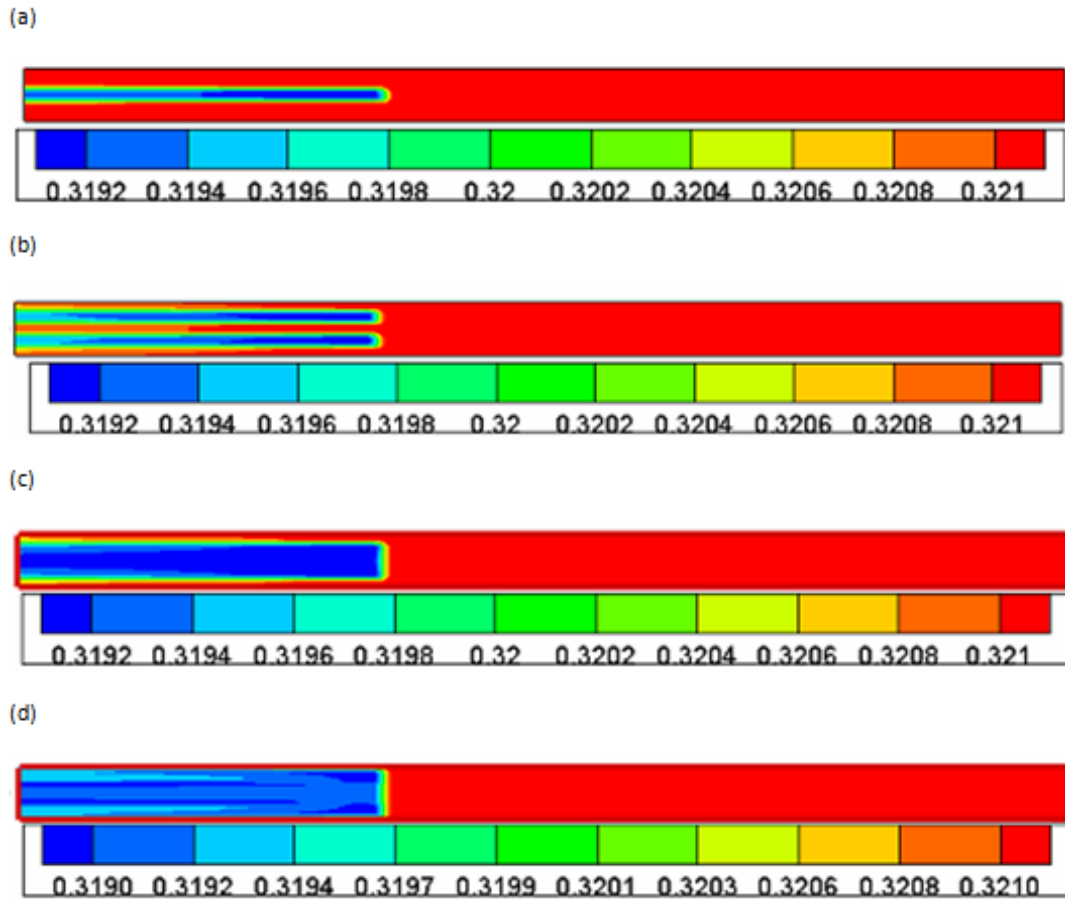


Figure 4-53. Humidity contours, (a) one injection, (b) two injections, (c) three injections, (d) four injections.

Figure 4-53 illustrates the effect of number of injections on the humidity distribution. When one injection is used in the channel, humidity is reduced only the central core of the channel. However by enhancing the number of the injections, humidity is reduced at regions close to the wall too.

4.2.5.1. Effect of number of injections on flow pattern on the horizontal centerline

The following figures show the profile of various parameters on the centerline of the chamber.

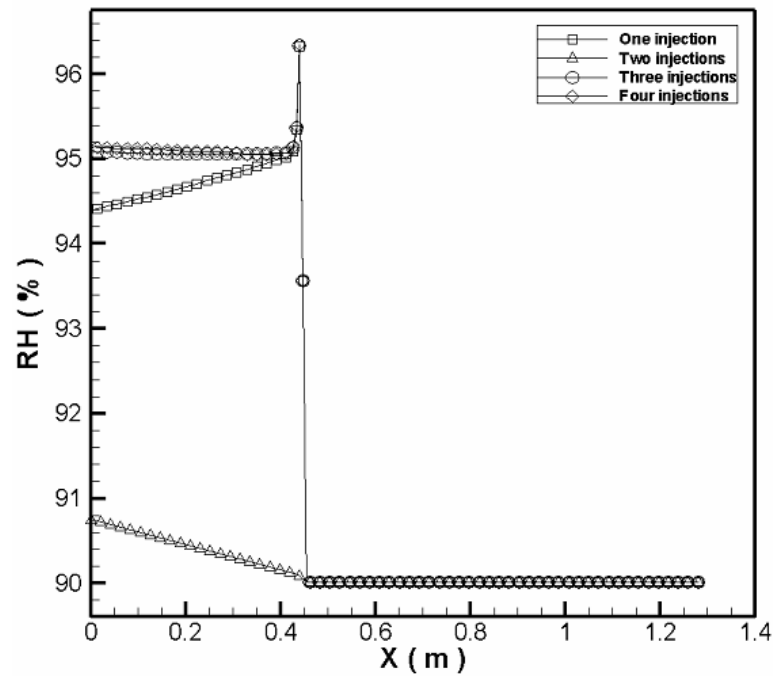


Figure 4-54. Effect of number of injections on relative humidity distribution on the horizontal centerline.

When one injection is used in the channel, the central axis of the nozzle is the same with the centerline of the chamber. For this reason effect of this injection is remarkable on the central core. When two injections are used, the axis of the injection is not the same with chamber centerline. Therefore its effect on the centerline is less. Figure 4-54 depicts that relative humidity is enhanced after the nozzle.

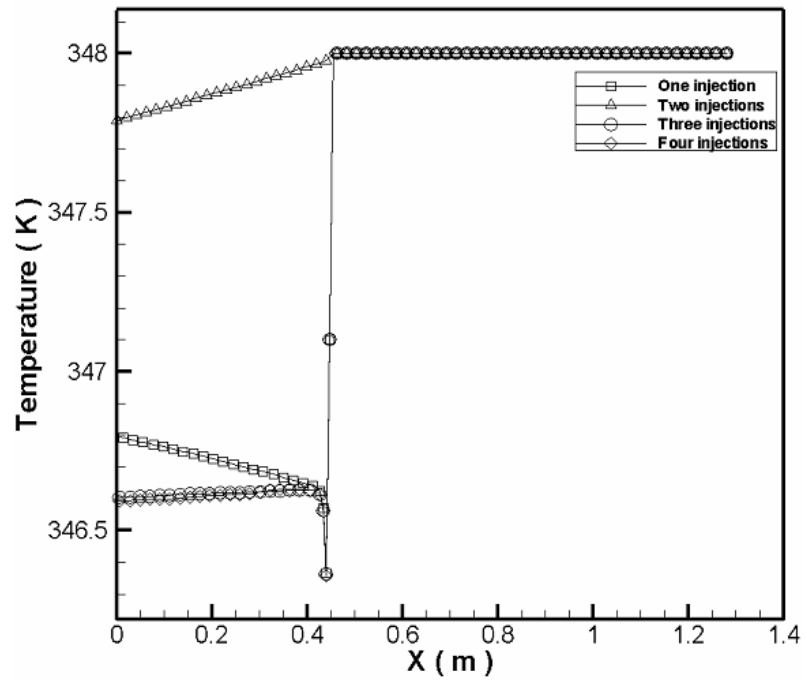


Figure 4-55. Effect of number of injections on temperature distribution on the horizontal centerline.

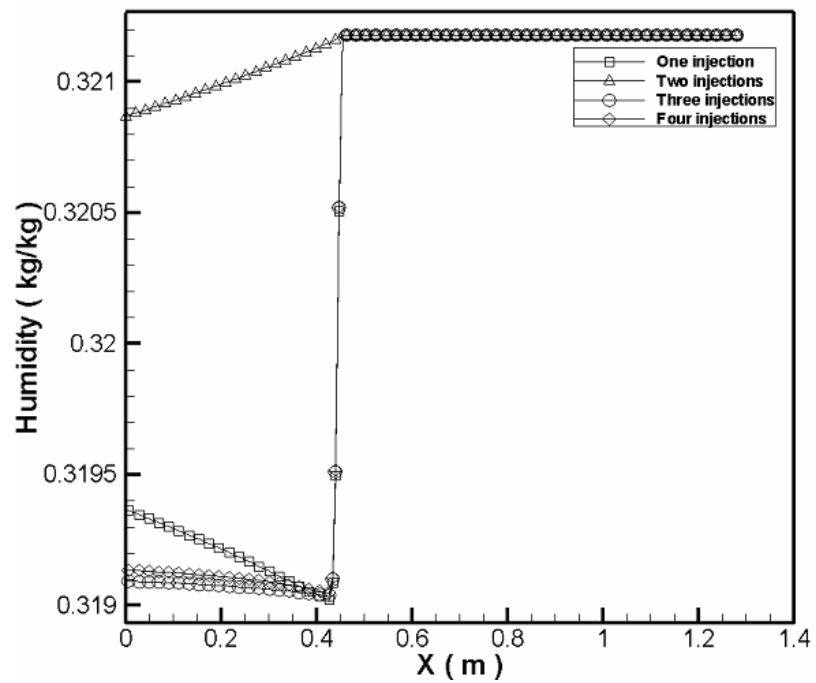


Figure 4-56. Effect of number of injections on humidity distribution on the horizontal centerline.

Figure 4-55 and 4-56 show the effect of number of the injections on the temperature and humidity profile, respectively. However the effect of number of the injections on condensation efficiency is obvious on mass weighted average values. Increasing the number of the nozzles spreads the spray influences in the y direction in the channel.

4.2.5.2. Effect of number of injections on flow pattern at the outlet cross section

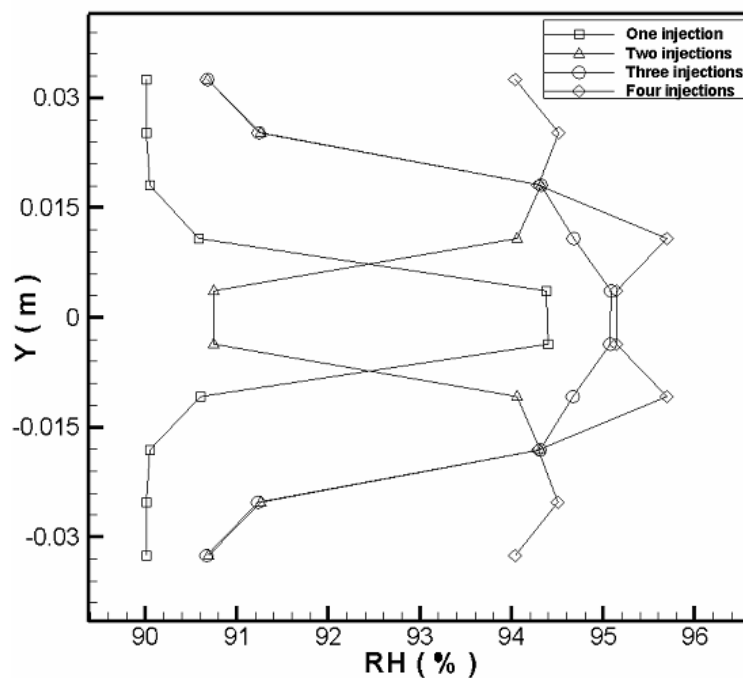


Figure 4-57. Effect of number of injections on relative humidity distribution at the outlet cross section.

Figure 4.57 depicts the effect of the number of injections on the relative humidity at the outlet. By using one injection, relative humidity is enhanced only at the central core of the channel. However when four injections are utilized, relative humidity is enhanced at regions close to the wall too.

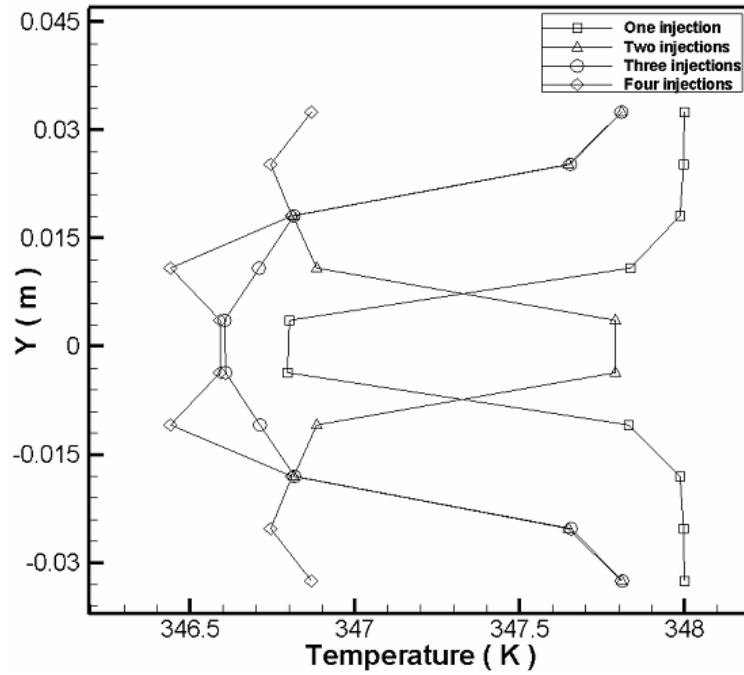


Figure 4-58. Effect of number of injections on temperature distribution at the outlet cross section.

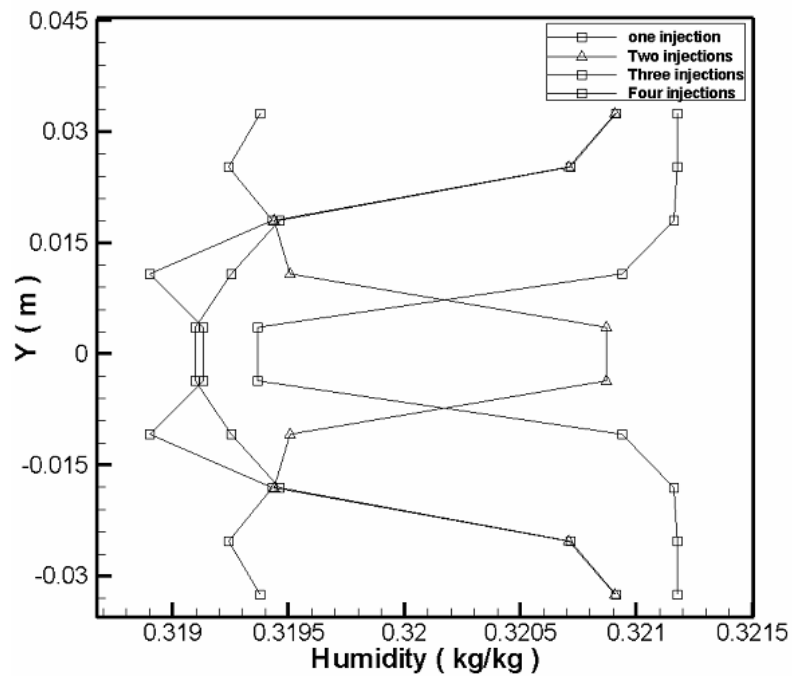


Figure 4-59. Effect number of injections on humidity distribution at the outlet cross section.

Figure 4-58 depicts the effect of the number of injections on the temperature distribution at the outlet. When the number of sprays in the channel is increased, dehumidification and cooling is more effective. For this reason temperature and humidity at the outlet reduce more. Figure 4-59 shows that humidity values are reduced remarkably close to the wall when four injections are utilized in the channel. However when one injection is used in the channel, only the regions close to the axis of the injection are cooled and dehumidified.

If the discharging mixture is heated to increase its temperature to 348 K, relative humidity of the mixture decreases. For the case with four injections, the relative humidity will decrease from 94.84 % to 89.12 %. If the same process is considered for the case with one injection, the relative humidity will decrease from 91.2 % to 89.39 %. Since during the heating process humidity is constant, the mixtures with lower humidity will have lower relative humidity. Consequently, by increasing the mixture temperature to 348 K, the relative humidity of the case with four injections decreases to lower values compared to case with one injection. Table 4-7 summarizes the effect of heating on relative humidity.

Table 4-7. Effect of heating the air-vapor mixture on RH.

Case	RH (%)	RH (%) at T = 348 K
One injection	91.2	89.39
Four injections	94.84	89.12

The temperature of the mixture at the outlet is reduced more by using four injections, therefore mixture requires more heat to increase its temperature to 348 K compared to the case with one injection. For example when four injections are used in the channel, 817 Watt energy is required to increase the mixture temperature from its value at the outlet to 348 K. Similarly for the case with one injection in the channel, 335.7 Watt energy is required to enhance the mixture temperature from its value at the outlet to 348 K.

4.2.5.3. Effect of number of injections on mass-weighted average values of the parameters

In order to depict the effect of the number of injections on the various parameters better, mass weighted average values of different parameters in the channel are calculated.

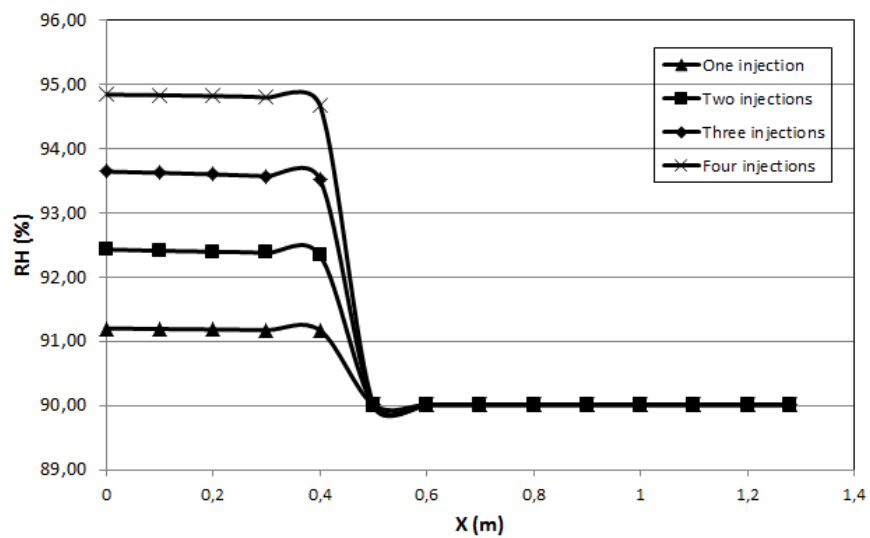


Figure 4-60. Effect of number of injections on mass-weighted average relative humidity.

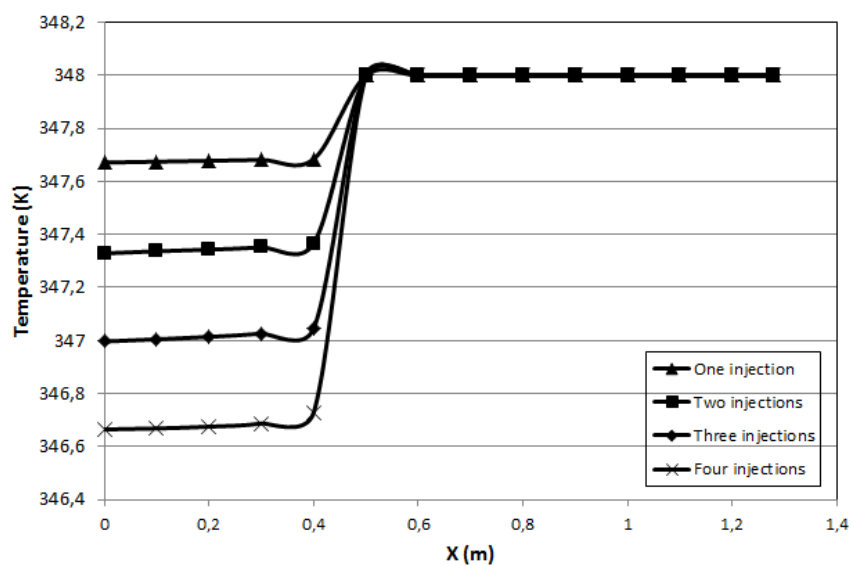


Figure 4-61. Effect of number of injections on mass-weighted average temperature.

Figure 4-60 depicts the effect of number of injections on mass weighted average relative humidity in the channel. It is found that by using more injections in the chamber, regions close to the wall get influenced by the spray dehumidification. Accordingly by increasing the number of the sprays, mass weighted average relative humidity increases more. Figure 4-61 illustrates that using more sprays leads to higher reduction of the mixture bulk temperature.

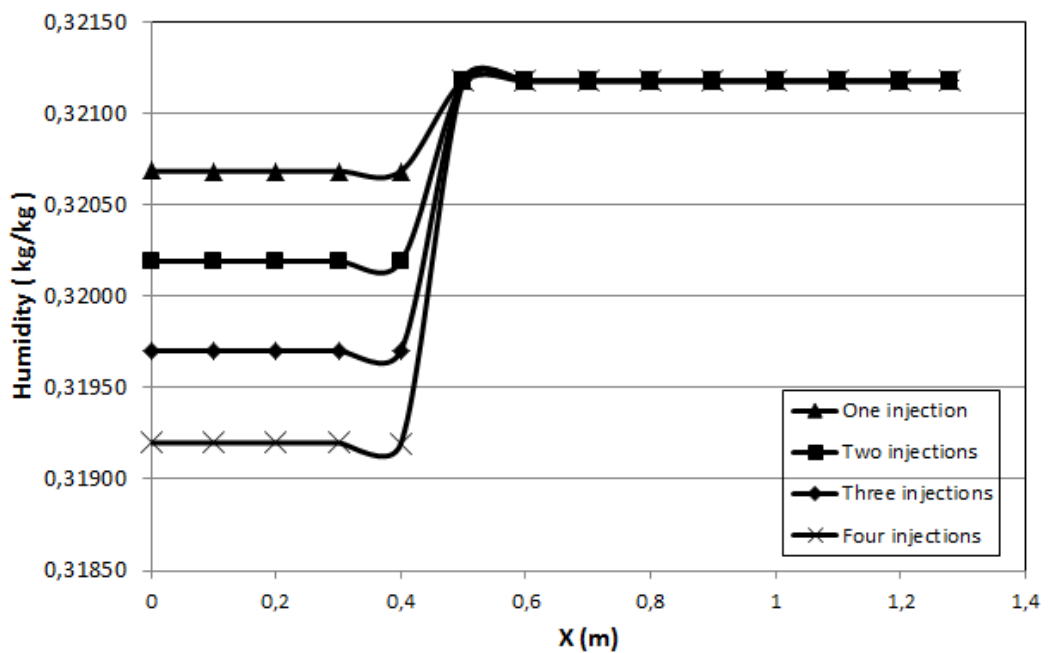


Figure 4-62. Effect of number of injections on mass-weighted average humidity.

Figure 4-62 shows that using more sprays causes more mass weighted average humidity reduction. This means that increasing the number of injections causes more effective dehumidification in the channel.

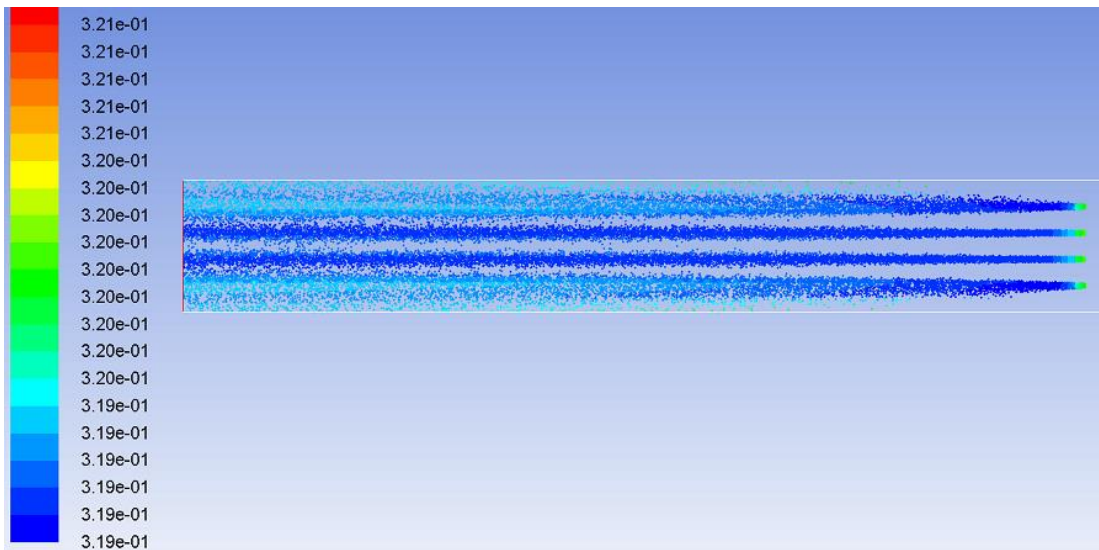


Figure 4-63. Particle trajectories colored by humidity.

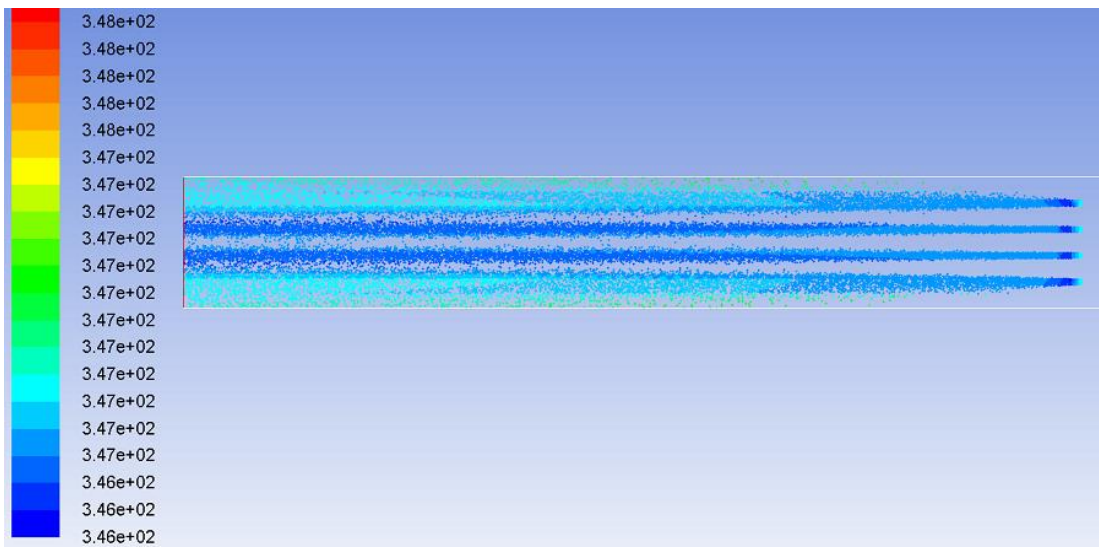


Figure 4-64. Particle trajectories colored by temperature.

Figure 4.63 shows the particle trajectories colored by mixture humidity when four injections are used in the channel. It is observed that humidity is reduced uniformly after the injections. Figure 4-64 illustrates the particle traces colored by mixture temperature. The mixture temperature is reduced even at regions close to the wall.

4.2.6. Effect of the Location of the Spray

In this chapter effect of the location of the spray on the flow pattern is discussed. The sprays are located on the chamber centerline at 44.5 cm, 80 cm, and 120 cm from the outlet.

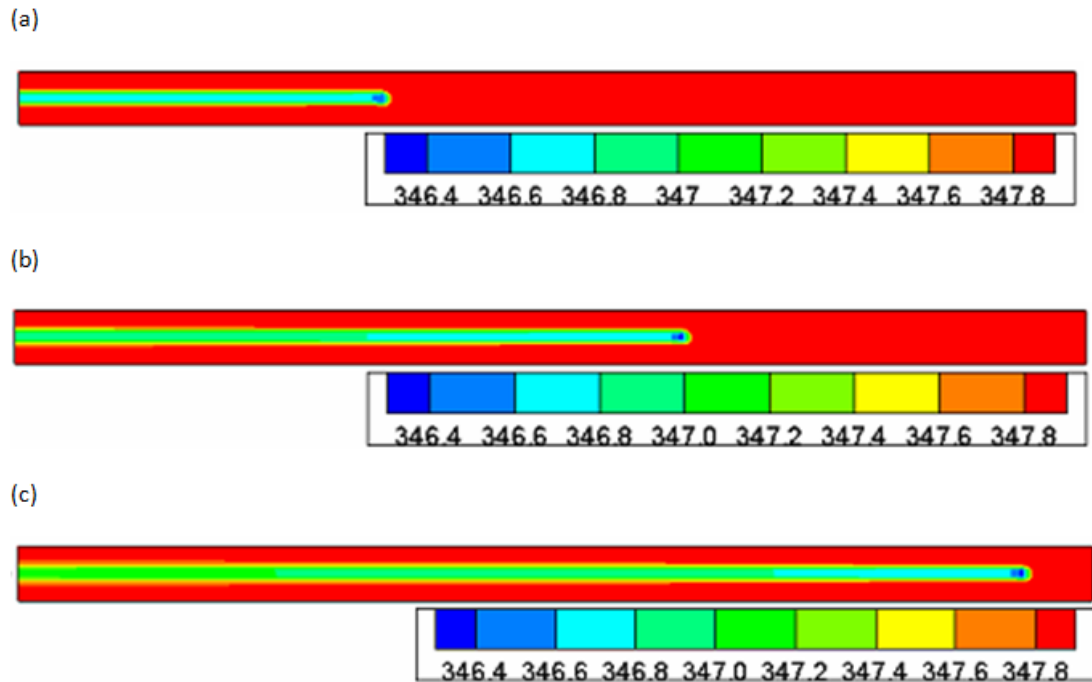


Figure 4-65. Temperature contours for sprays at different locations, (a) $x = 44.5$ cm, (b) $x = 80$ cm, (c) $x = 120$ cm.

Figure 4-65 shows the temperature contours for sprays at various locations. When the spray is closer to the outlet, temperature at the outlet central core reduces more. Sprays far from the outlet cause more penetration in the vertical direction, since droplets have more time to diffuse in y direction. However, temperature reduction at the outlet for case (c) is less compared to case (a).

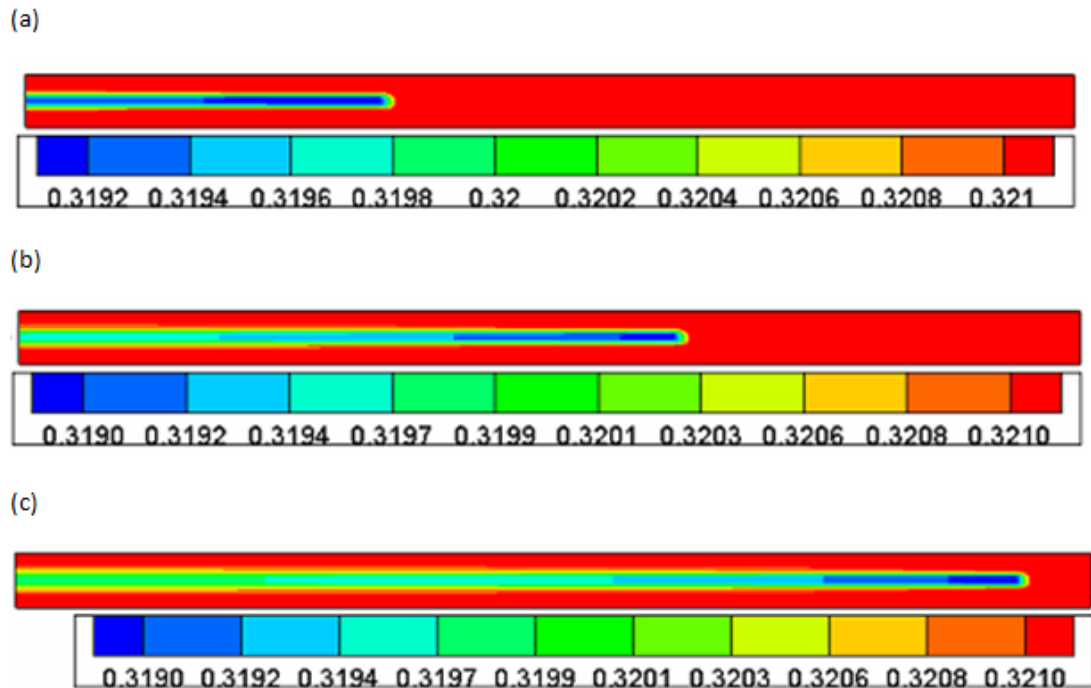


Figure 4-66. Humidity contours for sprays at different locations, (a) $x = 44.5$ cm, (b) $x = 80$ cm, (c) $x = 120$ cm.

Figure 4-66 illustrates the effect of the location of the spray on humidity pattern in the chamber. It is observed that as the location of the spray gets closer to the outlet, humidity reduction at the outlet increases. However by locating the spray far from the nozzle, dehumidification effect penetrates in vertical direction at the outlet which is an advantage for case (c).

4.2.6.1. Effect of the location of the spray on flow pattern on the centerline

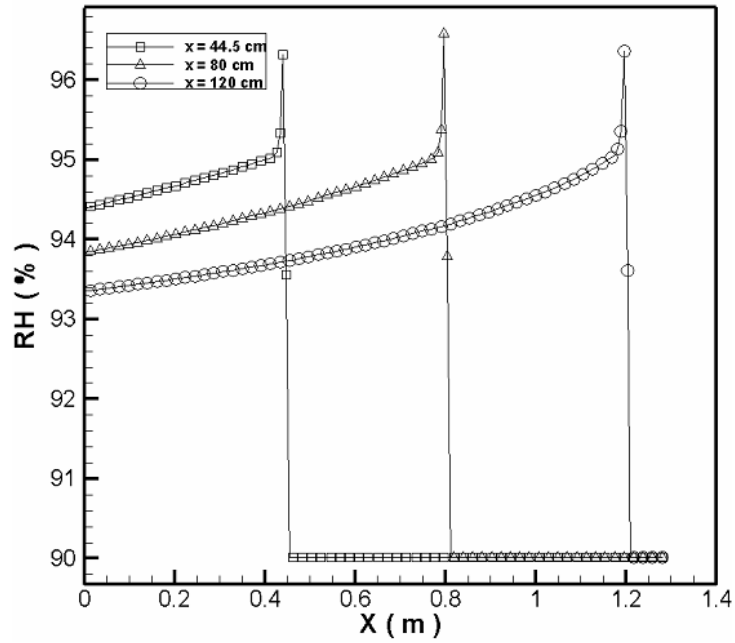


Figure 4-67. Effect of the spray location on relative humidity distribution on the horizontal centerline.

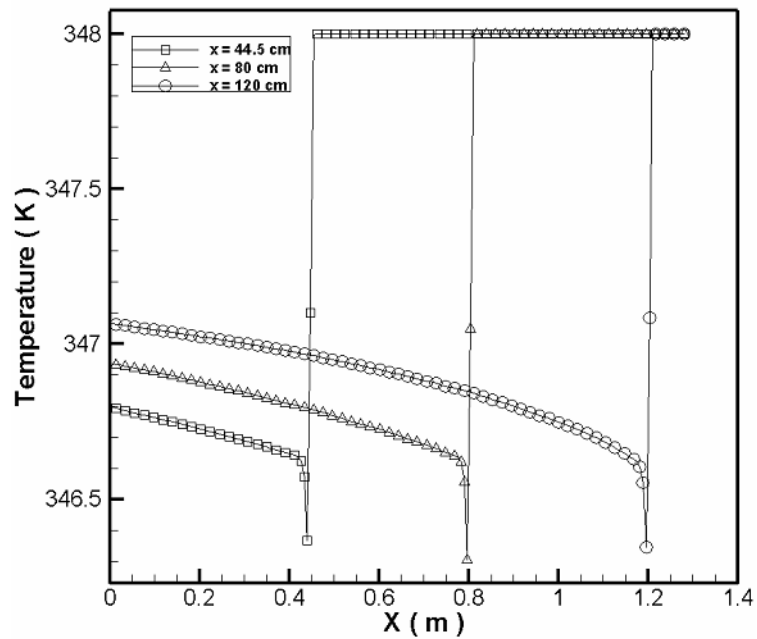


Figure 4-68. Effect of the spray location on temperature distribution on the horizontal centerline.

Figure 4-67 and 4-68 depict the effect of the spray location on the relative humidity and temperature, respectively. Figure 4-67 shows that by locating the spray close to the outlet, relative humidity on the centerline increases more. It is found that temperature reduction close to the nozzle is noticeable. Therefore if the spray is closer to the outlet, temperature reduction at the outlet will be more. Accordingly relative humidity will be higher. However it should also be considered that sprays far from the outlet penetrate better in the vertical direction.

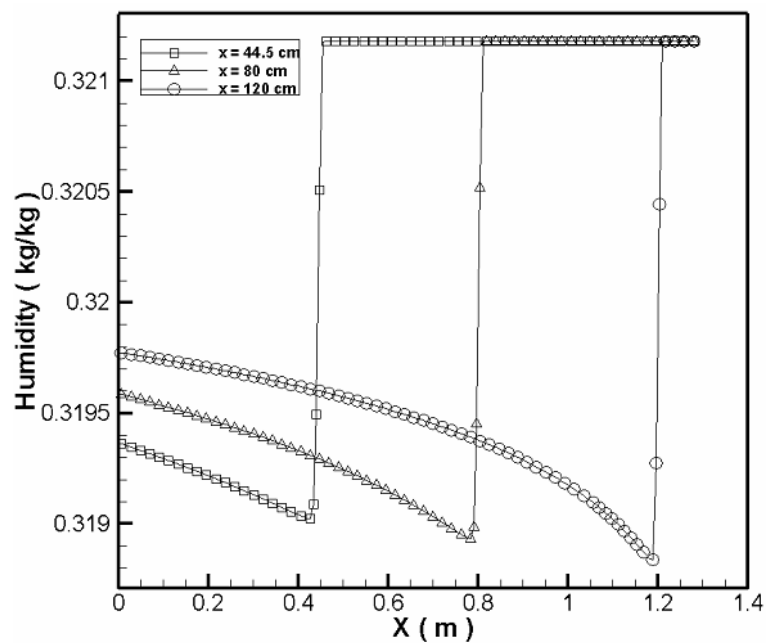


Figure 4-69. Effect of the spray location on humidity distribution on the horizontal centerline.

Figure 4-69 shows the effect of the spray location on the humidity on the centerline of the channel. It is found that right after the nozzle in the downstream direction condensation rate has the highest amount. At distances far from the nozzle condensation rate reduces. For this reason it is better to locate the nozzle close to the outlet. When the spray is located close to the outlet, humidity decreases more at the outlet.

4.2.6.2. Effect of the location of the spray on flow pattern at the outlet cross section

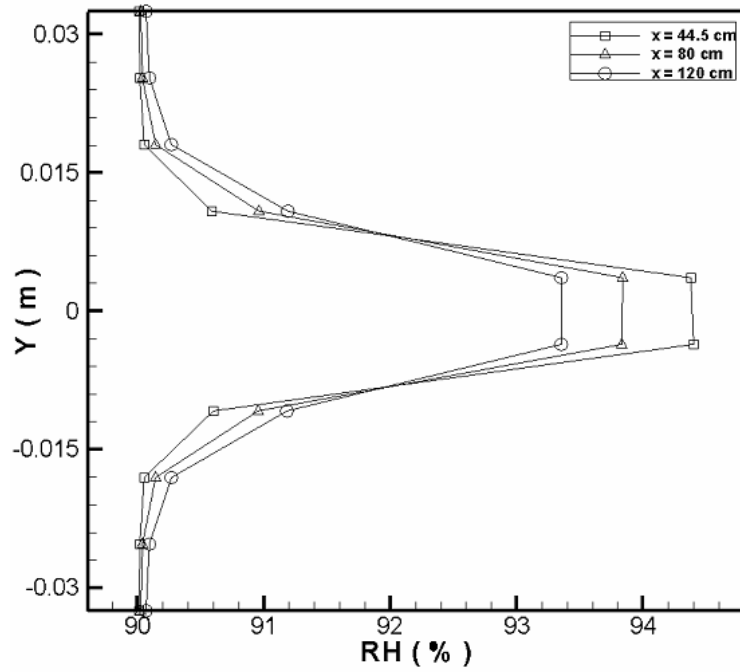


Figure 4-70. Effect of spray location on the relative humidity at the outlet.

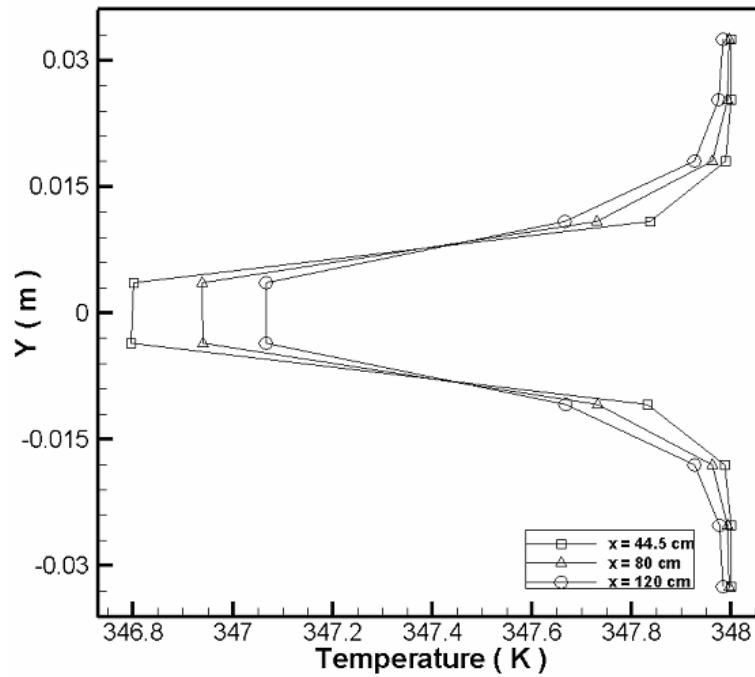


Figure 4-71. Effect of spray location on the temperature at the outlet.

Figure 4-70 and 4-71 show the effect of the spray location on the relative humidity and temperature at the outlet, respectively. When the spray is located close to the outlet, relative humidity enhances to higher values. On the other hand, by locating the spray at distances far from the outlet the temperature close to the wall also decreases since the water droplets are able to penetrate better in the vertical direction.

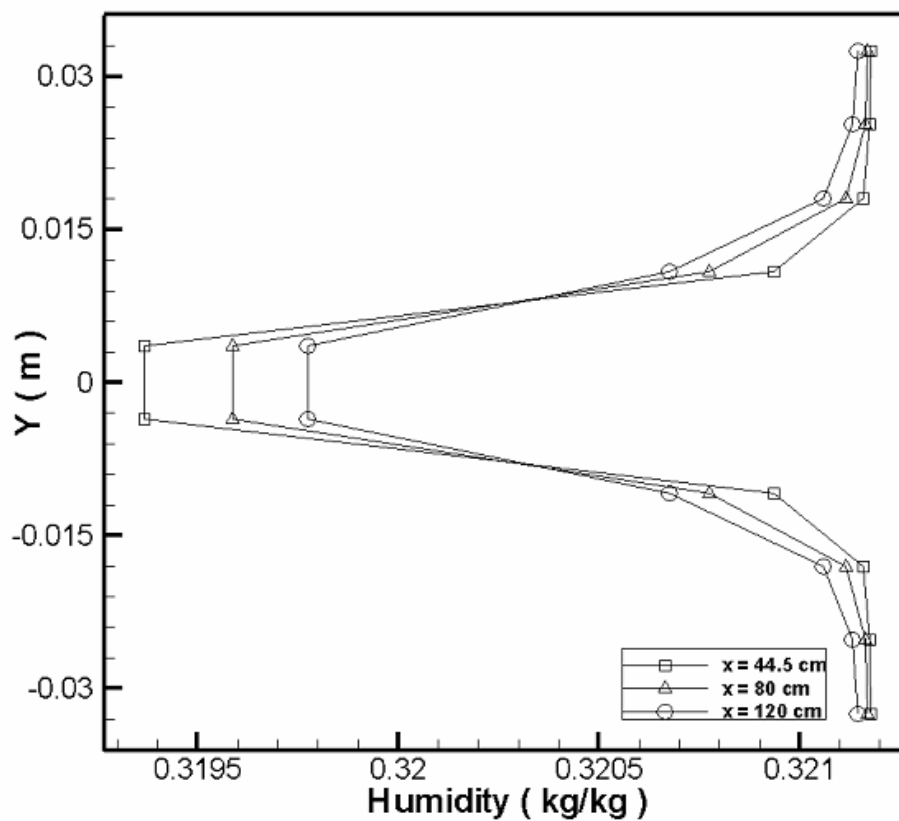


Figure 4-72. Effect of spray location on the humidity at the outlet.

Figure 4-72 depicts that by locating the spray close to the outlet, humidity reduces more. Since condensation rate right after the nozzle is higher, it is better to locate the spray close to the nozzle.

4.2.6.3. Effect of the location of the spray on mass-weighted average values of the parameters

In order to have a better understanding on the effect of the spray location, it is reasonable analyze the mass weighted average data of parameters.

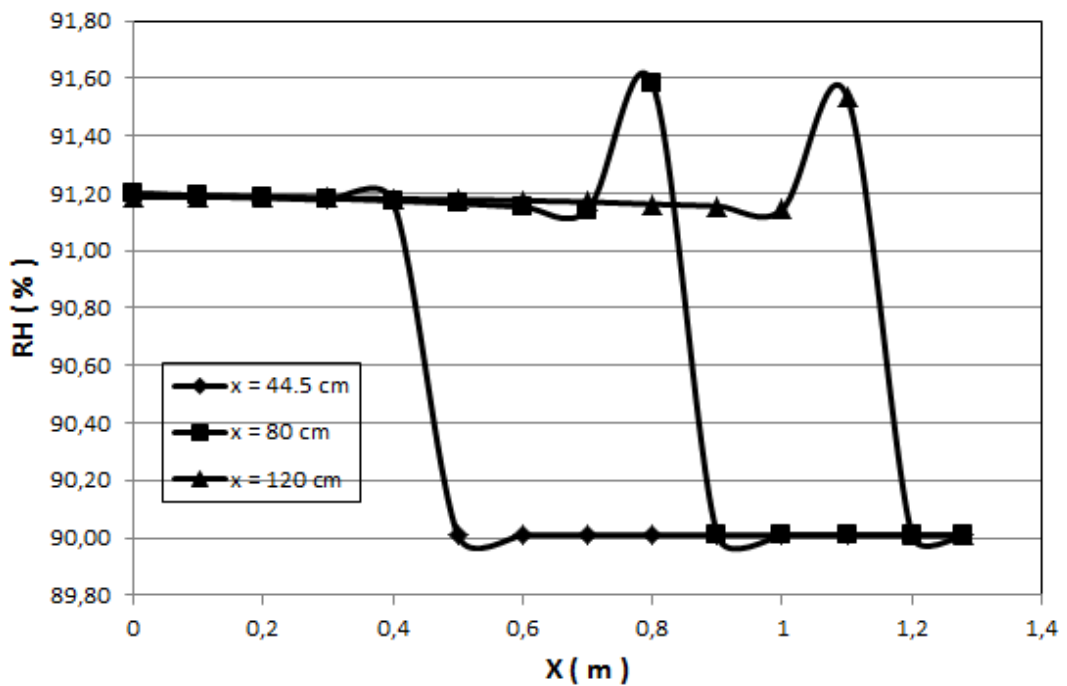


Figure 4-73. Effect of the spray location on mass-weighted average relative humidity.

Figure 4-73 depicts the effect of the spray location on the mass weighted average relative humidity. In all the cases, relative humidity increases after the spray. It is found that at the outlet, mass weighted average relative humidity approximately converges to a same value.

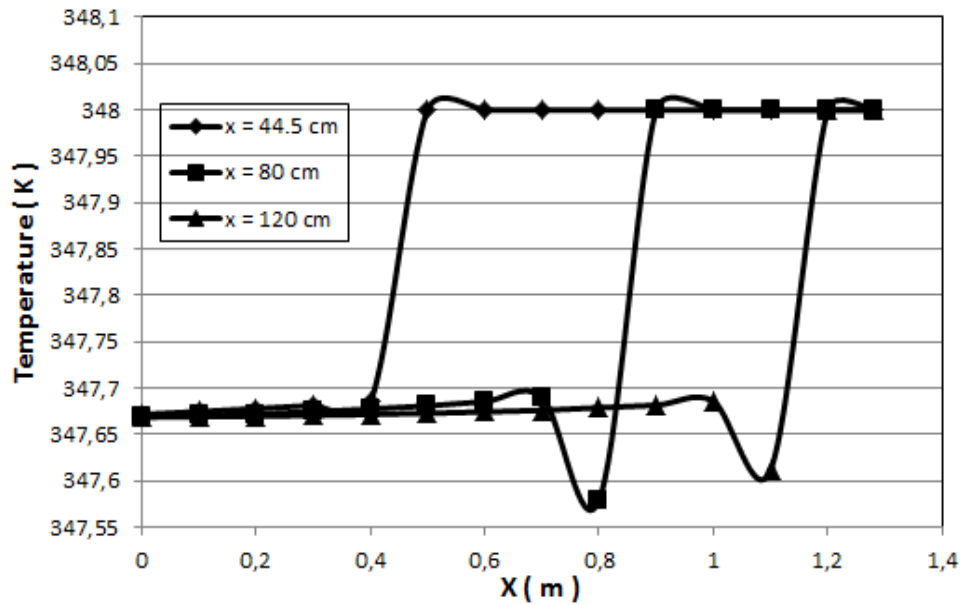


Figure 4-74. Effect of the spray location on bulk temperature.

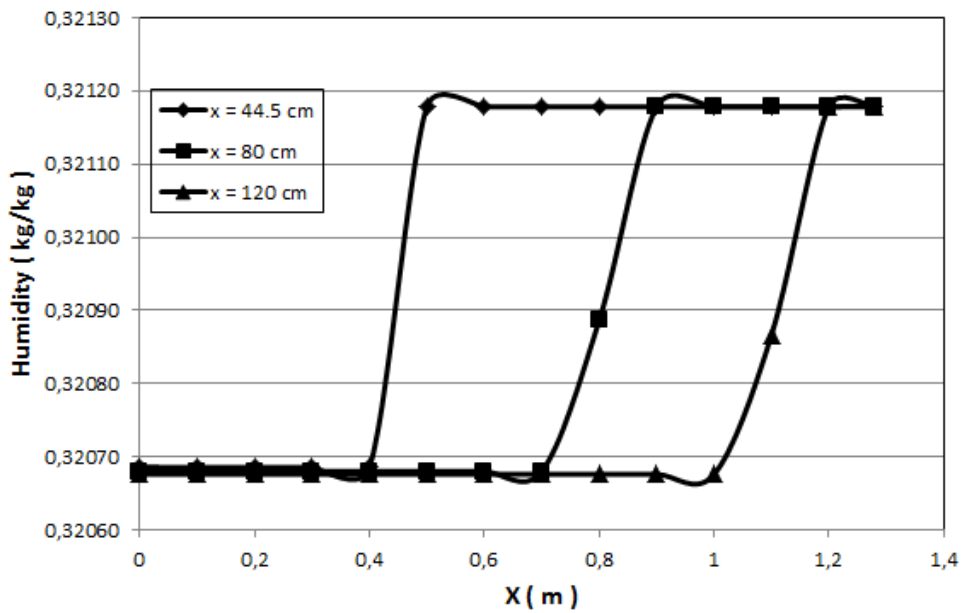


Figure 4-75. Effect of the spray location on mass-weighted average humidity.

Figure 4-74 clarifies the effect of the spray location on bulk temperature distribution in the channel. It is observed that right after the spray temperature reduces quickly and it converges to a specific value. Since all the sprays have the same initial conditions they approximately they converge to a same value. This fact clarifies that

location of the spray does not have significant effect on the bulk temperature at the outlet.

Figure 4-75 shows the effect of the spray location on the mass weighted average humidity. In all the cases right after the spray, a drastic reduction of the humidity occurs due to violent condensation of vapor on water droplets. After this reduction, humidity values of all the cases approximately converge to a same value. The results depict that location of the spray does not have a significant effect on the mass weighted average humidity at the outlet.

5. THREE DIMENSIONAL SIMULATIONS

In this part a three-dimensional model for the dehumidification process of moist air is developed. The chamber is a cylinder with length and diameter of 128 cm and 6.5 cm, respectively. The structural cells with edge size of 7 mm are used for the three dimensional simulations. The problem is simulated by considering unsteady particle tracking.

In this problem the mainstream flow is in the z-axis direction and flows from the right end of the chamber. Figure 5-1 depicts the geometry of the pipe. All the models which are used in two dimensional model are implemented in the three dimensional model.



Figure 5-1. Three dimensional geometry of the pipe.

Since three dimensional calculations are computationally expensive and results of two and three dimensional simulations are very similar, two dimensional simulations are considered to be sufficient for the parametric study. For this reason in this chapter just some sample cases for three dimensional simulations are shown.

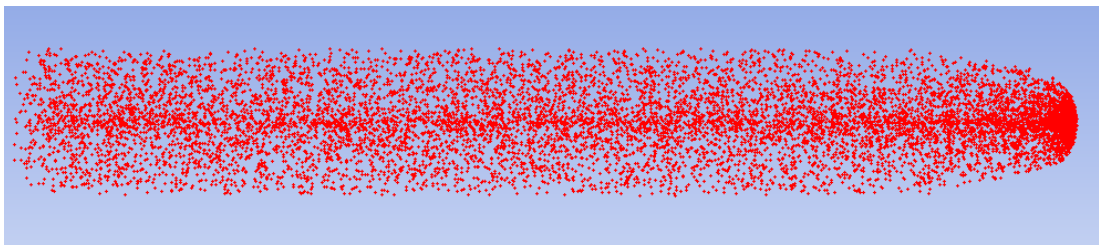


Figure 5-2. Particle trajectories for $dp = 80 \mu\text{m}$.

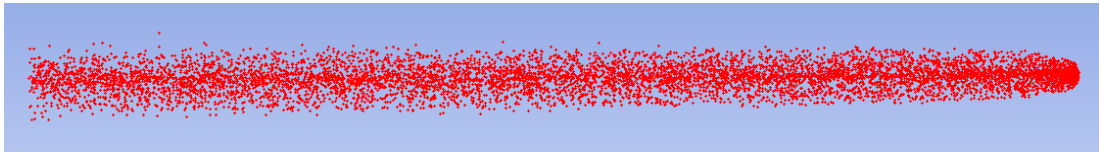


Figure 5-3. Particle trajectories for $d_p = 40 \mu\text{m}$.

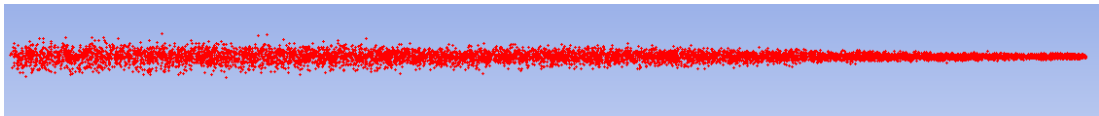


Figure 5-4. Particle trajectories for $d_p = 10 \mu\text{m}$.

Droplet trajectories for three different cases with $d_p = 80 \mu\text{m}$, $d_p = 40 \mu\text{m}$, and $d_p = 10 \mu\text{m}$ are calculated and shown in Figure 5-2, 5-3 and 5-4, respectively. Larger droplets diffuse in the radial direction, but smaller ones do not have the enough momentum to penetrate radially. Thickness of the particle trajectories reveals this fact.

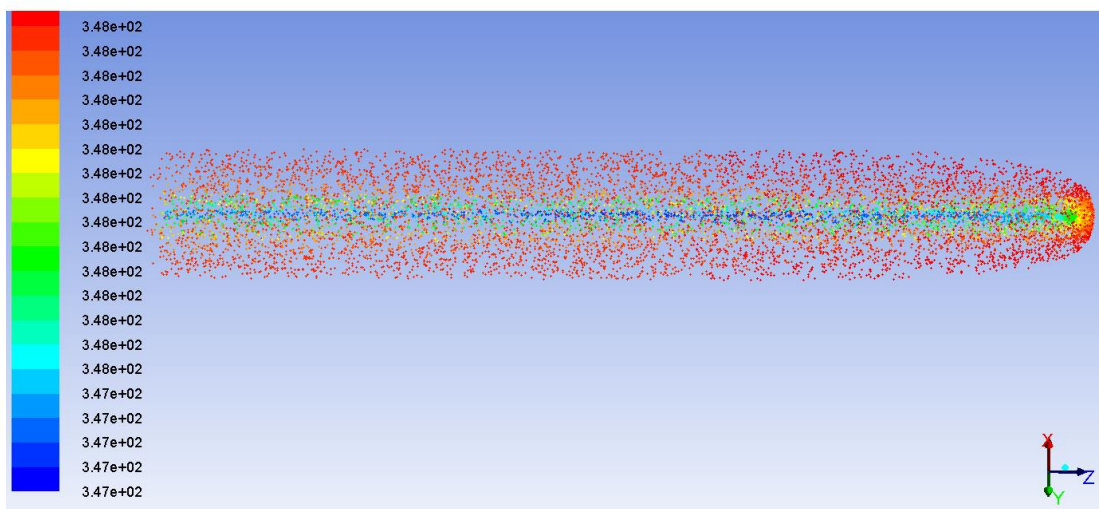


Figure 5-5. Particle traces colored by gas-phase temperature ($d_p = 80 \mu\text{m}$).

Figure 5-5 shows the droplet traces colored by temperature of the gas-phase for droplets with diameters of $80 \mu\text{m}$. It is observed that the central core of the chamber is cooled effectively compared to regions lose to the wall.

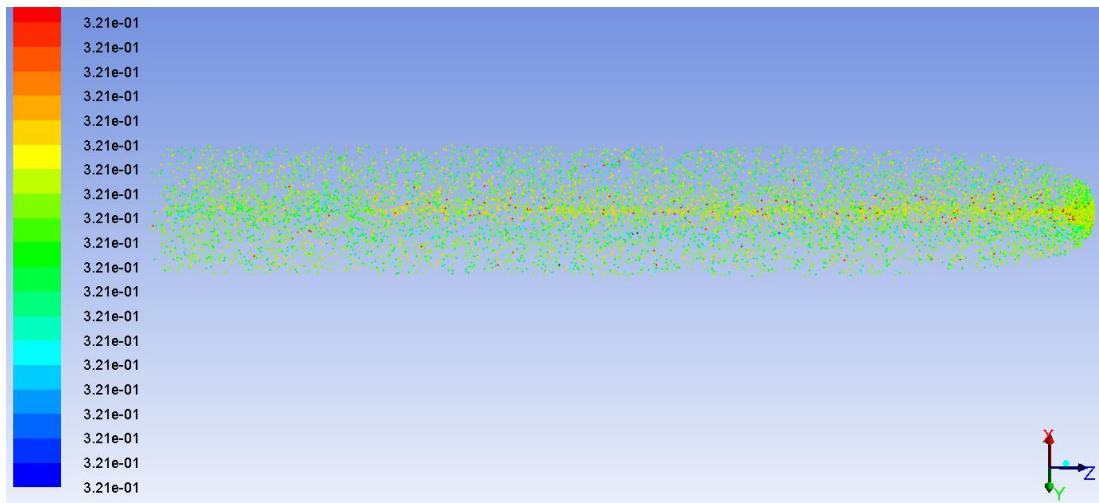


Figure 5-6. Particle traces colored by humidity ($d_p = 80 \mu\text{m}$).

Particle traces colored by humidity of the mixture are revealed in figure 5-6. As it is also noticed in chapter 4.2.1, large droplets such as particles with diameter of $80 \mu\text{m}$ are not able to reduce the humidity of the mixture.

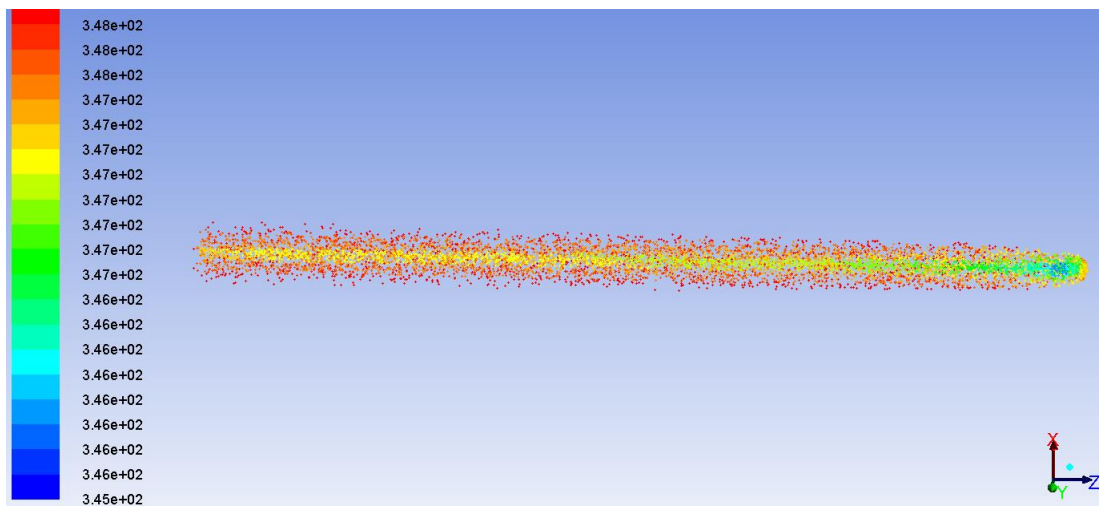


Figure 5-7. Particle traces colored by gas-phase temperature ($d_p = 40 \mu\text{m}$).

Figure 5-7 illustrates the particle trajectories for droplets with diameter of $40 \mu\text{m}$ which are colored by continuous phase temperature. Traces are thinner compared to traces of larger droplets which means droplets are not able to diffuse in radial direction effectively. In addition, due to lower momentum particles are not able to penetrate in the mainstream flow. It is noticed that in the nozzle region temperature

reduction has its highest amount. In regions far from the spray temperature reduction rate decreases.

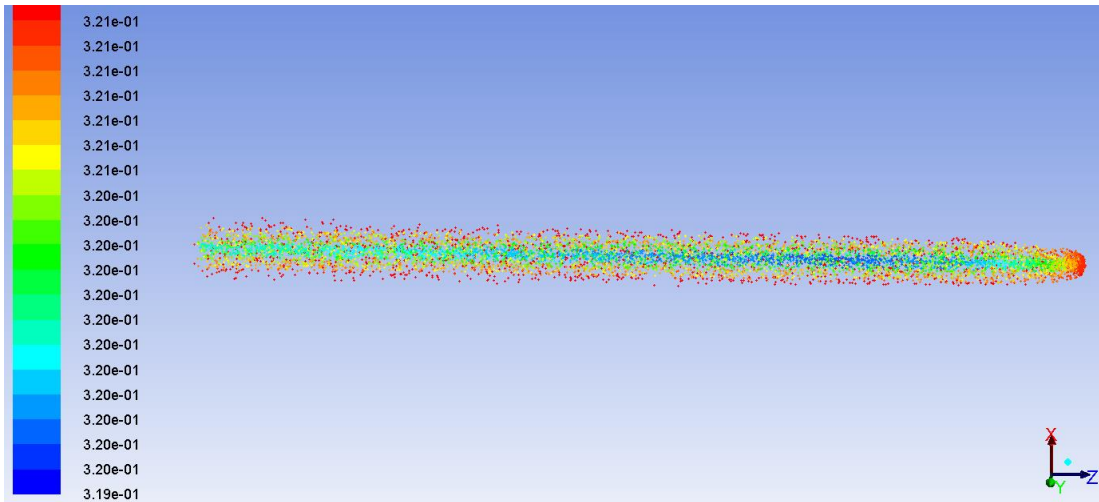


Figure 5-8. Particle traces colored by humidity ($d_p = 40 \mu\text{m}$).

Figure 5-8 shows the particle traces colored by humidity for the droplets with diameter of $40 \mu\text{m}$. Humidity around the centerline of the spray is declined. This reduction of vapor content in the continuous phase is because of the higher condensation of the steam on water droplets in these parts of the chamber.

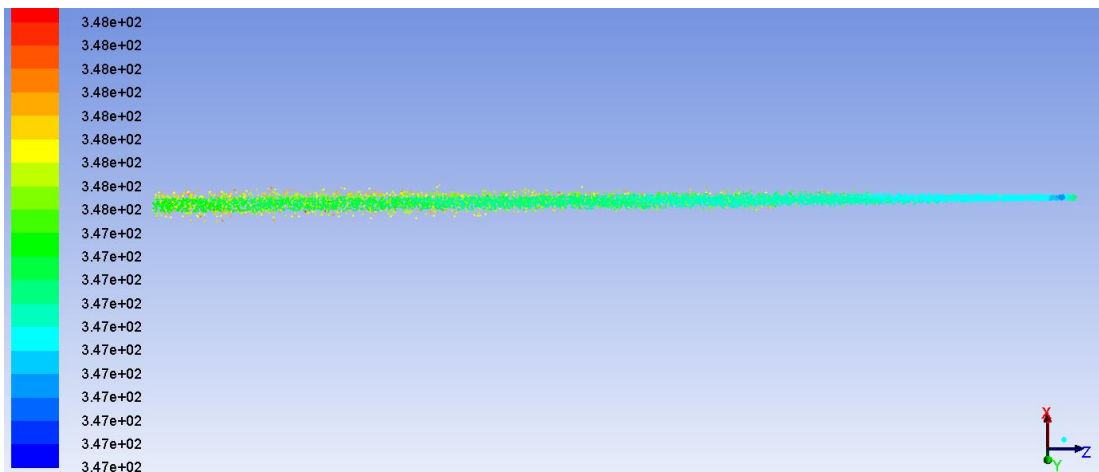


Figure 5-9. Particle traces colored by gas-phase temperature ($d_p = 10 \mu\text{m}$).

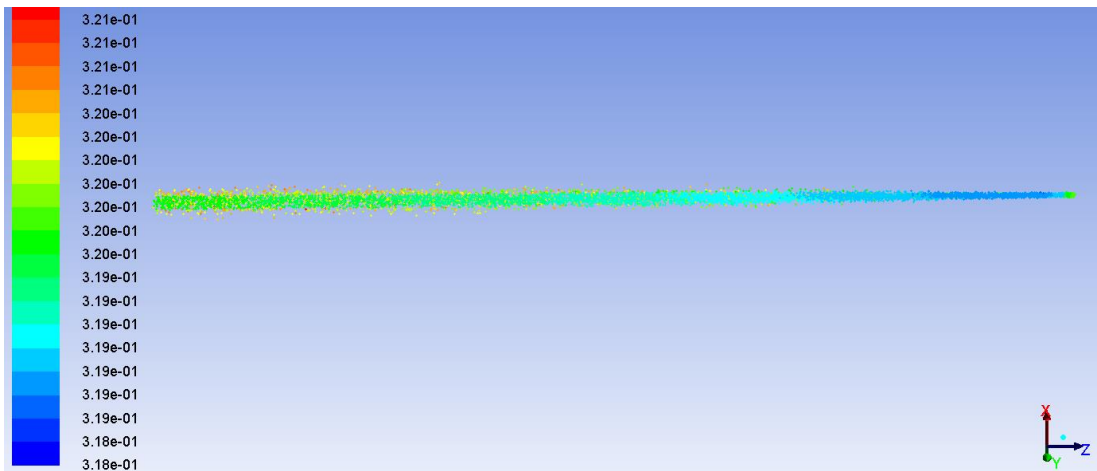


Figure 5-10. Particle traces colored by humidity ($d_p = 10 \mu\text{m}$).

Figure 5-9 shows the particle traces colored by gas-phase temperature while the droplets have the diameter of $10 \mu\text{m}$. Since momentum of the droplets is low, they could not stretch their effect on the flow field. These particles just reduce the temperature and humidity at the cone center of the chamber (Figure 5-9, Figure 5-10). When droplet size is reduced to $10 \mu\text{m}$, the highest mass transfer is achieved in the central core region compared to larger droplets. Therefore by using sprays of smaller droplets humidity reduction will have the highest rate which is the target of this research.

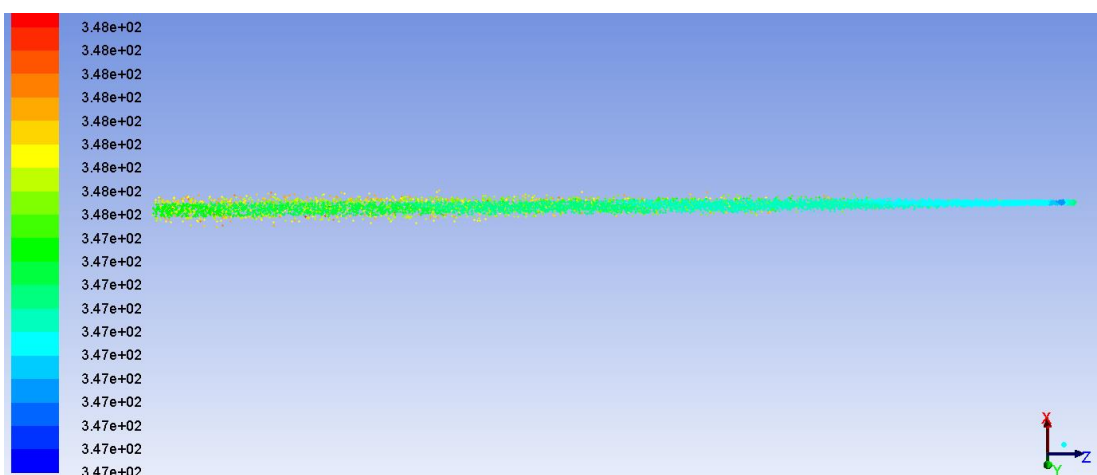


Figure 5-11. Particle traces colored by temperature ($T_w = 288 \text{ K}$).

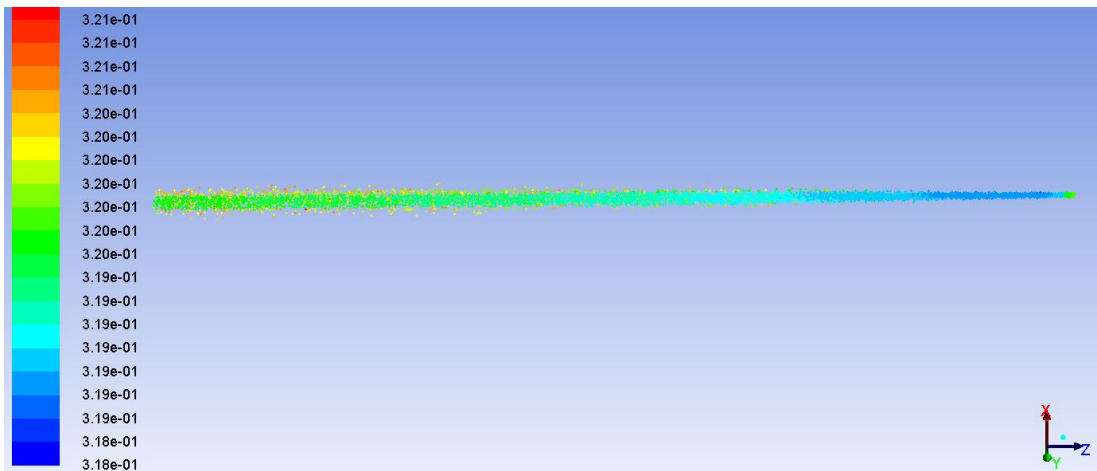


Figure 5-12. Particle traces colored by humidity ($T_w = 288$ K).

Figure 5-11 and 5-12 illustrate the particle traces colored by temperature and humidity, respectively. By decreasing the particle temperature, temperature difference between the droplets and the continuous phase enhances. For this reason more humidity and temperature reduction is expected. If the water temperature is increased to 323 K, the heat and mass transfer rates decrease as a result of temperature gradient reduction. Figure 5-13 and 5-14 illustrate the particle traces colored by temperature and humidity, respectively.

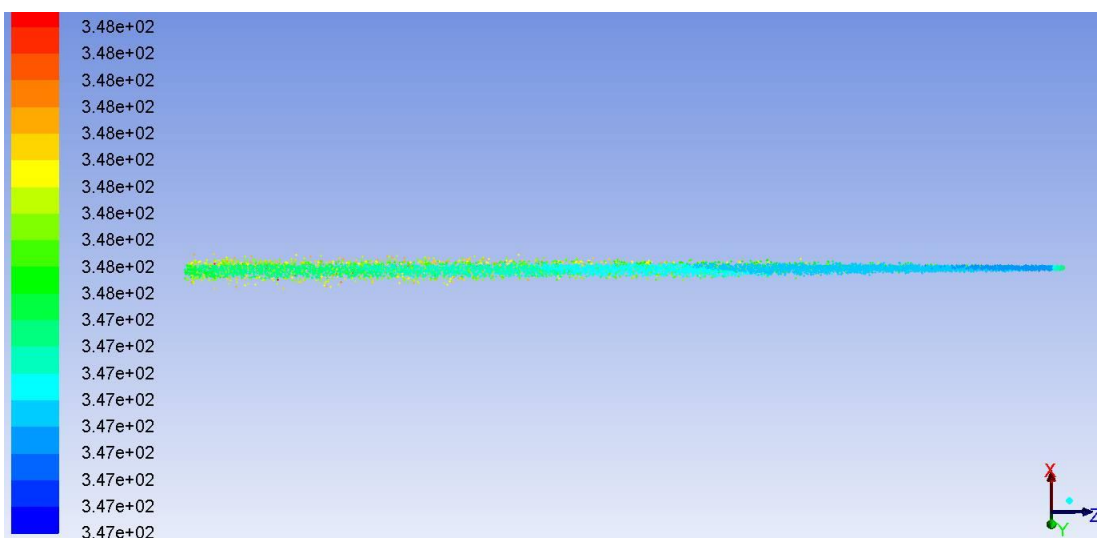


Figure 5-13. Particle traces colored by temperature ($T_w = 323$ K).

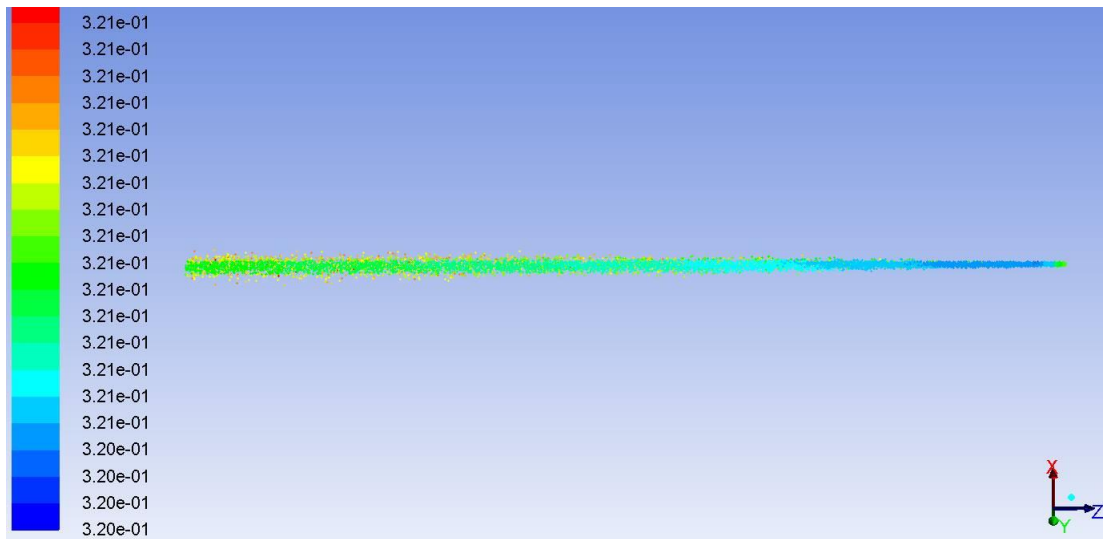


Figure 5-14. Particle traces colored by humidity ($T_w = 323$ K).

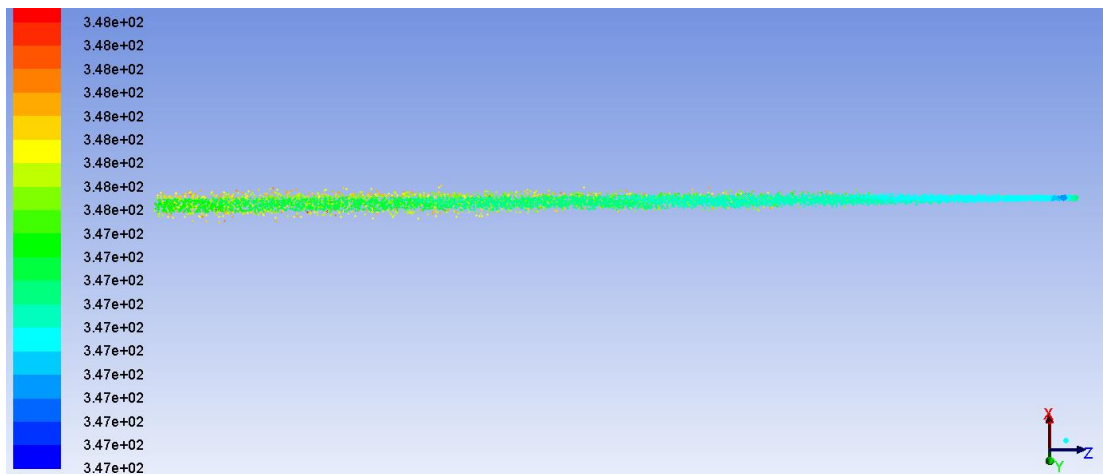


Figure 5-15. Particle traces colored by temperature (mass flow rate = 3 gr/s).

When the mass flow rate of the spray increases, heat and mass transfer between the droplets and the continuous phase enhances. Figure 5-15 and 4-16 illustrate the particle traces for spray with mass flow rate of 3gr/s.

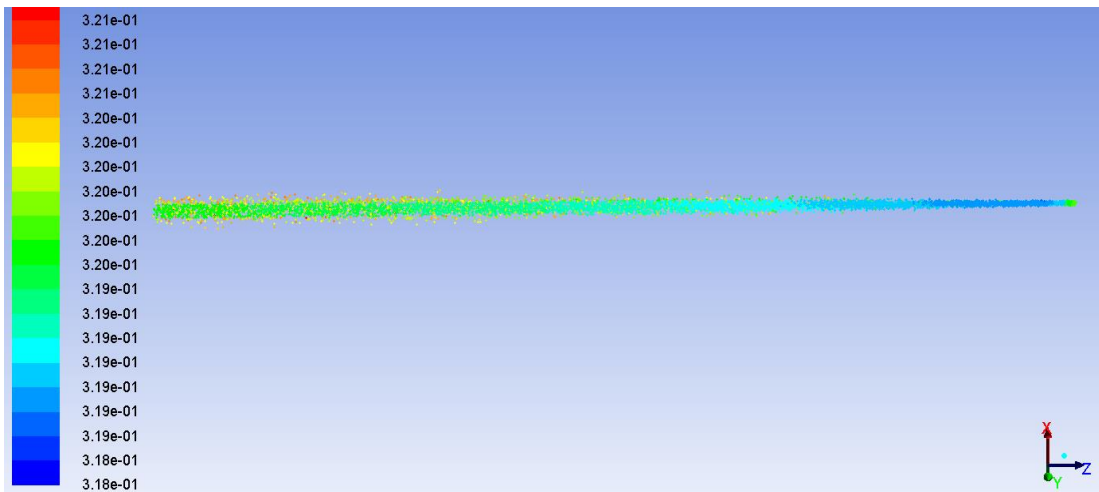


Figure 5-16. Particle traces colored by humidity (mass flow rate = 3 gr/s).

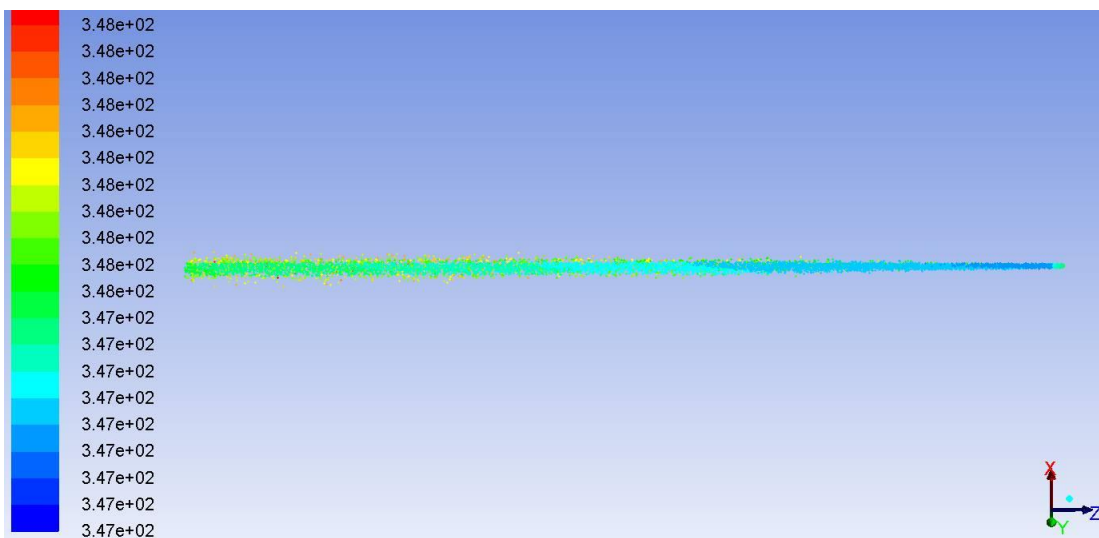


Figure 5-17. Particle traces colored by temperature (mass flow rate = 6 gr/s).

Figure 5-17 and 5-18 depict the particle traces for the spray with mass flow rate of 6gr/s. It is observed that heat and mass transfer for the sprays with higher mass flow rates is more. In other words, temperature and humidity reduction for sprays with higher mass flow rates is more.

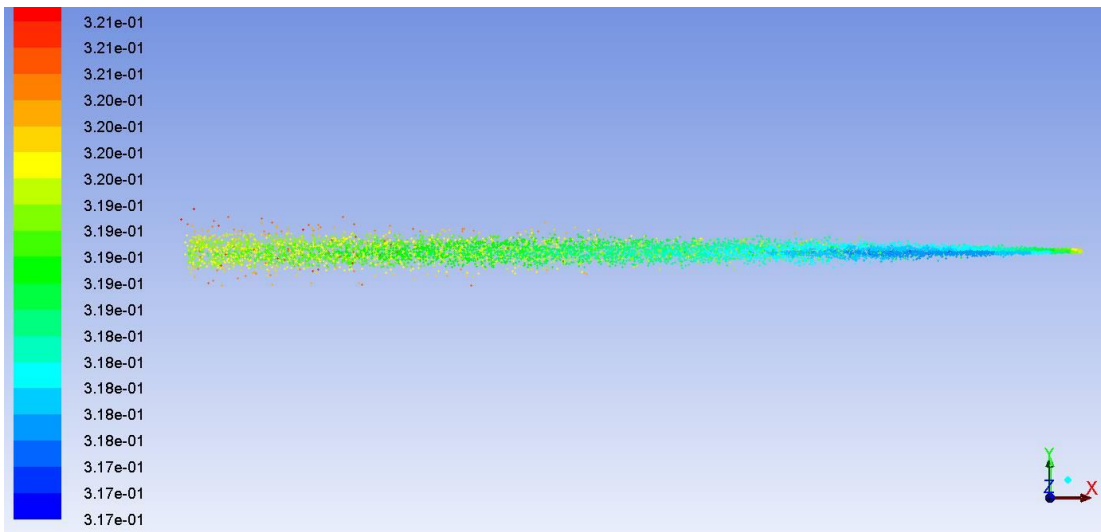


Figure 5-18. Particle traces colored by humidity (mass flow rate = 6 gr/s).

6. CONCLUSIONS

This work investigates the effect of various parameters on dehumidification process in a channel. The major objective of this study is to gain a complete understanding of the underlying phenomena in direct contact condensation heat and mass transfer. The main phenomenon in this two phase flow problem is direct contact condensation of vapor on water droplets. In this chapter the main results and conclusions of the research are presented.

The problem is solved by using ANSYS Fluent 14.5. The continuous phase (gas-vapor mixture) is solved in the Eulerian approach and the discrete phase is solved by applying Lagrangian approach.

In order to investigate the effect of various parameters on heat and mass transfer, each time one parameter is altered while different conditions are kept constant. The results of this research depict that by increasing the droplet diameter heat transfer initially enhances; however by passing an optimum diameter heat transfer decreases. The droplet size effect is always in contrast with mass transfer rate. It means that decreasing the droplet diameter results in enhancement of mass transfer. The goal of this investigation is to reduce the moisture content of the mixture. Accordingly droplets with the smallest diameters will be the favorable droplet sizes in this investigation.

It is concluded that increase in mass flow rate of the spray causes enhancement in heat and mass transfer. Since the mass flow rate rises gas-phase temperature and humidity decreases more. Consequently spray with the maximum mass flow rate should be chosen to have higher dehumidification rate.

Water temperature has vital effect on direct contact condensation of vapor on droplets surfaces. For this reason various water temperatures are studied to figure out temperature effect on DCC. It is noticed that decrease in water temperature increases the temperature gradient which leads to greater heat and mass transfer. That is why higher dehumidification rate will be achieved by using colder water droplets.

Furthermore the effect of different spray cone angles is studied. It is found that heat transfer is increased by increasing the cone angle of the spray. However the effect of cone angle on heat transfer is so small that it could be neglected.

Since a single spray is not efficiently spreading in the radial direction, the idea of using more nozzles in the channel is implemented to the problem. Increasing the number of the nozzles causes enhancement in mass weighted average relative humidity. By using two sprays in the channel mass weighted average humidity and temperature decreases. In order to increase the dehumidification efficiency number of sprays should increase.

It is found that the location of the spray does not have a significant effect on the mass weighted average humidity and temperature.

REFERENCES

- [1] http://en.wikipedia.org/wiki/Air_conditioning , access date: 12 November 2014.
- [2] Nagengast, B., The First 80 Years of Air-Conditioning, ASHRAE Journal, Vol.34, No.1, pp.S164-S175, 1992.
- [3] Kreith, F., Boehm, R. F., Direct Contact Heat Transfer, Hemisphere Pub. Corp., 1988.
- [4] Hasson, D., Luss, D., and Navon, V., An Experimental Study of Steam Condensing on a Laminar Water Sheet, International Journal of Heat and Mass Transfer, 7, 983-1001, 1964.
- [5] FORD, J. D. & LEKIC, A., Rate of growth of drops during condensation. Int. J. Heat Mass Transfer, 16, 61-64, 1973.
- [6] Simpson, M.E., Chan, C.K., Hydrodynamics of a subsonic vapor jet in subcooled liquid., Journal of Heat Transfer 104, 271–278, 1982.
- [7] Jeje, A., Asante, B., Ross, B., Steam bubbling regimes and direct contact condensation heat transfer in highly subcooled water. Chemical Engineering Science 45, 639–650, 1990.
- [8] Garimella S. V., Christensen R. N., Transient condensation in the presence of noncondensables at a vertical wall. Nuclear Technology 89, 388 – 398, 1990.
- [9] Celata, G. P., Cumo, M., Annibale, F. D., & Farello, G. E., Direct Contact Condensation of Steam on Droplets, Int. J. Multiphase Flow, 17(2), 191–211., 1991.
- [10] Aya, I., Nariai, H., Evaluation of heat-transfer coefficient at direct-contact condensation of cold water and steam, Nuclear Engineering and Design, 131, 17–24., 1991.
- [11] Liang, K.-S., 1991, Experimental and analytical study of direct contact condensation of steam in water. PhD Thesis, Massachusetts Institute of Technology.

- [12] Mayinger, F. and Chavez A., Measurement of direct-contact condensation of pure saturated vapour on a injection spray by applying pulsed laser holography, *International Journal of Heat Mass Transfer*, 35(3), 691-702, 1992.
- [13] Akira, M., Fiji, H., & Takamoto, S., Prediction of heat transfer by direct contact condensation at a steam-subcooled water interface. *International Journal of Heat and Mass Transfer*, 35(1), 101–109, 1992.
- [14] Lock, G. S. H., *Latent Heat Transfer: An Introduction to Fundamentals*, Oxford University Press, Oxford, 1994.
- [15] Kuhn S. Z., Schrock V. E., Peterson P. F., An investigation of condensation from steam-gas mixtures flowing downward inside a vertical tube. *Nuclear Engineering and Design* 177, 53 – 69, 1997.
- [16] Karl J., Weiss T., Measurement of condensation heat transfer coefficients at stratified flow using Linear Raman Spectroscopy. *Proceedings of The 1st Pacific Symposium on Flow Visualization and Image Processing*, Honolulu, 479 – 484., 1997.
- [17] Anderson M. H., Herranz L. E., Corradini M. L., Experimental analysis of heat transfer within the AP600 containment under postulated accident conditions. *Nuclear Engineering and Design* 185, 153 – 172, 1998.
- [18] Ju, S. H., No, H. C., Mayinger, F., Measurement of heat transfer coefficients for direct contact condensation in core makeup tanks using holographic interferometer. *Nuclear Engineering and Design*, 199, 75–83, 2000.
- [19] Lee, H., Kim, M., Park, S., The Effect of Noncondensable Gas on Direct Contact Condensation of Steam/Air-mixture *Journal of the Korean Nuclear Society*, 33(6), pp.585-595, 2001.

- [20] Kim, H.W., Bae, Y.Y., Song, C.H., Park, J.K., Choi, S.M., Experimental study on stable steam condensation in a quenching tank. *International Journal of Energy Research* 25, 239–252, 2001.
- [21] Pikkula, B. M., Torres, J. H., Tunnell, J. W., Anvari, B., Cryogen Spray Cooling: Effects of Droplet Size and Spray Density on Heat Removal, *Lasers in Surgery and Medicine* 28:103-112, 2001.
- [22] Cheng, W. L., Han, F. Y., Liu, Q. N., Fan, H. L., Spray Characteristics and Spray Cooling Heat Transfer in the non-boiling Regime, *Energy*, 36, 3399-3405, 2001.
- [23] Chen, R. H., Chow, L. C., Navedo, J. E., Effects of spray characteristics on critical heat flux in subcooled water spray cooling, *International Journal of Heat and Mass Transfer*, 45, 4033–4043, 2002.
- [24] Martinez-Galvan, E., Anton, R., Ramos, J. C., & Khodabandeh, R., Effect of the spray cone angle in the spray cooling with R134a. *Experimental Thermal and Fluid Science*, 50, 127–138, 2013.
- [25] Zhang, H., Bai, B., Liu, L., Sun, H., & Yan, J., Droplet dispersion characteristics of the hollow cone sprays in crossflow. *Experimental Thermal and Fluid Science*, 45, 25–33, 2013.
- [26] Minkowycz W. J., Sparrow E. M., Condensation heat transfer in presence of noncondensables, interfacial resistance, superheating, variable properties, and diffusion. *International Journal of Heat and Mass Transfer* 9, 1125 – 1144, 1966.
- [27] Sparrow E. M., Minkowycz W. J., Saddy M., Forced convection condensation in presence of noncondensables and interfacial resistance. *Int. J. Heat Mass Transfer* 10, 1829 – 1845, 1967.

- [28] Taitel, Y., Tamir, A., Condensation in the presence of a noncondensable gas in direct contact, *International Journal of Heat and Mass Transfer*, 12(9), 1157–1169, 1969.
- [29] Sage F. E., Estrin J., Film condensation from a ternary mixture of vapours upon a vertical surface, *International Journal of Heat and Mass Transfer*, 19, 323 – 333, 1976.
- [30] Frediani, H. A. and Smith, N., Mathematical model of spray cooling systems, *Journal of engineering for power*, 279-283, 1977.
- [31] Ghosh, S. and Hunt, J. C. R., Induced Air Velocity Within Droplet Driven Sprays, *Proceedings of the Royal Society of London A*, 444, 105-127, 1994.
- [32] Akimoto, H., Kozawa, Y., Inoue, A., & Aoki, S., Analysis of Direct Contact Condensation of Flowing Steam onto Injected Water with Multifluid Model of Two-Phase Flow. *Journal of Nuclear Science and Technology*, 20(12), 1006–1022, 1983.
- [33] Huang, L. J., Ayyaswamy, P. S., Heat and mass transfer associated with a spray drop experiencing condensation: a fully transient analysis., *International Journal of Heat and Mass Transfer*, 30(5), 881–891, 1987.
- [34] Turkoglu, H., Farouk, B., Yang, L., Modeling of Interfacial Transport Processes in a Direct-Contact Condenser For Metal Recovery, *Numerical Heat Transfer, Part A*, 33, 457-475, 1998.
- [35] Lin, L., & Ponnappan, R., Heat transfer characteristics of spray cooling in a closed loop. *International Journal of Heat and Mass Transfer*, 46(20), 3737–3746, 2003.
- [36] Shah, A., Chughtai, I. R., & Inayat, M. H., Numerical Simulation of Direct-contact Condensation from a Supersonic Steam Jet in Subcooled Water. *Chinese Journal of Chemical Engineering*, 18(4), 577–587, 2010.

- [37] Shaver, D., Antal, S., Podowski, M., Kim, D., Modeling and Analysis of Direct Steam Condensation in a Passive Safety System of Advanced PWR, 7th International Conference on Multiphase Flow ICMF 2010, 1–8, Florida, USA, 2010.
- [38] Alnaimat, F., Klausner, J. F., & Mei, R., Transient analysis of direct contact evaporation and condensation within packed beds. *International Journal of Heat and Mass Transfer*, 54(15-16), 3381–3393, 2011.
- [39] Cui, X., Li, X., Sui, H., & Li, H., Computational fluid dynamics simulations of direct contact heat and mass transfer of a multicomponent two-phase film flow in an inclined channel at sub-atmospheric pressure. *International Journal of Heat and Mass Transfer*, 55(21-22), 5808–5818, 2012.
- [40] Lan, Z., Wen, R., Wang, A., & Ma, X., A droplet model in steam condensation with noncondensable gas. *International Journal of Thermal Sciences*, 68, 1–7, 2013.
- [41] ANSYS FLUENT Theory Guide, ANSYS, Inc., Release 14.0, 2011.
- [42] Morsi, S. A. and A. J. Alexander., *Journal of Fluid Mechanics*, 55(2), 193-208, 1972.
- [43] W. E. Ranz and W. R. Marshall, Jr., Vaporation from Drops, Part I., *Chem. Eng. Progr.* 48(3), 141–146, 1952.
- [44] R. S. Miller, K. Harstad and J. Bellan., Evaluation of Equilibrium and Non-Equilibrium Evaporation Models for Many Droplet Gas-Liquid Flow Simulations, *International Journal of Multiphase Flow*, 24(6), 1025 –1055, 1998.
- [45] S. S. Sazhin., *Advanced Models of Fuel Droplet Heating and Evaporation*, *Progress in Energy and Combustion Science*, Elsevier Science, 32, 162–214, 2006.
- [46] Ashgriz, N., *Handbook of Atomization and Sprays: Theory and Applications*, Springer, 2011.

- [47] Takahashi, M., Nayak A. K., Kitagawa, S. I., Murakoso, H., Heat Transfer in Direct Contact Condensation of Steam to Subcooled Water Spray, *Journal of Heat Transfer*, 123(4), 703-710, 2001.
- [48] Cheng, L., Mewes, D., *Advances in Multiphase Flow and Heat Transfer*, Vol. 1, Bentham Science Publishers, 2009.
- [49] Chadderton, D., V., *Air Conditioning: A Practical Introduction*, Third Edition, , Routledge, New York, 2014.
- [50] Ananthanarayanan, P., N., *Basic Refrigeration and Air Conditioning*, Third Edition, McGraw-Hill, New Delhi, 2006.
- [51] Singh, P., Singh, V. P., *Snow and Glacier Hydrology*, Kluwer Academic Publishers, Netherlands, 2001.
- [52] Liu, X., Jiang, Y., Zhang, T., *Temperature and Humidity Independent Control (THIC) of Air-conditioning System*, Springer, Heidelberg, 2013.
- [53] DUTTA, B., K., *PRINCIPLES OF MASS TRANSFER AND SEPERATION PROCESSES*, New Delhi, PHI, 2009.
- [54] Wang, S., *Intelligent Building and Building Automation*, Spon Press, New York, 2010.
- [55] Petchers, N., *Combined Heating, Cooling and Power Handbook: Technologies and Applications*, Fairmont Press, New York, 2003.
- [56] El-Morsi, M. S., 2002, *Optimization of Direct-Contact-Spray-Coolers*, PhD Thesis, University of Wisconsin-Madison.
- [57] Chen, R. H., Chow, L. C., Navedo, J. E., Effects of spray characteristics on critical heat flux in subcooled water spray cooling, *International Journal of Heat and Mass Transfer*, 45(19), 4033–4043, 2002.

- [58] Sarkar, M., Multiphase Flow Modeling of Spray Cooling to Improve Heat Transfer, ProQuest LLC, Ann Arbor, United States of America, 2008.
- [59] Hwang, G. J., Transport Phenomena In Thermal Control, Hemisphere publishing Corporation, United States of America, 1989.
- [60] L. Ortiz and J. E. Gonzalez, Experiments on Steady-State High Heat Fluxes Using Spray Cooling, Experimental Heat Transfer, 12, 215–233, 1999.
- [61] Cabrera, E., Gonzalez, J. E., HEAT FLUX CORRELATION FOR SPRAY COOLING IN THE NUCLEATE BOILING REGIME, Experimental Heat Transfer, 16, 19–44, 2003.
- [62] Yao, S. C., Choit, K. J., Heat transfer experiments of mono-dispersed vertically impacting sprays, International Journal of Multiphase Flow, 13(5), 639–648, 1987.
- [63] Lefebvre, A. H., Atomization and Sprays, Taylor & Francis, United States of America, 1989.
- [64] ANSYS FLUENT UDF Manual, ANSYS, Inc., Release 14.5, October 2012.

RESUME

Personal Information

Surname, Name : FARNOUD, Ali
Nationality : IRAN
Birth Date and Place : 21.09.1989, IRAN
Marital Status : Single
Phone : +90 (536) 638 43 49
Fax : -
E-mail : alifarnod@gmail.com

Education

Degree	Date	Education Department	Graduation
Bachelor of Science		University of Tabriz/ Mecanical Engineering	2011
Master of Science		TOBB University of Economics and Technology /Department of Mechanical Engineering	2014

Academic Work Experience

Year	Place	Task
03.2013-12.2014	TOBB University of Technology and Economics , Ankara, Turkey	Research Assistant

Foreign Language

Persian, English, Turkish, Arabic, German

Awards

Full Tuition Award (B.Sc.)	2007-2011
Paul Eisenklam Travel Award for Young Researchers	ILASS14, 26th European Conference Liquid Atomization & Spray Systems, Bremen, Germany, September 2014
German Excellence Initiative	Doctoral fellow-2015-2018

Publications

1. Farnoud, A., Duru, C., Kasap, F., Şahin, Y., AKTAŞ, M. K., SPREYLE SOĞUTMA İŞLEMİNİN SAYISAL ANALİZİ, ULIBTK 2013 19. Ulusal Isı Bilimi ve Tekniği Kongresi, Samsun, Eylül, 2013.
2. Farnoud, A., Gumruk, S., Aktas, M. K., NUMERICAL INVESTIGATION OF HEAT TRASFER ENHANCEMENT AND DEHUMIDIFICATION OF MOIST AIR, Proceedings of CONV-14: Int. Symp. on Convective Heat and Mass Transfer, Turkey, June, 2014.
3. Farnoud, A., Aktas, M. K., PARAMETRIC STUDY OF DIRECT CONTACT STEAM CONDENSATION ON DROPLETS IN A HORIZONTAL CHANNEL, ILASS – Europe 2014, 26th Annual Conference on Liquid Atomization and Spray Systems, Bremen, Germany, September, 2014.